# UPPER BOUND ERRORS IN FAR-FIELD ANTENNA PARAMETERS DETERMINED FROM PLANAR NEAR-FIELD MEASUREMENTS PART 2: ANALYSIS AND COMPUTER SIMULATION



Allen C. Newell

Lecture Notes for National Bureau of Standards Short Course,
Antenna Parameter Measurements by Near-Field Techniques

July 7-11, 1975
Boulder, Colorado

IMPORTANT NOTICE



This material will appear shortly as NBS Technical Note 671.

Contents

List of Figures

# UPPER BOUND ERRORS IN FAR-FIELD ANTENNA PARAMETERS DETERMINED FROM PLANAR NEAR-FIELD MEASUREMENTS PART 2: ANALYSIS AND COMPUTER SIMULATION


## Abstract

In recent years, planar near-field antenna measurements have been developed and used in a number of applications. One of the primary concerns with this, or any, measurement approach is the accuracy of the results; that is, how do errors in measured near-field quantities affect the accuracies of far-field parameters such as gain, sidelobe levels, monopulse difference level, beam width, etc. Some efforts have been made in the past to estimate these errors, but the results have been limited in generality and primarily of a qualitative nature.

A two-fold approach is used in this study to obtain equations giving reasonable upper-bound errors resulting from systematic errors in the near-field measurements. The strategy has been to derive error expressions from the equations relating near and far-field quantities and also to computer simulate errors using actual measured near-field data. The simulation has both given some direction to, and confirmed the results of the analysis. The errors which have been investigated are: x, y, and z-position errors of the probe, amplitude and phase uncertainties of the measured data, and multiple reflections between the probe and test antenna. The results not only give the effects of errors in a given quantity, but also specify the form of the error (i.e., linear, quadratic, periodic, etc.) which will produce the largest effect in the far-field parameters. This information is very valuable in designing the measuring equipment so that these types of errors can be avoided, or minimized.


## 1.0 Introduction

During the last few years, a large amount of work has gone into the development of a Planar Near-Field (PNF) antenna measurement technique. A detailed and rigorous theory was formulated by Kerns and Dayhoff [1] and further developed by Kerns [2-4] which has served as the basis for all of this work. There have been advances in electronic measuring equipment and digital computers which have made the measurements possible and practicable. Experimental work has developed the measurement techniques to successfully apply this approach to a number of antennas over a broad frequency range. There have been indications in most of this experimental work that high accuracy results were possible, but we have lacked a thorough error analysis to confidently estimate the magnitude of errors in the results of PNF measurements. Efforts have been made to demonstrate the accuracy of these measurements by comparing them with

conventional far-field measurements, but this approach could not determine the size or the source of errors in the results of near-field measurements. At best, it demonstrated that the results were compatible with conventional measurements and thereby increased confidence in the newer measurement, but the errors inherent in far-field range measurements prevent it from being used as an accuracy standard.

The best approach to prove measurement accuracy is to thoroughly analyze the sources of error in the measurements and determine how they affect the calculated far-field quantities, and that is the purpose of this study.

This study is one of three error analyses which have appeared recently and together they provide a rather complete treatment. Rodrique et al. [5] used computer simulation on a hypothetical near-field distribution to derive tables and curves to show the effects of certain near-field errors. Their work identified certain error sources as primary or major contributors, and found that others had little effect on their model. Due to the specific model and error types studied, however, it was difficult to generalize the results to other antenna types or know if the error curves were upper bounds or not. Recently Yaghjian [6] has done an extensive analysis using the geometrical theory of diffraction and asymptotic evaluation of integral equations to arrive at upper bound error equations. He treated the effects of using a finite scan area which is not considered in either this or the earlier work by Rodrique, as well as treating position and instrumentation errors.

The unique results in this report are due to a different analytical approach coupled with an error simulation on actual measured near-field data. By using a Fourier transform analysis three main new results were obtained.

1. The error analysis was extended to steerable beam antennas for all sources of error.
2. The functional forms of the worst case error functions were determined. This will be especially valuable in designing future measurement systems.
3. The results of the analysis were confirmed and guided by the companion computer simulation.

Section 2, which follows, contains some background material necessary for the analysis and includes a brief outline of the theoretical formulation and notation, and some results from previous measurement studies. In section 3, general equations are derived to give the errors in far-field parameters resulting from errors in the measured near-field data. These equations are then applied to a sample antenna in section 4. The final section contains a summary of the conclusions resulting from this study and some suggestions for areas where additional work needs to be done.

## 2.0 Background Material on Planar Near-Field Antenna Measurements

### 2.1 Notation and Theory

The rigorous theoretical foundation of the PNF measurements is one of the key reasons for the success and general applicability of this technique. The theory is very general and rigorous, does not have built in approximations which might limit its accuracy or applicability, and the major numerical calculations can be accomplished with highly efficient computer algorithms. Specifically, neither the antenna under test nor the probe antenna need possess special polarization, symmetry, or field separability properties, and the transformation from near to far-field domains does not involve small angle approximations. The theory includes the directive effects of the measuring probe and therefore provides a means of correcting the final results for the probe receiving pattern. Neither is it necessary to assume that the probe measures a single component of the electric field at a point. Because of the above factors the results are more accurate than previous attempts at near-field measurements.

The scope of this report does not allow a complete discussion or development of the theory. Such treatments are available elsewhere [1-8] and may be referred to for more detailed study. We will list here the definition of important quantities and the key equations which are taken from the above references. Further discussion of some relationships will occur elsewhere in the report.

$\underline{k}$ = Propagation vector for plane waves.

$k_x, k_y, k_z$ = Rectangular components of $\underline{k}$.

$\underline{K} = k_x \underline{e}_x + k_y \underline{e}_y$ = Transverse part of $\underline{k}$.

$\gamma = \sqrt{k^2 - K^2}, = \pm k_z$.

$e^{-i\omega t}$ = assumed time dependence.

$\lambda$ = wavelength of operating frequency.

$f$ = operating frequency.

$\underline{s}_{10}(\underline{K})$ = Complete vector transmitting characteristic for the test antenna.

$\underline{s}_{01}(\underline{K})$ = Complete vector receiving characteristic for the test antenna.

$\underline{r}_{10}(\underline{K})$ and $\underline{r}_{01}(\underline{K})$ = Similar transmitting and receiving characteristics for the probe antenna.

$\underline{P} = x\underline{e}_x + y\underline{e}_y$ = transverse position vector for the probe.

$a_o$ = Incident wave amplitude at the input terminal of the test antenna.

$b_o$ = Emergent wave amplitude at the input terminal of the test antenna.

$b_o'(\underline{P})$ = Output wave amplitude at the output terminal of the probe antenna.

$\underline{E}$ = Electric field.

$\delta_x, \delta_y$ = Data point spacings in x and y-direction.

$L_x, L_y$ = Antenna dimensions in x and y-directions.

$S_x, S_y$ = Scan lengths in x and y directions.

$\Gamma_g, \Gamma_\ell, \Gamma_s, \Gamma_r$ = Complex reflection coefficients for generator terminal (input to test antenna) load terminal, test antenna and probe antenna respectively.

$Y_o$ = Characteristic admittance of free space = $\sqrt{\varepsilon_o/\mu_o}$.

$\eta_o$ = Characteristic admittance of the waveguide port connected to the antennas.

$G(K)$ = Power gain function.

$\sigma(\underline{K})$ = Receiving cross section function.

$\rho_\ell(\underline{K})$ = Complex ratio of linear polarization.

$R(\underline{K})$ = Right circular component of the transmitting spectrum.

$L(\underline{K})$ = Left circular component of the transmitting spectrum.

$A(\underline{K})$ = Axial ratio in the direction specified by $\underline{K}$.

$\tau(\underline{K})$ = Tilt angle in the direction specified by $\underline{K}$.

It should be noted that the complete vector quantities $\underline{s}_{10}(\underline{K})$ and $\underline{s}_{01}(\underline{K})$ will be used in this report, and most of the previous formulation has been given in terms of the transverse vectors $\underline{S}_{10}(\underline{K})$ and $\underline{S}_{01}(\underline{K})$. Either form may be chosen to fit the application if the correct relations are applied. In the present case it appeared more efficient to use the complete vectors.

Assume now that we have an antenna whose characteristics are to be determined. Let us define a coordinate system fixed to the antenna such that x-y plane is approximately normal to the electrical boresight direction of the antenna, and the origin is at the center of the antenna. These coordinates could be defined by fiducial marks placed on the antenna structure, and the results of the measurements will be defined with respect to this system. The antenna with its coordinate system is shown schematically in figure 1 where the rectangular and spherical unit vectors are also defined. Let the probe antenna be placed in a receiving position on a mechanical planar scanning structure and the test antenna aligned so that its x-y plane is parallel to the scan plane of the mechanical scanner.

The probe is aligned so that its own coordinate system is rotated 180° about the y-axis of the test antenna. The relative orientation of the antennas and their coordinate systems is shown schematically in figure 2, along with other important terminal planes and defined quantities.

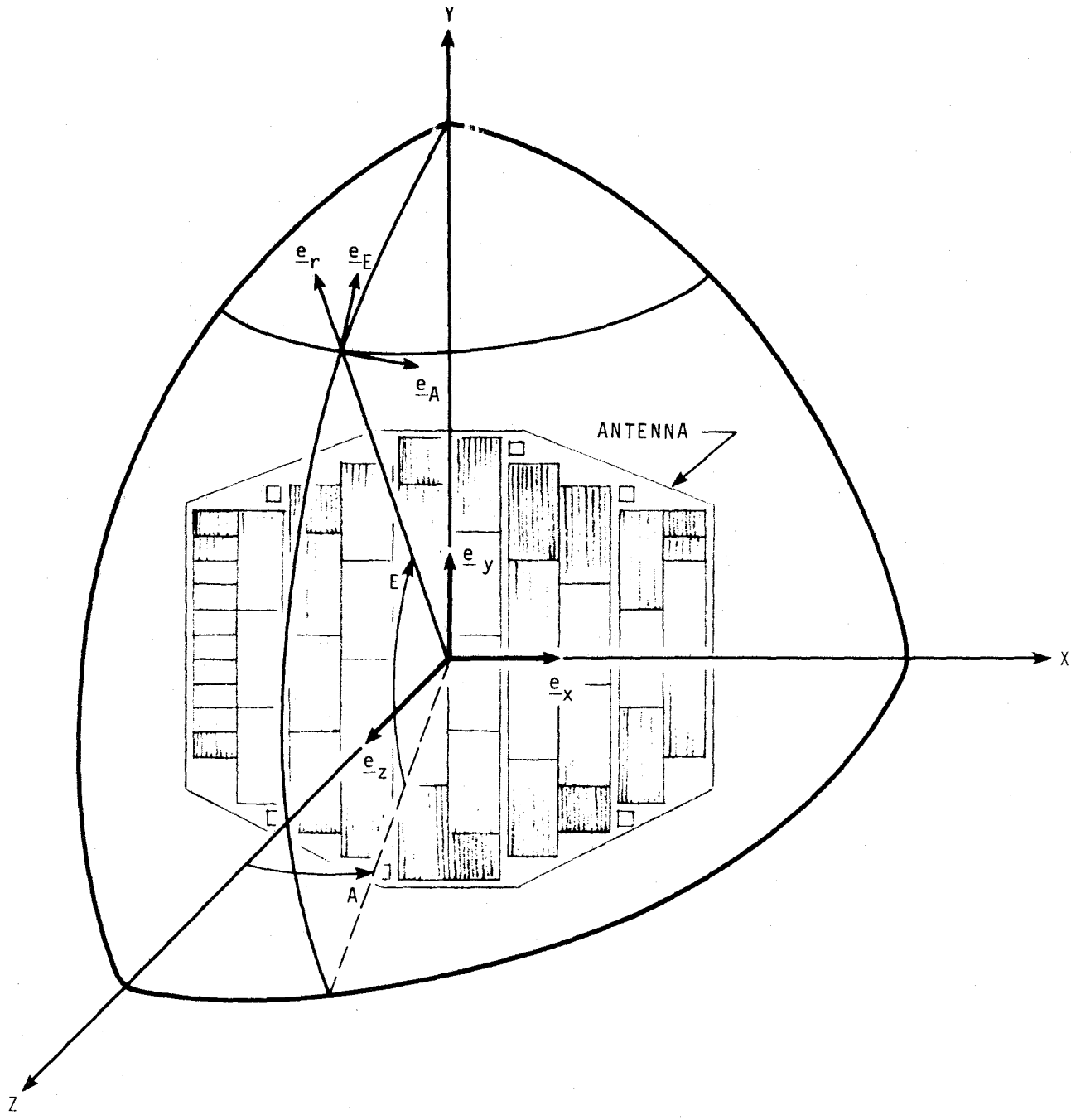


Figure 1. Antenna Coordinate System.

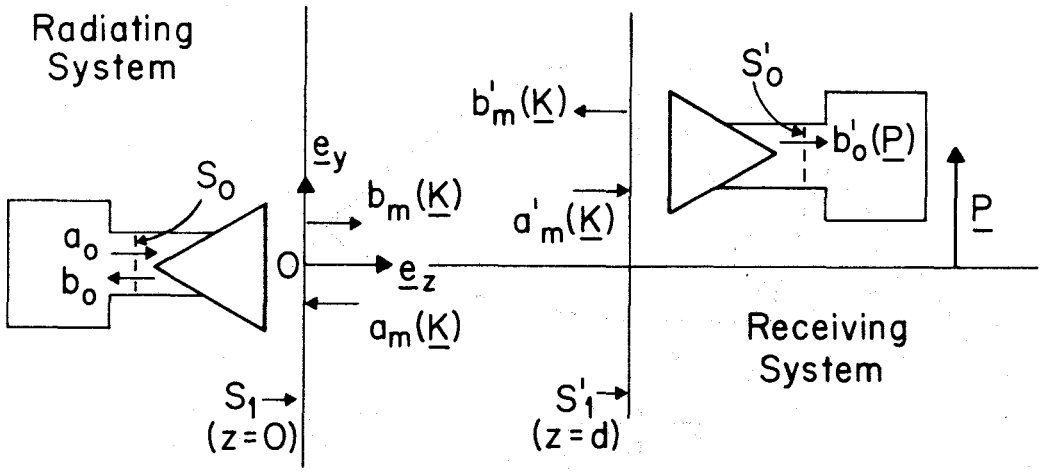


Figure 2. Test Antenna and Probe Schematic.

Let the probe be moved in the plane z=d by a transverse displacement $\underline{P} = x\underline{e}_x + y\underline{e}_y$ and denote the complex probe output amplitude by $b'_o(\underline{P})$. If we now assume that multiple reflections between the antennas are small enough to neglect, the transmission equation is given by

$$b'_o(\underline{P}) = \frac{a_o}{(1-\Gamma_\ell\Gamma_r)} \int \left[\underline{r}'_{01}(\underline{K}) \cdot \underline{s}_{10}(\underline{K})\ e^{i\gamma d}\right] e^{i\underline{K}\cdot\underline{P}}\, d\underline{K} \qquad (1)$$

where $d\underline{K} \equiv dk_x\, dk_y$, and where integration is over all significant values of the integral. The prime on the probe receiving characteristic represents the change in description of $\underline{r}_{01}(\underline{K})$ when the probe is placed in the receiving position. $\underline{r}_{01}(\underline{K})$ is the description of the probe from its coordinate system, while $\underline{r}'_{01}(\underline{K})$ describes the probe response from the test antenna coordinate system.

It should be noted that $b'_o(\underline{P})$ is the actual observed quantity, essentially the complex voltage observed at the output terminals of the probe. To solve for the transmitting characteristics of the test antenna in terms of this observed data, we note that eq. (1) is a Fourier integral transform, and therefore

$$D'(\underline{K}) = \frac{e^{-i\gamma d}(1-\Gamma_\ell\Gamma_r)}{4\pi^2\, a_o} \int b'_o(\underline{P})\ e^{-i\underline{K}\cdot\underline{P}}\, d\underline{P} \qquad (2)$$

where

$$D'(\underline{K}) = \underline{r}'_{01}(\underline{K}) \cdot \underline{s}_{10}(\underline{K}). \qquad (3)$$

Equation (3) gives one equation for the two spherical components of $\underline{s}_{10}(\underline{K})$ in terms of the Fourier transform of the measured data, $D'(\underline{K})$, and the probe receiving pattern $\underline{r}'_{01}(\underline{K})$. To obtain the required second equation, the measurement is repeated with a second "independent" probe. If the probe is not circularly polarized, the second probe can be obtained in effect by rotating the probe about its z-axis by 90°. The second equation in any case is

$$D''(\underline{K}) = \underline{r}''_{01}(\underline{K}) \cdot \underline{s}_{10}(\underline{K}), \tag{4}$$

where

$$D''(\underline{K}) = \frac{e^{-i\gamma d}(1-\Gamma_\ell \Gamma_r)}{4\pi^2 a_o} \int b''_o(\underline{P})\, e^{-i\underline{K}\cdot\underline{P}}\, d\underline{P} \tag{5}$$

and $b''_o(\underline{P})$ and $\underline{r}''_{01}(\underline{K})$ are respectively the received signal and probe receiving characteristic for the second orientation.

To obtain the components of $\underline{s}_{10}(\underline{K})$, the simultaneous equations implied in eqs. (3) and (4) are solved. For instance, if we desire the spherical (Azimuthal = A, Elevation = E) components of $\underline{s}_{10}(\underline{K})$ as defined in figure 1, and therefore have previously measured the spherical components for the probe, eqs. (3) and (4) give

$$s_{10A}(\underline{K}) = [D'(\underline{K}) r''_{01E}(\underline{K}) - D''(\underline{K}) r'_{01E}(\underline{K})]/\Delta \tag{6}$$

$$s_{10E}(\underline{K}) = [D''(\underline{K}) r'_{01A}(\underline{K}) - D'(\underline{K}) r''_{01A}(\underline{K})]/\Delta \tag{7}$$

where

$$\Delta = r'_{01A}(\underline{K})\, r''_{01E}(\underline{K}) - r''_{01A}(\underline{K})\, r'_{01E}(\underline{K}). \tag{8}$$

Once the components of $\underline{s}_{10}(\underline{K})$ are obtained, other quantities are easily derived. For instance if the antenna is reciprocal, then its receiving characteristic is given by

$$\underline{s}_{01}(\underline{K}) = \frac{Y_o\, \gamma}{\eta_o\, k}\, \underline{s}_{10}(-\underline{K}) \tag{9}$$

In the direction specified by the unit vector $\frac{\underline{k}}{|\underline{k}|}$, and at a large distance d from the antenna, the electric field is given by

$$\underline{E}(d) = \frac{-i\gamma\, \underline{s}_{10}(\underline{K})\, a_o\, e^{ikd}}{d}, \tag{10}$$

where $\underline{d} = d\, \frac{\underline{k}}{|\underline{k}|}$.

The gain function $G(\underline{K})$ and the receiving cross section functions $\sigma(\underline{K})$ are given in terms of $\underline{s}_{10}(\underline{K})$ and $\underline{s}_{01}(\underline{K})$ by

$$G(\underline{K}) = \frac{4\pi Y_o \gamma^2}{(1-|\Gamma_s|^2)\eta_o} |\underline{s}_{10}(\underline{K})|^2, \quad \text{and} \tag{11}$$

$$\sigma(\underline{K}) = \frac{4\pi^2 \eta_o}{(1-|\Gamma_s|^2)Y_o} |\underline{s}_{01}(\underline{K})|^2. \tag{12}$$

The linear polarization ratio is the ratio of the two components of $\underline{s}_{10}(\underline{K})$

$$\rho_\ell(\underline{K}) = \frac{s_{10A}(\underline{K})}{s_{10E}(\underline{K})}, \tag{13}$$

while the two circular components are given by

$$R(\underline{K}) = \frac{s_{10A}(\underline{K}) - i\, s_{10E}(\underline{K})}{\sqrt{2}}, \text{ and} \tag{14}$$

$$L(\underline{K}) = \frac{s_{10A}(\underline{K}) + i\, s_{10E}(\underline{K})}{\sqrt{2}}. \tag{15}$$

From these complex polarization quantities the axial ratio and tilt angle are obtained from the relations

$$A(\underline{K}) = \frac{|R(\underline{K})| + |L(\underline{K})|}{|R(\underline{K})| - |L(\underline{K})|} \tag{16}$$

$$\tau(\underline{K}) = 1/2 \arg\left[\frac{R(\underline{K})}{L(\underline{K})}\right]. \tag{17}$$

Therefore the usual far-field antenna parameters are all easily obtained once $\underline{s}_{10}(\underline{K})$ has been determined from the near-field measurements. Although the discussion here has been in terms of a measurement arrangement where the test antenna is used in the transmitting mode, the opposite configuration may also be used. The test antenna can be used in the receive mode, $\underline{s}_{01}(\underline{K})$ determined, and receiving cross section and receiving polarization determined. If the antenna is reciprocal, eq. (9) may be used to obtain the transmitting parameters.

In summary then the steps in the planar near-field measurement technique are:

1. Define the coordinate axes of the reference measurement system, the test antenna, and the probe.
2. Measure or calculate from theory the probe receiving characteristic for all values of $\underline{K}$ for which the test antenna characteristics are to be determined.

3. Place the test antenna and probe in the measurement system in the prescribed orientation and verify that multiple reflections are small enough to neglect.
4. Measure $b_o'(\underline{P})$ and $b_o''(\underline{P})$ over a sufficient area and at adequate spacing in x and y.
5. Evaluate the integrals in eqs. (2) and (5) and solve eqs. (6) and (7) for the two spherical components of $\underline{s}_{10}(\underline{K})$ or $\underline{s}_{01}(\underline{K})$.
6. Compute power gain, transverse components, polarization ratios or other desired quantities, or use $\underline{s}_{10}(\underline{K})$ to obtain the field in any other transverse plane to evaluate antenna performance.

## 2.2 Examples of Previous Results Using PNF Techniques

The experience gained from previous measurements and from NBS studies were used extensively in this investigation. They cover a broad range of frequencies and antenna types and have been indispensible in arriving at meaningful conclusions. Table 1 summarizes some of the antennas which have been measured at the National Bureau of Standards using PNF techniques which relate to the present study.

In most of these past measurements it has been possible to compare the results from near-field measurements with conventional far-field measurements, and therefore to demonstrate the general feasibility of this approach.

Table 1. Antenna Measurements Considered in Study.

| Antenna Type | Frequency (GHz) | Major Dimension in Wavelengths | Gain (dB) |
|---|---|---|---|
| Horn Lens | 48.0 | 90 | 47.0 |
| Conical Horn (JPL) | 8.4 | 6 | 22.08 |
| Cassegrain Reflector | 60.0 | 91 | 46.5 |
| Lens Array (Constrained Lens) | 9.2 | 23 | 30.0 |
| Corporate Fed Array (Volphase) | 8.4 | 17 | 21.5 |
| Dipole Array | 1.4 | 5 | 20.3 |

In the case of the JPL conical horn, both pattern and gain comparisons were made. The far-field measurements were performed by JPL [10] and NBS performed both near-field and extrapolation [9] measurements. The ohmic loss in the antenna was also determined from the near-field data by integrating the computed pattern to obtain transmitted power, and the loss was obtained from the ratio of transmitted to input powers. This result was compared with a loss calculation performed by JPL. The results of these comparisons along with a similar comparison for the mm-wave antenna are summarized in Table 2. They illustrate that for both medium and high gain antennas, PNF techniques are capable of high accuracy. More will be said about this in a later section.

Table 2. Summary of Comparisons

| | Measurement Technique | | |
|---|---|---|---|
| Antenna | Far-Field | Extrapolation | Near-Field |
| JPL Horn (Gain) | 22.03 dB | 22.08 dB | 22.05 dB |
| JPL Horn (loss) | 0.021 dB | | 0.039 dB |
| Cassegrain Reflector | | 46.30 dB | 46.42 dB |

Pattern Comparisons

Far-Field Measurements vs.
Computed From Near-Field Data

1 -- JPL Horn
2 -- Cassegrain Reflector
3 -- Lens Array (Constrained Lens)
4 -- Corporate Fed Array (Volphase)

Far field pattern comparisons have yielded similar results. Figures 3-7 are samples of some of these comparisons for three different antennas. Over most of the patterns the agreement is very good and most differences are well within the errors to be expected in either measurement. The largest differences, as in figure 3 for off axis angles greater than 45°, and in figure 7 for angles greater than +35° are due to insufficient scan area in the near-field data. In both of these measurements a small portable scanner was being used which limited the size of the scan area and therefore reduced the reliable angular region. This effect will be discussed further in succeeding sections.

The sum total of all our work in PNF measurements confirms that high accuracy results are obtainable. Since the theory is rigorous, the basic formulation does not set a limit on the attainable accuracy. The errors which do result in computed far-field parameters are primarily due

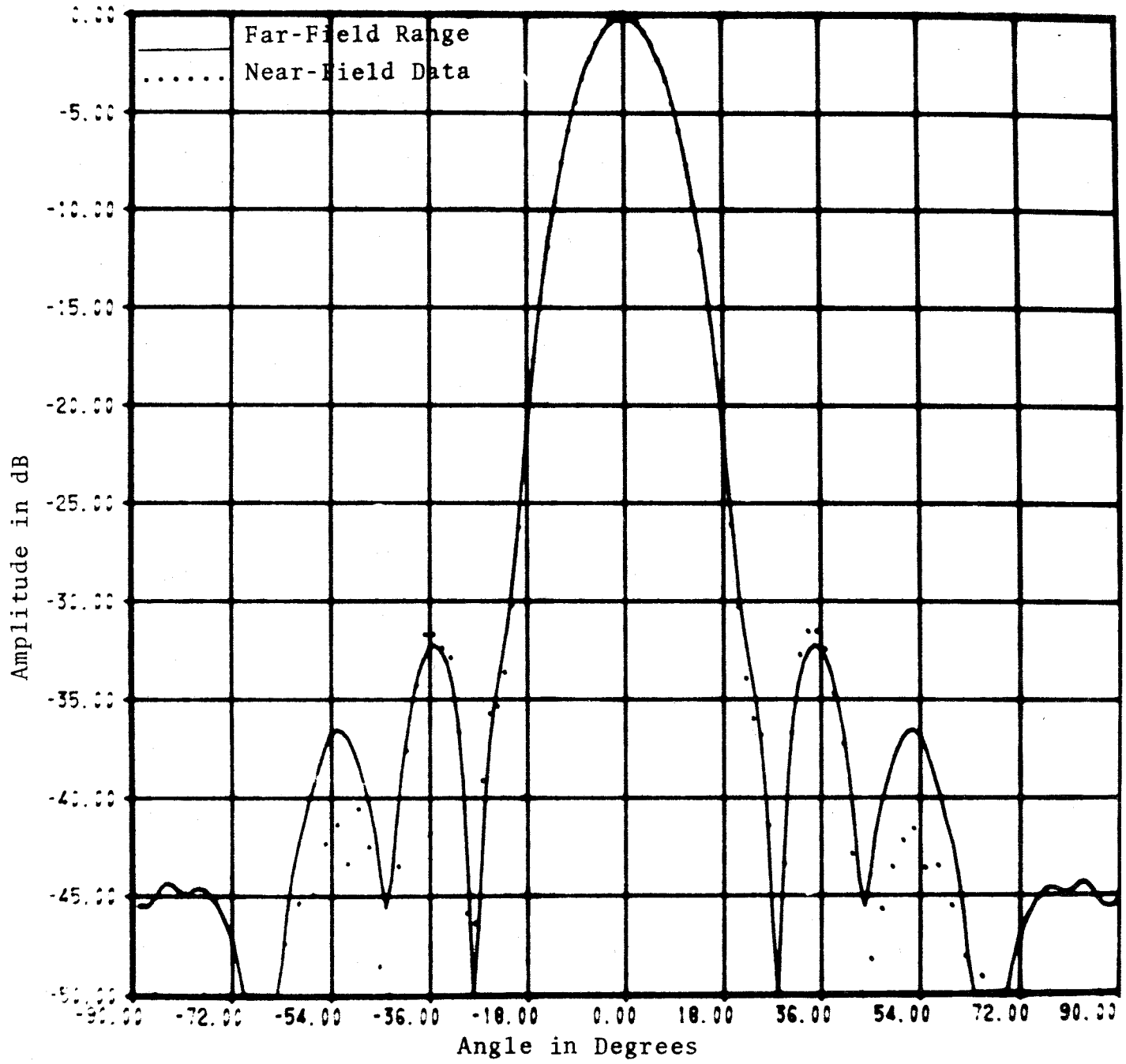


Figure 3. Pattern Comparison for JPL Horn.

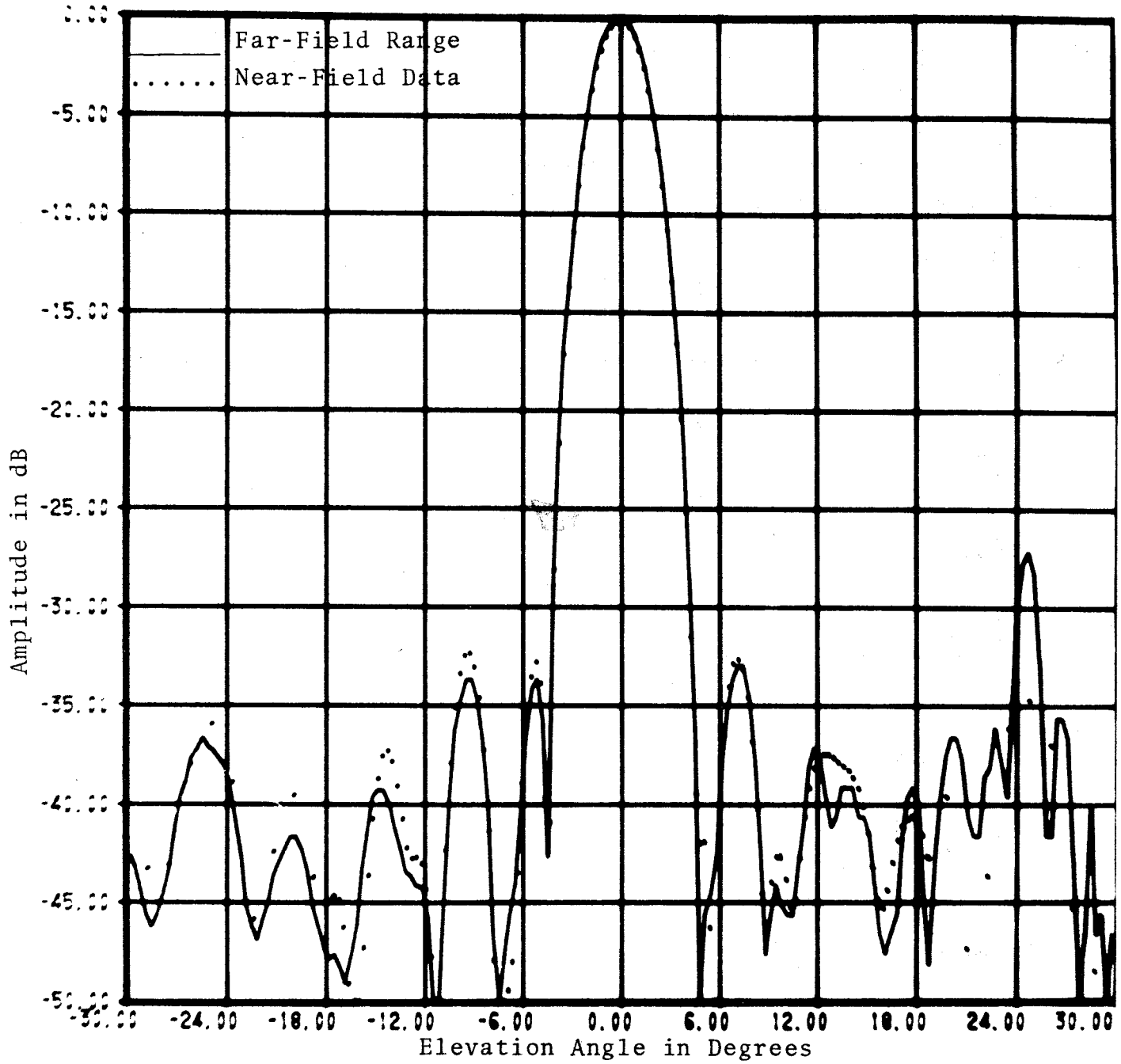


Figure 4. Pattern Comparison for Lens Array Sum Pattern.

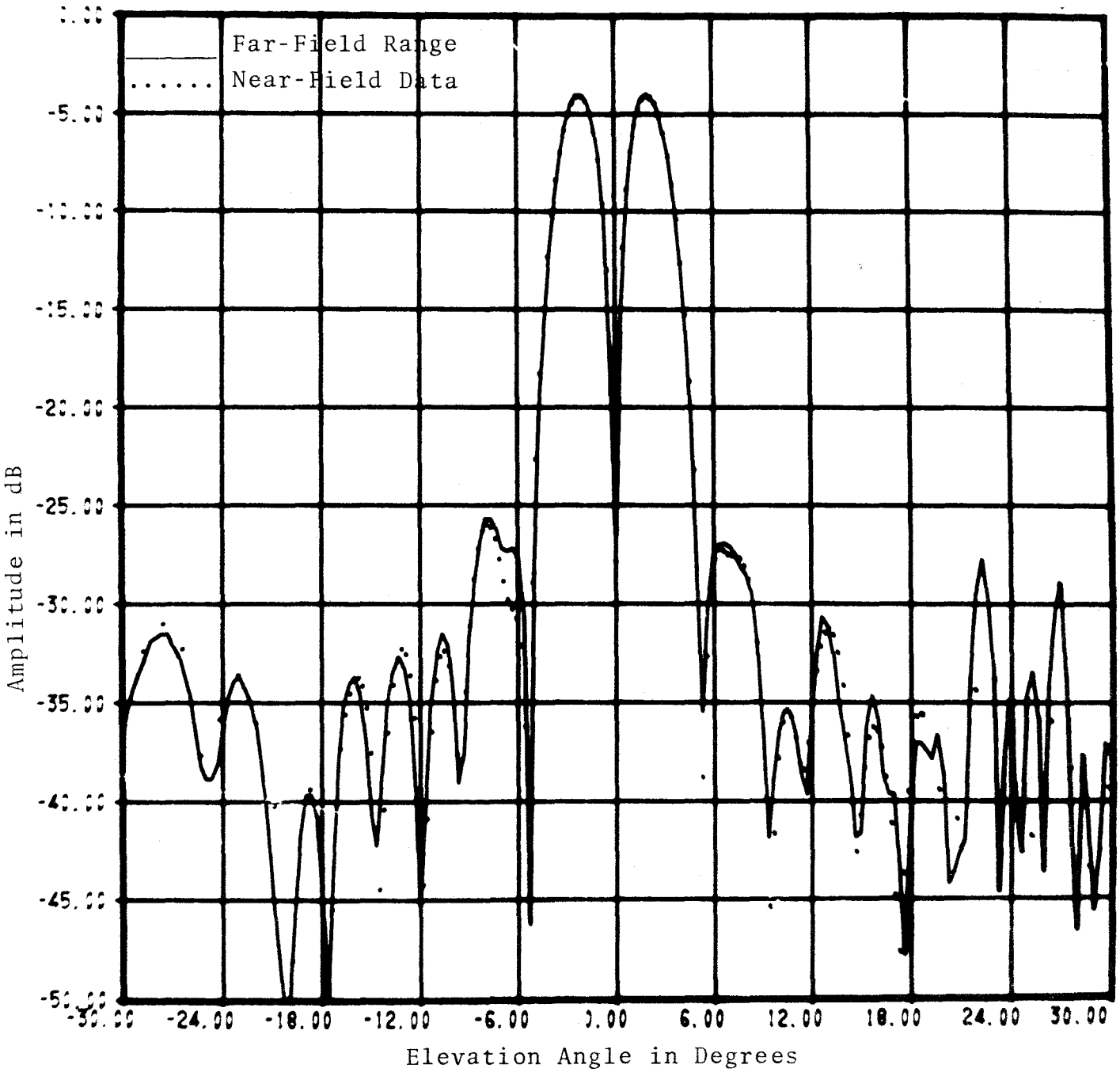


Figure 5. Pattern Comparison for Lens Array Difference Pattern.

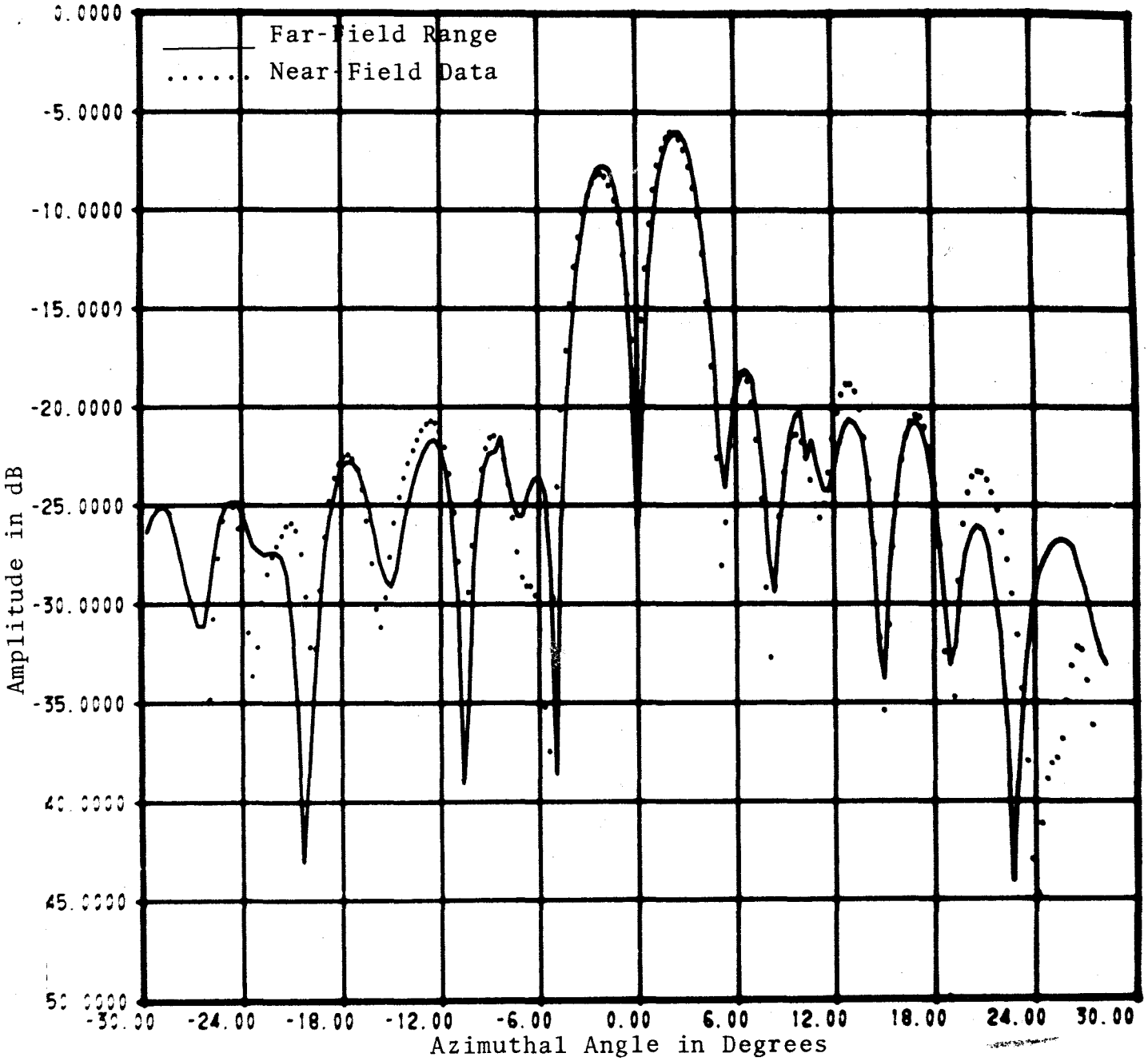


Figure 6. Pattern Comparison for Corporate Fed Array 0° Beam.

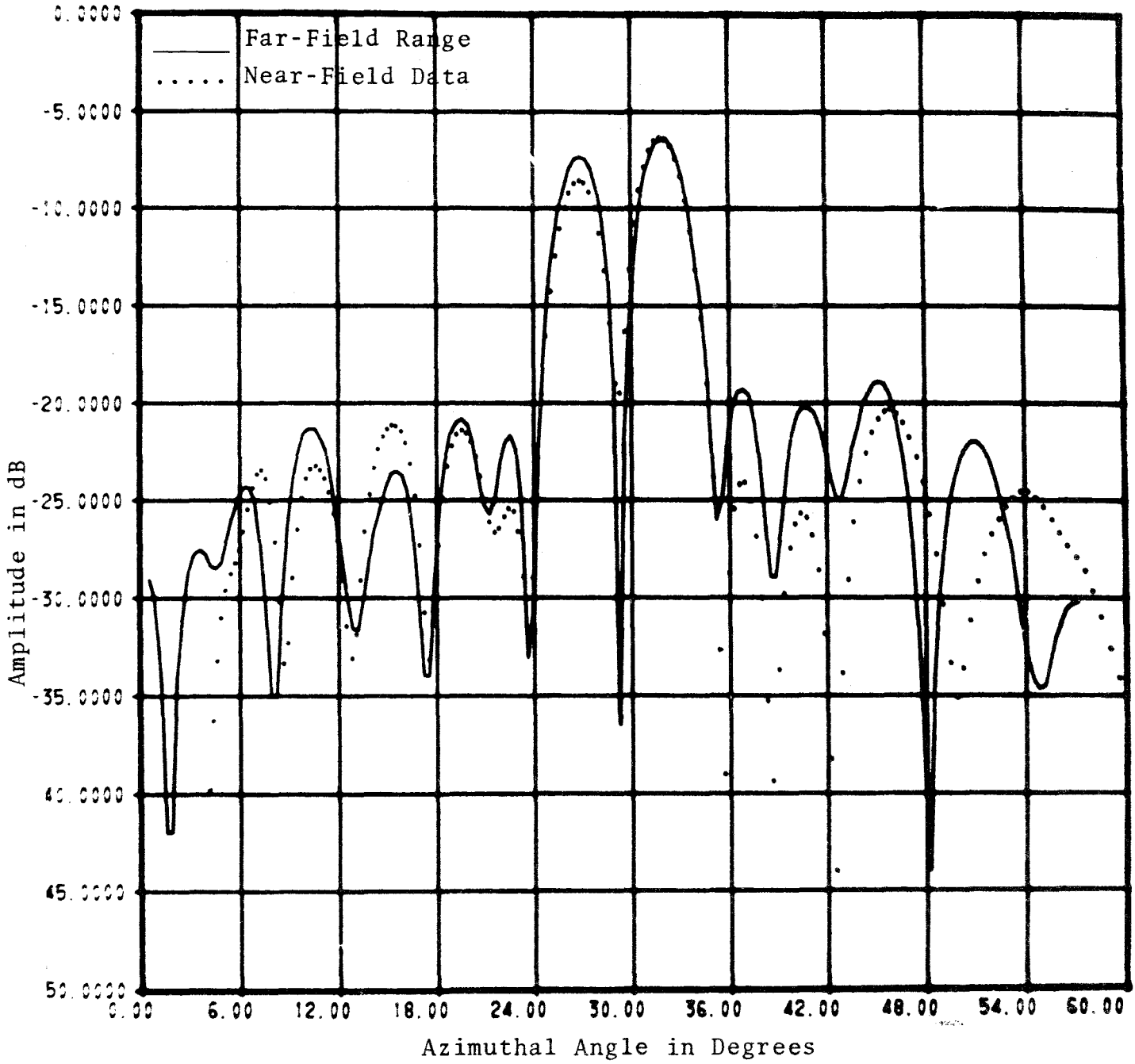


Figure 7. Pattern Comparison for Corporate Fed Array 30° Beam.

to the errors in the measured near-field data. The effects of some errors have been studied in the past and guidelines have been established to specify the parameters of the measurement system in order to achieve a given level of accuracy. These guidelines will be reviewed in the following section. A more complete analysis of the effects of measurement errors was developed for this study and appears in section 3.1.

## 2.3 Measurement Guidelines

One of the first questions to be answered relates to the scan parameters. That is, what is the size of the scan area, what data point spacings are required, and what separation distance between test antenna and probe is optimum?

Previous work has shown [11] that for a directive antenna, the size of the scan area and the separation distance between the probe and test antenna determine the maximum off-axis angle to which accurate far-field patterns can be calculated. If the dimension of the antenna in the x-direction is $L_x$, the scan length in the x-direction $S_x$, and the separation distance d, then the reliable pattern region will be bounded by

$$|\theta_x| \leq \tan^{-1}\left(\frac{S_x - L_x}{2d}\right) \tag{18}$$

where $\theta_x$ is the off axis angle in the $k_x$ direction. A similar relation will define the reliable region in the $k_y$ direction.

The data point spacings are determined by a two-dimensional form of the sampling theorem. This theorem states that if $b_o'(\underline{P})$ is the Fourier transform of a band limited function of $\underline{K}$ with band limits

$$|k_1| = \frac{\pi}{\delta_x}, \quad |k_2| = \frac{\pi}{\delta_y} \tag{19}$$

then the minimum required spacings are $\delta_x$ and $\delta_y$. Furthermore, the integrals in eqs. (2) and (5) can be replaced by summations without approximation for such band limited data. The function which must be band limited is the quantity within the brackets of eq. (1) and the band limiting can be due to the directivity of the test antenna and/or probe (from the product $\underline{r}_{01}'(\underline{K}) \cdot \underline{s}_{10}(\underline{K})$) or arise from the factor $e^{i\gamma d}$. The latter term produces very sharp attenuation in the evanescent mode region where $K^2 > k^2$ and $\gamma$ is therefore imaginary. In this region the band limits are

$$k_1 \geq k = \frac{2\pi}{\lambda}, \quad k_2 \geq k = \frac{2\pi}{\lambda}$$

which result in data point spacings of

$$\delta_x \leq \lambda/2, \qquad \delta_y \leq \lambda/2.$$

Our experience has shown that for directive antennas, even when steered away from the z-direction, $\delta_x$ and $\delta_y$ need be only a few percent smaller than $\lambda/2$, and for directive antennas whose main beam is in the z-direction, the data point spacings can be larger than $\lambda/2$. In the latter case, spacings of $0.8\lambda$ to $\lambda$ are not uncommon.

It is assumed in the theoretical development that multiple reflections between the two antennas or due to other sources of reflection are small enough to neglect. Absorbing material is used behind and on metal surfaces of the scanner as shown in figure 9 to reduce extraneous reflections. Scattering from the probe is minimized by using a small probe (one whose area is about 1/100 of the test antenna) and tapering its edges at the probe aperture. The magnitude of the multiple reflections can be reduced by increasing the separation distance, but this improvement must be weighed against the resulting increase in required scan area.

The actual level of multipath and its effect on computed results must be checked for each measurement. Fast and simple tests have been developed [11] for accomplishing this, and consist of measuring partial data on planes separated by $\lambda/8$. Gain and pattern variations resulting from data in the different planes are an approximate measure of errors due to multipath. In all of our measurements on directive antennas where the probe was much smaller than the antenna, multiple reflections have not been a major source of error.

In addition to its scattering characteristics, the gain, pattern, and polarization of the probe should be considered in choosing one for a particular measurement. The probe should be large enough so that its gain is not more than 30 dB below that of the test antenna. This will improve the gain measurement by reducing the insertion loss between probe and test antenna. (This will be discussed further in section 3.1.5 on gain accuracy.) Where pattern information is only required over a limited angular region, a larger probe can be used to filter out the wide angle information. This allows wider data point spacing and results in improved accuracy over the smaller angular region. When wide angle information is needed, the probe must have a broad beam to avoid attenuation of needed information. In any case, the probe pattern should not have nulls or minima below about -25 to -30 dB within the angular region of interest.

If the test antenna is nominally linearly polarized, then the logical choice for probe polarization is also linear. The data $(b_o'(\underline{P}))$ obtained with the probe polarization is essentially matched to the test antenna will contain the primary information for the principal polarization pattern of the test antenna. If the probe polarization is sufficiently linear over the angular region of interest, this single set of data may be sufficient

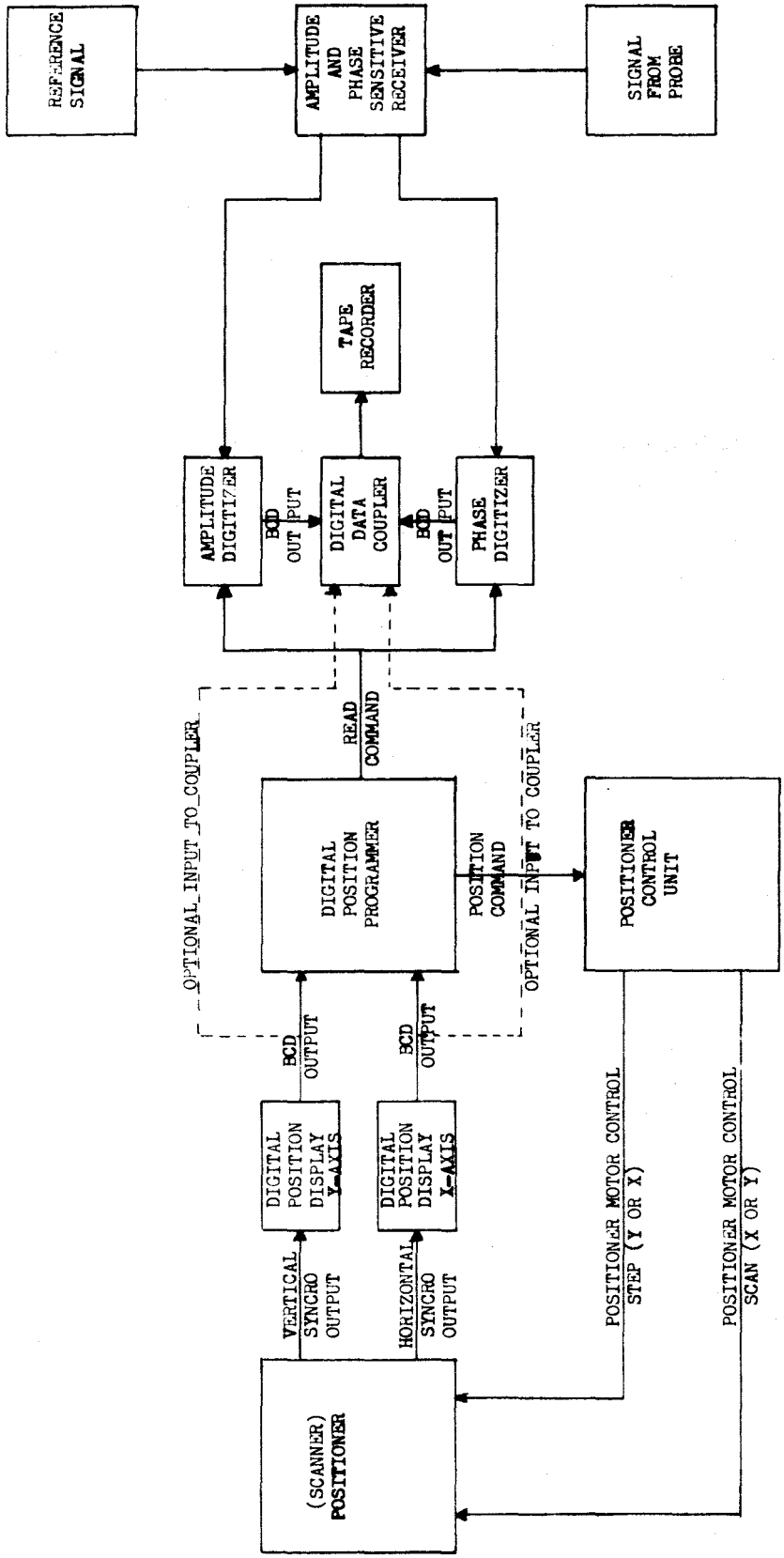


Figure 8. Block Diagram of Measurement System.

to determine principal polarization patterns. That is, if $r'_{01E}(\underline{K}) \simeq 0$ for all values of $\underline{K}$ within the region of interest, then eq. (6) reduces to

$$s_{10A}(\underline{K}) = \frac{D'(\underline{K})}{r'_{01A}(\underline{K})} \quad . \tag{20}$$

Furthermore, when the probe is almost linearly polarized, the "independent antenna" can be obtained by rotating the probe about its axis by 90°. Two different probes are therefore not required, and both $\underline{r}'_{01}(\underline{K})$ and $r''_{01}(\underline{K})$ can be derived from the same pattern, gain, and polarization measurements.

The linear probe may also be used in the same way when the test antenna is circularly polarized. But in this case both sets of data must be measured, and $b'_o(\underline{P})$ and $b''_o(\underline{P})$ will be of approximately equal magnitudes. The principal polarization component will essentially be determined from the sum of these two sets of data while the cross component will be obtained from their difference. This can produce a larger uncertainty in the cross component than when the probe is polarization matched to the test antenna. The other alternative in this case is to use two separate probes with nominal right and left hand circular polarizations. They should have good polarization purity over the angular region of interest, and this may be difficult to achieve. Measurements on circularly polarized antennas are one area where little work has been done and more needs to be done to optimize the measurement techniques.

The measurement hardware required to implement PNF measurement is illustrated in the block diagram of figure 8, and the photographs of the NBS system in figures 9 and 10. There are three basic subsystems which are shown in these figures: the RF source and receiver, the data recording system, and the x-y scanner with its associated automatic position controls. The accuracy requirements for each of these systems is examined in the following section.

## 3.0 Error Analysis

### 3.1 Introduction

In analyzing the effects of PNF measurement errors on calculated antenna parameters, we have attempted to make the following results as general and useful as possible. Ideally one would like to obtain a concise relationship giving a realistic upper bound or probable value for the effects of a given type of error. The relationship should apply to a large class of antennas without major modification. It is also very desirable that the error relations be given in terms of easily obtainable antenna parameters such as diameter, approximate gain, first sidelobe level, etc., rather than

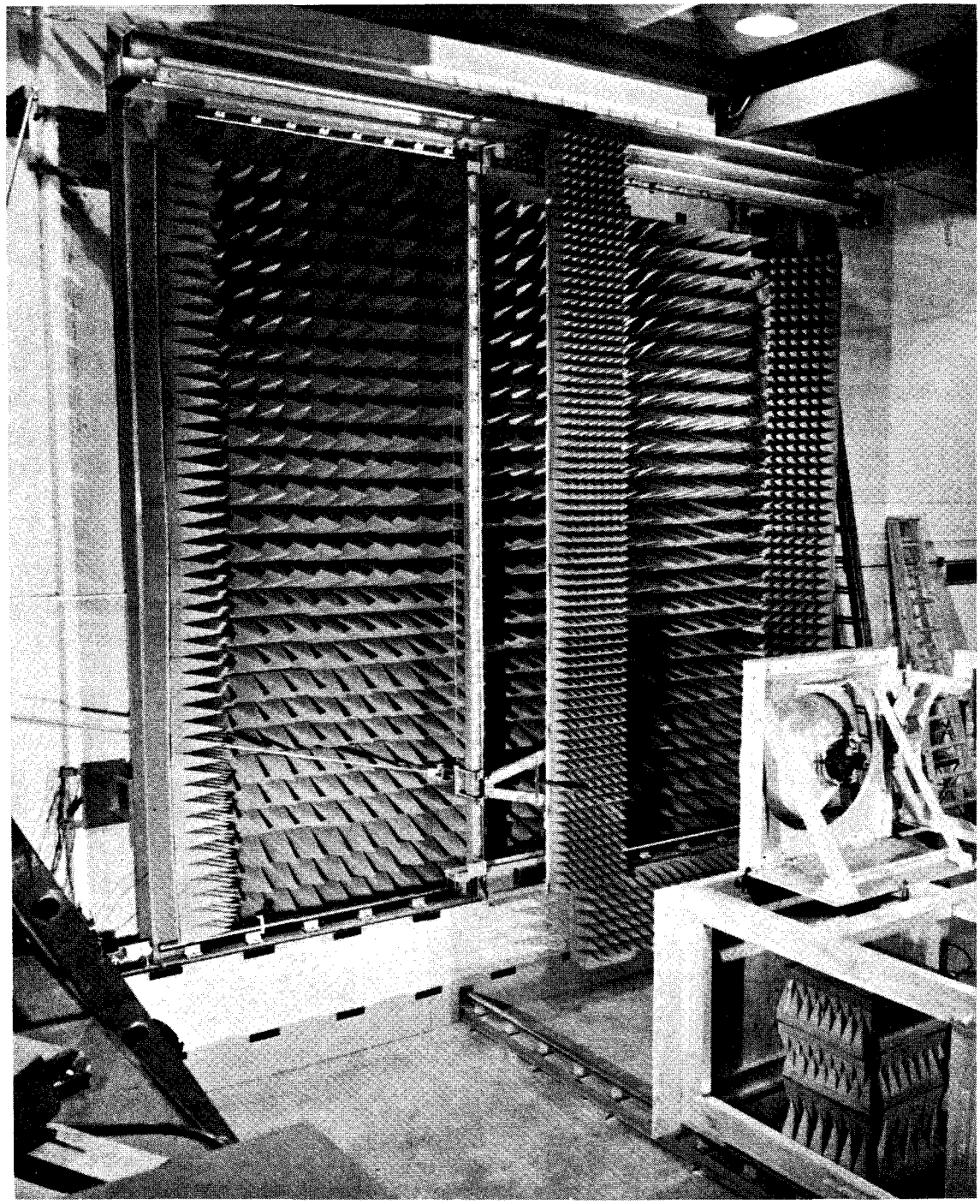

Figure 9. Planar near-field scanner at NBS.

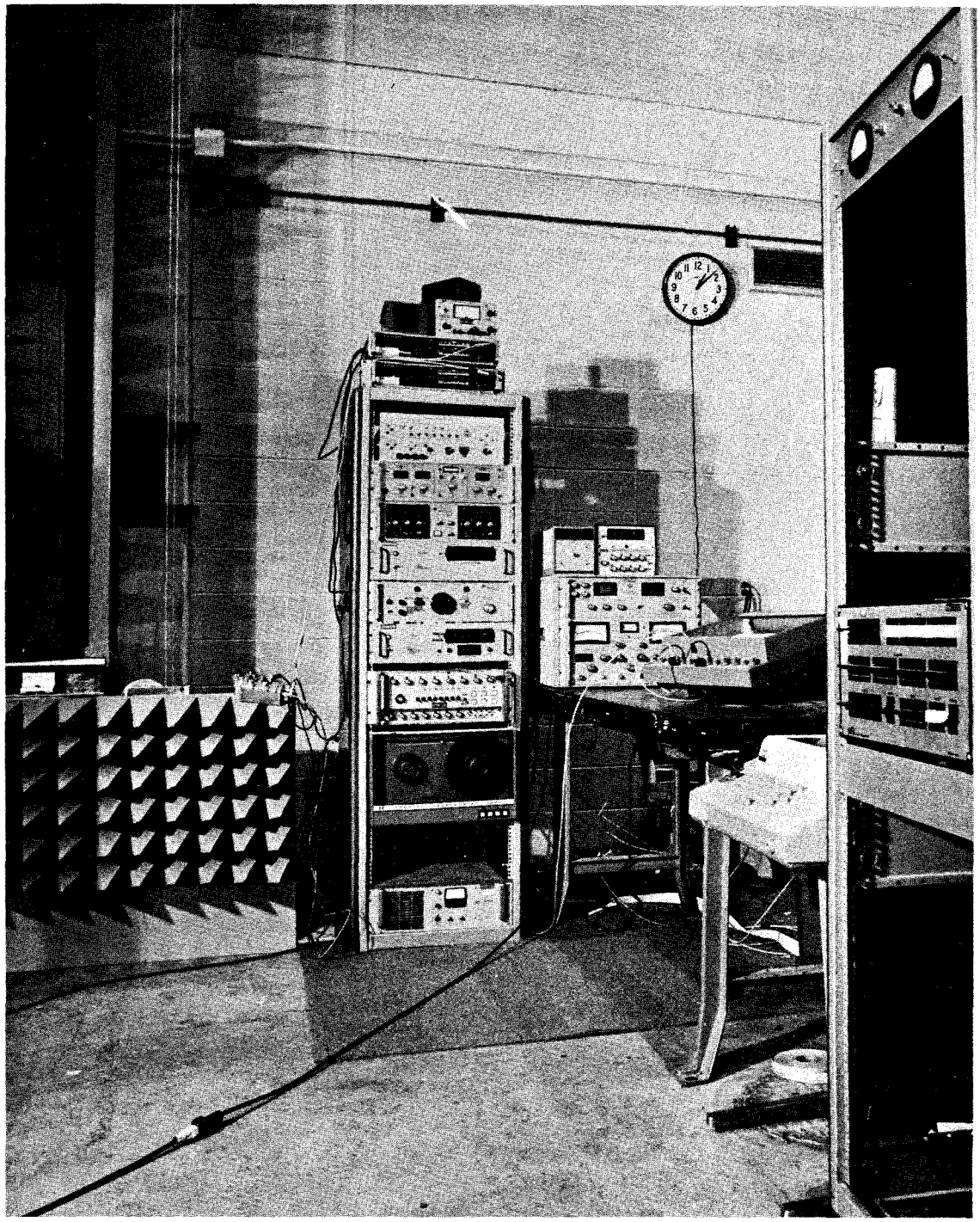

Figure 10. Electronic equipment associated with planar scanner.

requiring a detailed knowledge of the near-field pattern, and that the error analysis should define the form of near-field errors (i.e., linear, periodic, etc.) which have the largest effects.

Each of these objectives has been considered in the following analysis, and in most cases they have been achieved. The general approach will be to derive a general equation for the error in $D'(\underline{K})$ due to one type of error in the near-field data. The general equation will then be applied to specific cases such as a narrow beam antenna operating in the sum mode with the beam along the z-axis. Other cases will be considered to cover all modes of interest to this study. For each case we will determine an upper bound for the far-field error and the form of the near-field error which would produce this upper bound. In some cases the form of the resulting near-field error is not physically possible or reasonable, and so a smaller upper bound is determined consistent with a more realistic near-field error.

To illustrate the various errors, and as a guide in some of the analysis, some of the errors were simulated on a computer using actual measured near-field data. This simulation has proven very valuable in giving a graphic display of the effects of various errors, and to verify whether or not the upper bounds obtained in the analysis are realistic.

In all of the following analysis, we will determine the error in $D'(\underline{K})$ due to errors in the measured near-field data. While $D'(\underline{K})$ is generally not the desired end result in the calculations, it is usually simply related to the final results and is more closely related to the measured data. For example, if both the probe and test antenna are nearly linearly polarized in the vertical direction then $D'(\underline{K})$ will be primarily due to the coupling of principal (elevation) components. From eq. (7) and (10), the elevation component pattern of the far electric field along the E and H-planes are then respectively

$$\frac{E_E(0,k_y)}{E_E(0,0)} = \frac{D'(0,k_y)\ \cos(E)}{D'(0,0)\ r'_{01E}(0,k_y)} \tag{21a}$$

$$\frac{E_H(k_x,0)}{E_H(0,0)} = \frac{D'(k_x,0)\ \cos(A)}{D'(0,0)\ r'_{01E}(k_x,0)}\ . \tag{21b}$$

For the waveguide type probes, and for narrow beam test antennas over the region of interest

$$\frac{\cos(E)}{r'_{01E}(0,k_y)} \cong \frac{\cos(A)}{r'_{01E}(k_x,0)} \cong 1. \tag{22}$$

The pattern of $D'(\underline{K})$ is very nearly equal to the pattern of the far electric field, and errors in the two quantities will be essentially the same.

In the following analysis the prime or primes on $D(\underline{K})$ and $b(\underline{P})$ which were used to denote the two sets of data will be deleted, since the results will apply to either case. We will also use the normalized near-field data, $B(\underline{P})$, rather than $b_o'(\underline{P})$. The quantity $\frac{b_o'(\underline{P})}{a_o}$ in eq. (2) is actually obtained in a two step process. First relative near field data, $B(\underline{P})$, are measured which are normalized to $b_o'(\underline{P})$ at one arbitrary point in the measurement lattice, $\underline{P} = \underline{P}_o$, which is usually at or near the maximum amplitude.

$$B(\underline{P}) = \frac{b_o'(\underline{P})}{b_o'(\underline{P}_o)} \tag{23a}$$

When the relative measurements are completed, the probe is placed at $\underline{P}_o$ and an insertion loss measurement is used to determine the normalization factors

$$A_n' = \frac{a_o}{b_o'(\underline{P}_o)}, \quad A_n'' = \frac{a_o}{b_o''(\underline{P}_o)} . \tag{23b}$$

The magnitude of the $A_n$'s is essentially the ratio of the amplitude at the input to the test antenna to that at the output of the probe. With these modifications eq. (2) becomes

$$D(\underline{K}) = \frac{e^{-i\gamma d}}{4\pi^2 F A_n} \int B(\underline{P}) e^{-i\underline{K}\cdot\underline{P}} \, d\underline{P}, \tag{24}$$

where F is the mismatch factor $1/(1-\Gamma_\ell\Gamma_r)$. This form will be used in the following analysis.

### 3.1.1 Probe x-y Position Errors

We will first consider the effects of x-y position errors and much of the analysis here will also be useful in other sections. The position errors are one of the most important to consider in this study because the mechanical scanner and its feasibility are key considerations. The basis for this analysis is the two Fourier transform relations which relate $D(\underline{K})$ and $B(\underline{P})$.

$$B(\underline{P}) = FA_n \int D(\underline{K}) e^{i\gamma d} \, e^{i\underline{K}\cdot\underline{P}} \, d\underline{K} = FA\,\mathcal{F}^{-1}[D(\underline{K})e^{i\gamma d}] \tag{25a}$$

$$D(\underline{K}) = \frac{e^{-i\gamma d}}{4\pi^2 F A_n} \int B(\underline{P}) e^{-i\underline{K}\cdot\underline{P}} \, d\underline{P} = \frac{e^{-i\gamma d}}{FA}\mathcal{F}[B(\underline{P})] \tag{25b}$$

where the script $\mathcal{F}$ denotes the Fourier transform and its inverse $\mathcal{F}^{-1}$. Let us assume that due to an x-y position error, the data are measured at $\underline{P}'$

rather than at $\underline{P}$ where

$$\underline{P}' = \underline{P} + \underline{\Delta}(\underline{P}) = \underline{P} + \Delta x(\underline{P})\underline{e}_x + \Delta y(\underline{P})\underline{e}_y. \tag{26}$$

The effect of two special position errors can be formulated exactly using well known Fourier transform relations, and will be discussed first. If the position error is constant over the entire scan area, $\underline{\Delta}(\underline{P})$ = constant = $\underline{C}_1$, then the spectrum computed from this data is

$$D_e(\underline{K}) = e^{-i\underline{K}\cdot\underline{C}_1} D(\underline{K}). \tag{27}$$

In eq. (27) and the following analysis, $D(\underline{K})$ will denote the true spectrum which would be obtained if there were no errors in the measured data, and $D_e(\underline{K})$ will denote the calculated results which include the effects of the error under consideration and will be referred to as the error-contaminated spectrum.

We note from eq. (27) that the only effect of a constant position error is to uniformly alter the phase of the spectrum. In many cases the far-field phase is not of interest, and so a constant shift of the position of all the data points is acceptable. Two cases where it could cause a problem are where the two sets of near-field data are required to compute circular components or linear spherical components in directions far off the z-axis. In these cases the relative phase of the two spectral components is important, and if the constant shift was different for the two measurements, the relative phase would not be correct.

The second special position error may be referred to as a scale error, and would result from incorrect calibration of position encoders or linear expansion of position encoder drives. In these cases the apparent position vector is proportional but not equal to the actual position vector.

$$x' = \alpha x, \quad y' = \beta y. \tag{28}$$

The effects on the computed spectrum are a change of beam widths and gain given by

$$D_e(\underline{K}) = \frac{D(\frac{k_x}{\alpha}, \frac{k_y}{\beta})}{\alpha\beta}. \tag{29}$$

In general, the position error will be more complicated than these special cases, and it is the more general ones which require additional analysis. Since the data are measured at intervals of approximately $\lambda/2$, and the position errors will be a small fraction of that interval, we can express the change in the data as the first term in a Taylor series

expansion.

$$B(\underline{P}') = B(\underline{P}) + \nabla B(\underline{P}) \cdot \underline{\Delta}(\underline{P})$$
$$= B(\underline{P}) + \frac{\partial B(\underline{P})}{\partial x} \Delta x(\underline{P}) + \frac{\partial B(\underline{P})}{\partial y} \Delta y(\underline{P}) \qquad (30)$$

Since the integrand of eq. (25a) is an analytic function, the derivatives in eq. (30) can be obtained by differentiating under the integral sign of eq. (25a) to give

$$\nabla B(\underline{P}) = iFA_n \int \underline{K} D(\underline{K}) e^{i\gamma d} e^{i\underline{K}\cdot\underline{P}} d\underline{K}$$
$$= iFA_n \mathcal{F}^{-1}[\underline{K} D(\underline{K}) e^{i\gamma d}] \qquad (31)$$

It is instructive to give a physical interpretation to eq. (31) as this kind of relation will appear frequently. Consider a narrow beam antenna whose main beam is along the z-axis. $|D(\underline{K})|$, which is essentially the far-field pattern of the antenna will be large for $|\underline{K}| \cong 0$ near the z-axis and small for large $\underline{K}$ which corresponds to angles far off the main beam. In the integration of eq. (31), large values of $D(\underline{K})$ will be multiplied by small values of $\underline{K}$ and vice versa which will result in a relatively small value for $\nabla B(\underline{P})$. If the main beam is steered sufficiently far off the z-axis so that the large values of $D(\underline{K})$ coincide with large values of $\underline{K}$, then the integral will be large, and the rate of change of $B(\underline{P})$ will be significant. Also if the antenna has a fairly broad beam $\nabla B(\underline{P})$ will be significant. Equation (31) simply expresses the fact that the more relative energy there is at wide angles (large $\underline{K}$ values) the more variation there will tend to be in the near field as a function of x and y-position. We can therefore expect the effects of x-y position errors to be the largest for broad beam and steered beam antennas and smallest for narrow beam antennas directed along the z-axis.

If the spectrum is computed from the data taken at $\underline{P}'$ we obtain from eqs. (25b) and (30)

$$D_e(\underline{K}) = \frac{e^{-i\gamma d}}{FA_n} \mathcal{F}[B(\underline{P}')]$$
$$= \frac{e^{-i\gamma d}}{FA_n} \mathcal{F}[B(\underline{P}) + \nabla B(\underline{P}) \cdot \underline{\Delta}(\underline{P})]$$
$$= D(\underline{K}) + \frac{e^{-i\gamma d}}{4\pi^2 FA_n} \int \nabla B(\underline{P}) \cdot \underline{\Delta}(\underline{P}) e^{-i\underline{K}\cdot\underline{P}} d\underline{P} \qquad (32)$$

where $D(\underline{K})$ and $D_e(\underline{K})$ are respectively the true spectrum and the erroneous spectrum resulting from the position errors. If we now use eq. (31) for $\nabla B(\underline{P})$ in eq. (32) we can obtain an expression for the error in D(K) in terms

of spectral rather than near-field quantities.

$$\Delta D(\underline{K}) = D_e(\underline{K}) - D(K) = \frac{e^{-i\gamma d}}{FA_n} \mathcal{F}\left[ iFA_n \underline{\Delta}(\underline{P}) \cdot \mathcal{F}^{-1}[\underline{K} D(\underline{K}) e^{i\gamma d}] \right] \qquad (33)$$

Making use of the convolution theorem [12] that the transform of a product is equal to the convolution of the transforms of the terms in the product we obtain

$$\Delta D(\underline{K}) = i(\underline{K} D(\underline{K})) \overset{\cdot}{*} \underline{F}(\underline{K}) \qquad (34)$$

where

$$\underline{F}(\underline{K}) = \mathcal{F}[\underline{\Delta}(\underline{P})]. \qquad (35)$$

and the dot and asterisk denote convolution of the dot product of $\underline{F}(\underline{K})$ and $D(\underline{K})\underline{K}$. Rewriting eq. (32) in a slightly different form we obtain

$$\Delta D(\underline{K}) = \frac{e^{-i\gamma d}}{4\pi^2 FA_n} \int (\nabla B(\underline{P}) e^{-i\underline{K}\cdot\underline{P}}) \cdot \underline{\Delta}(\underline{P}) \, d\underline{P}. \qquad (36)$$

We now have two general equations for the effect of x-y position errors which will serve as the basis for examining certain special cases. Both forms are useful at various stages in the analysis. Equation (36) is used to determine the functional form of the worst-case type position error, while eq. (34) is more useful for deriving the magnitude of the error in $D(\underline{K})$. The generality of eqs. (34) and (36) should be emphasized since they will be used in a number of cases. Since we have not assumed any special antenna characteristics at this point, they apply to both narrow and broad beam antennas, sum and difference patterns, beams near and far from the z-axis, and errors close to the main beam and at the remote sidelobes.

The first task is to determine the functional form of $\underline{\Delta}(\underline{P})$ which will produce the largest realizable error in a given part of the pattern in the direction specified by $\underline{K}_a$. $\underline{K}_a$ could define the direction of the main beam, the monopulse null, or a given sidelobe, and we would like to know what type of x-y position error will have the maximum effect in that direction, and the magnitude of the error in $D(\underline{K})$. Let us assume that the maximum position errors in each direction are $\Delta_{mx}$ and $\Delta_{my}$, and that the RMS position error over the measurement area is $\sigma_{xy}$.

$$\sigma_{xy}^2 = \frac{1}{L_x L_y} \int \{[\Delta x(\underline{P})]^2 + [\Delta y(\underline{P})]^2\} \, d\underline{P} \qquad (37)$$

In order that all possible error functions are evaluated on a common basis, the RMS position error for each one must be the same. This guarantees that the difference in the effect of the various types of errors will be due to their functional form and not to varying amounts of total error "energy."

The Schwartz inequality [13] is used in the following analysis to determine the form of the worst case errors. This approach leads to the requirement that the error functions are complex quantities while in fact they must be real. In an attempt to satisfy both the analysis and reality, we chose either the real or imaginary part of the complex error function prescribed by the Schwartz inequality as the functional form for the realizable worst-case error. The validity of this approach is confirmed by the computer simulation and by a recent more rigorous approach used by D.M. Kerns of NBS. In his approach, the constraint of a real error function is applied initially, and an inequality incorporating that constraint is used in place of the Schwartz version. The results of this approach for antennas whose near-fields have either even or odd symmetry are the same as those reported here, and since the antenna types being studied do have these symmetry properties, the conclusions of this report are correct. Because of the added analysis required in the newer approach, it will not be described in detail here.

If we now use the Schwarz inequality on eq. (36), an upper bound for the error in $D(\underline{K})$ is

$$\left|\Delta D(\underline{K}_a)\right|^2 \leq \frac{1}{4\pi^2 F A_n}\left\{\int\left|\frac{\partial B(\underline{P})}{\delta x}\, e^{-i\underline{K}_a\cdot\underline{P}}\right|^2 d\underline{P}\int|\Delta x(\underline{P})|^2\, d\underline{P} + \int\left|\frac{\partial B(\underline{P})}{\partial y}\, e^{-i\underline{K}_a\cdot\underline{P}}\right|^2 d\underline{P}\int|\Delta y(\underline{P})|^2\, d\underline{P}\right\}. \tag{38}$$

The maximum value will be realized only when

$$\frac{\Delta x(\underline{P})}{c} = \left\{\frac{\partial B(\underline{P})}{\delta x}\, e^{-i\underline{K}_a\cdot\underline{P}}\right\}^* \quad \text{and} \tag{39a}$$

$$\frac{\Delta y(\underline{P})}{c} = \left\{\frac{\delta B(\underline{P})}{\delta y}\, e^{-i\underline{K}_a\cdot\underline{P}}\right\}^*. \tag{39b}$$

That is, the position error must be proportional to the complex conjugate (denoted by the *) of the derivative of the near field data multiplied by the kernel to produce the maximum error in $D(\underline{K}_a)$. The c's are in general complex constants which are chosen to satisfy the required RMS value of the error function.

The particular form of $\Delta x(\underline{P})$ or $\Delta y(\underline{P})$ will depend upon the character of the near-field data, and the direction of interest. To illustrate this, consider a one dimensional problem and denote the near-field amplitude and phase by

$$B(x) = a(x)\, e^{i\phi(x)}$$

where both $a(x)$ and $\phi(x)$ are real functions. The worst-case position error is given by

$$\frac{\Delta x(x)}{c} = \left\{\left[\frac{\partial a(x)}{\partial x} + ia(x)\frac{\partial \phi(x)}{\partial x}\right]e^{i(\phi(x)-k_{ax}x)}\right\}^*$$

$$a'(x)\cos[\phi(x)-k_{ax}x] - a(x)\phi'(x)\sin[\phi(x)-k_{ax}x]$$

$$- i\left[a'(x)\sin[\phi(x)-k_{ax}x] - a(x)\phi'(x)\cos[\phi(x)-k_{ax}x]\right] \qquad (40)$$

where the primes in eq. (40) denote the derivatives with respect to x. Since $\Delta x(x)$ must be a real function, the worst-case conditions cannot in general be realized. The largest realizable error will occur when $\frac{\Delta x(x)}{c}$ is equal to either the real or imaginary part of eq. (40), and in the remaining discussions, the term "worst-case" will imply the realizable worst-case condition. The important character of eq. (40) can be illustrated by some typical examples. For a narrow beam sum pattern centered on the z-axis, the near-field data will be similar to figure 11. Over the significant part of the near-field $\phi_s(x) \cong$ const and $a_s(x)$ = smoothly varying function.

Without a loss of generality we can take $\phi_s(x) = 0$, and eq. (40) becomes

$$\Delta x_s = c\, a_s'(x)\, \cos(k_{ax}x). \qquad (41)$$

The amplitude in this case will be approximately of the form

$$a_s(x) \cong \cos^2\left(\frac{\pi x}{L_x}\right) \qquad (42)$$

giving

$$a_s'(x) \cong -\frac{\pi}{L_x}\sin\left(\frac{2\pi x}{L_x}\right). \qquad (43)$$

where $L_x$ is the antenna aperture dimension. We can interpret the role of the factors in eq. (41) in a way which will give further insight into the character of a worst-case type error, and help to determine whether or not this type of error is reasonable or not. The factor $a_s'(x)$ will maximize the error in $\Delta D(\underline{K})$ since $\underline{\Delta}(\underline{P})$ will be proportional to $(\nabla B(\underline{P}))^*$ in eq. (36). The factor $\cos(k_{ax}x)$ will determine where the maximum error occurs. Since the spectrum of $\cos(k_{ax}x)$ is composed of two equal amplitude sidebands at $\pm k_{ax}$, the maximum errors will also occur in these two directions.

The type of error described above is one that could occur, and yet with the knowledge provided by the error analysis, the scanner can be designed and aligned to minimize the error in the important region of interest. The factor $a_s'(x)$ for the sum pattern being considered is a low frequency sine function with a period equal to the scan length similar to figure 12. This figure is an example of an x-position error which was simulated on actual measured near-field data. The simulated error was proportional to the

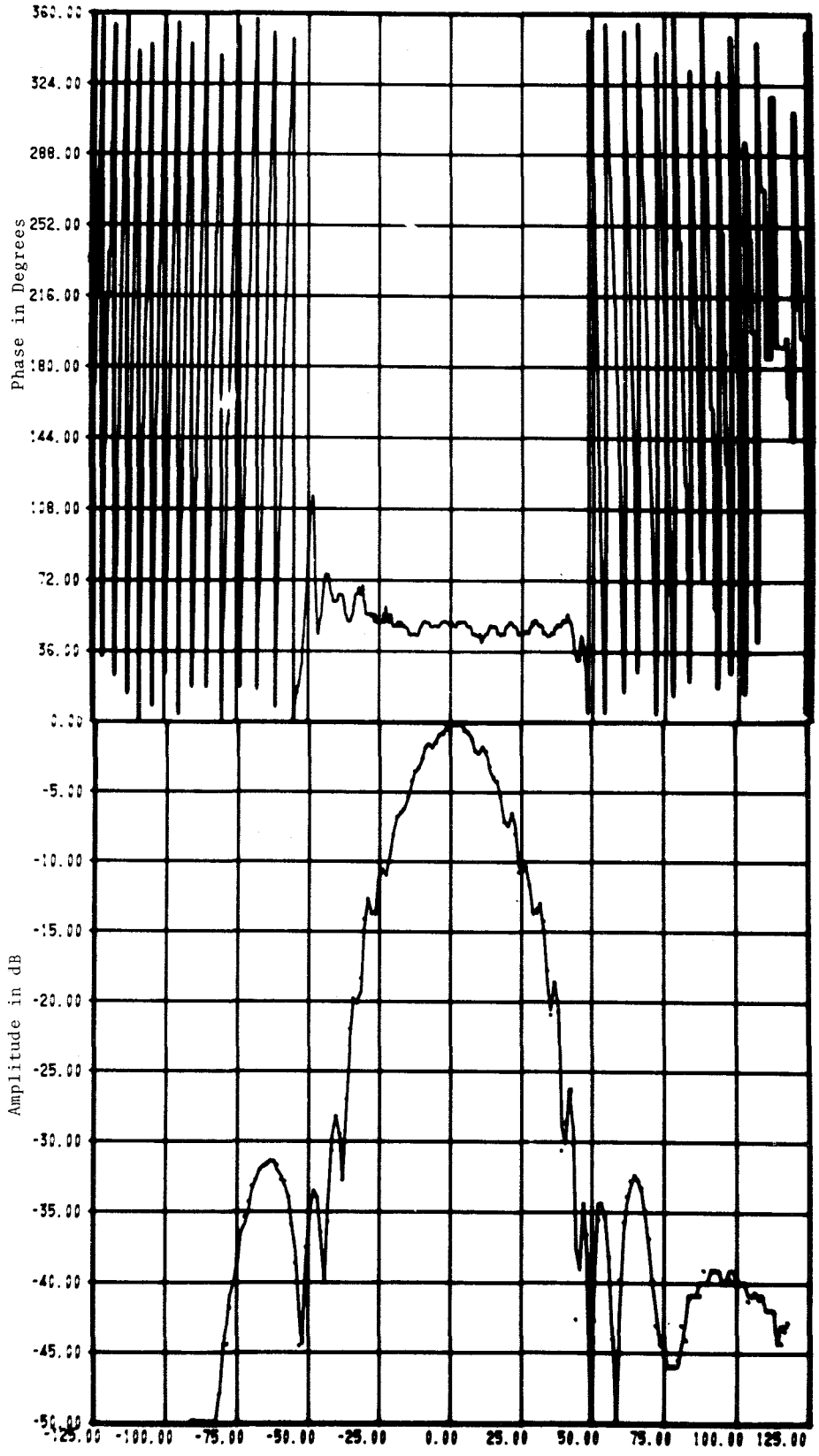


Figure 11. Near-Field Data, B(X,0), for Sum Pattern Antenna.

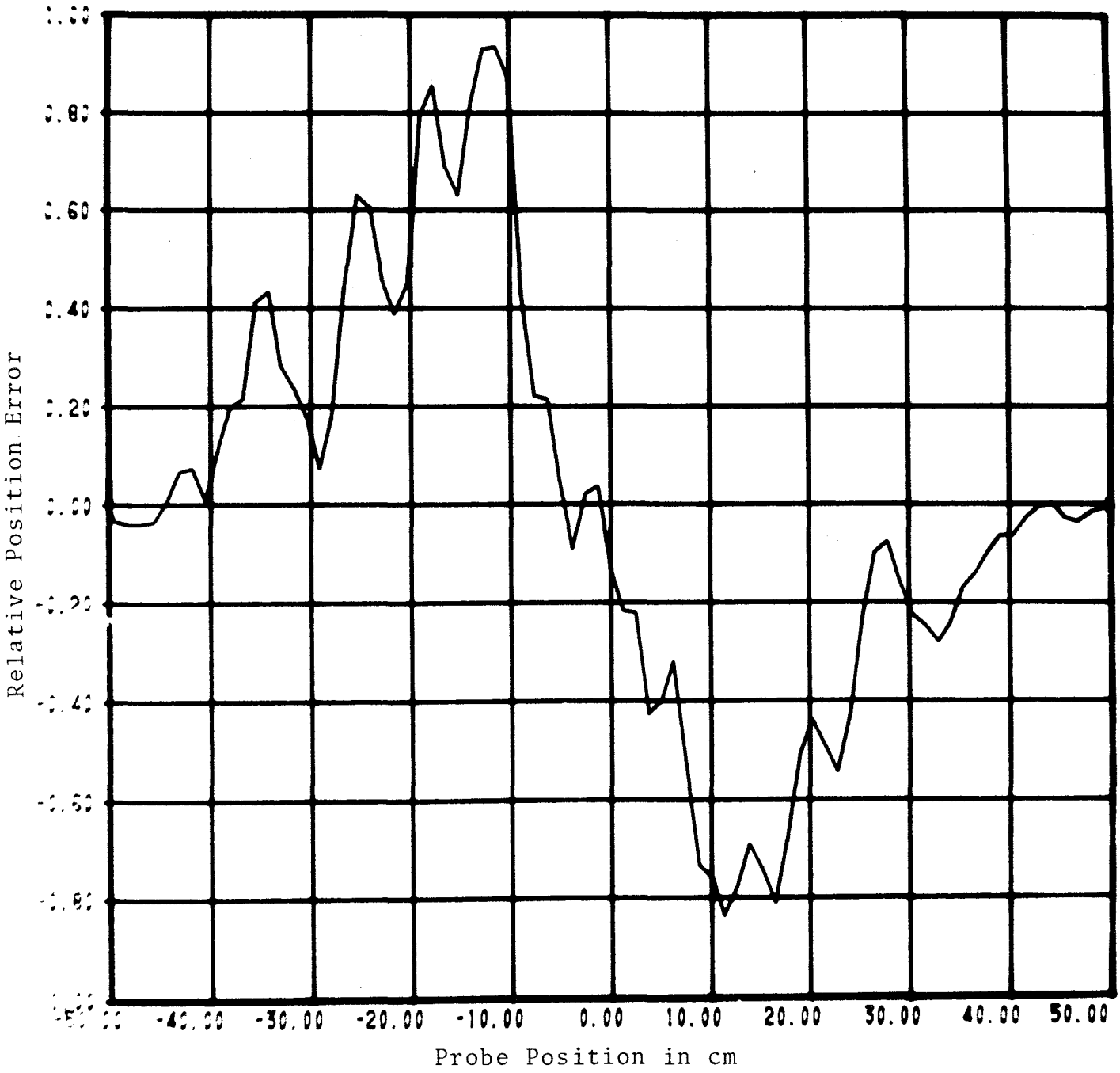


Figure 12. Worst Case Position Error for Sum Pattern.

derivative of the near-field amplitude shown in figure 11. It is apparent why this error produces the maximum change in the far-field when we note the change it produces in the near-field as shown in figure 13. There is very little phase change, and though the amplitude change is small, it has the same sign over the complete scan length and therefore produces the maximum change in the on-axis far field.

The factor $\cos(k_{ax}x)$ will have a period of

$$T_a = \lambda/\sin\theta_{ax} \tag{44}$$

and the low frequency variations produce errors close to the main beam while higher frequency position errors effect the sidelobes.

For a difference pattern centered on the z-axis the near-field can be approximated by

$$a_d(x) \cong \begin{cases} \sin^2\left(\frac{2\pi x}{L_x}\right) & x < 0 \quad (45a) \\ -\sin^2\left(\frac{2\pi x}{L_x}\right) & x > 0 \quad (45b) \end{cases}$$

$$\phi(x) \cong 0,$$

and again the only significant term in eq. (40) is $a_d'(x)\cos(k_{ax}x)$. The derivatives are given by

$$a_d'(x) \cong \begin{cases} \frac{2\pi}{L_x}\sin\left(\frac{4\pi x}{L_x}\right) & x < 0 \\ -\frac{2\pi}{L_x}\sin\left(\frac{4\pi x}{L_x}\right) & x > 0. \end{cases} \tag{46}$$

and the worst-case position error function is twice the frequency of the one for the sum beam pattern, but is still of relatively long wavelength.

As a third example let us look at a narrow beam sum pattern with the beam shifted away from the z-axis. If the main beam is at $k_x = k_b$ then the near field and its derivatives are

$$a_b(x) \cong \cos^2\left(\frac{\pi x'}{L_x}\right) \tag{47}$$

$$x' = x + d\tan\theta_b \tag{48}$$

$$\phi(x) = k_b x \tag{49}$$

$$a_b'(x) = -\frac{\pi}{L_x}\sin\left(\frac{2\pi x'}{L_x}\right) \tag{50}$$

$$\phi'(x) = k_b = \frac{2\pi}{\lambda}\sin\theta_b. \tag{51}$$

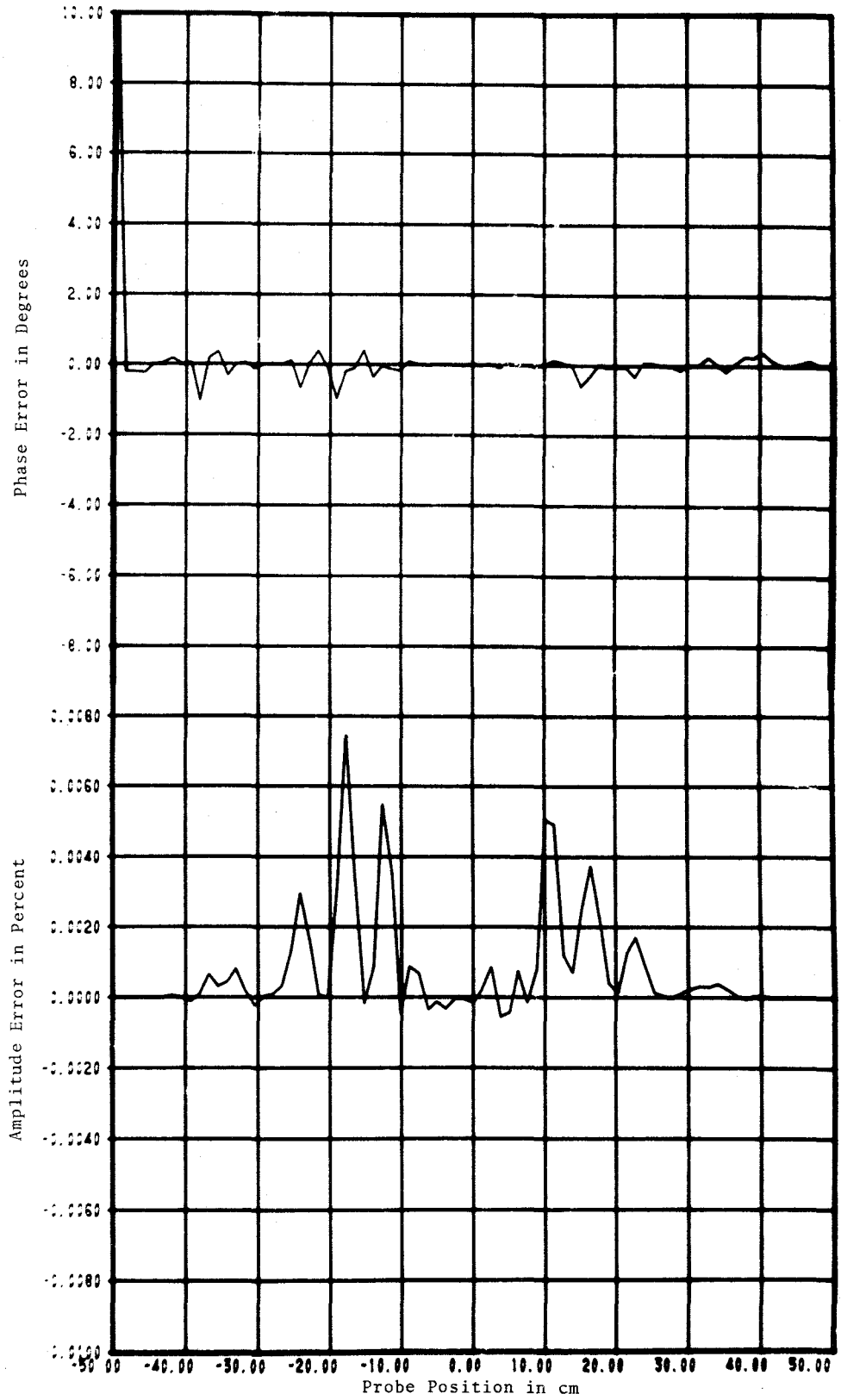


Figure 13. Error in Near-Field Amplitude and Phase Due to Transverse (x-y) Position Error.

Substituting there values in eq. (40) we obtain

$$\Delta_b(x) = c[a'(x)\cos[(k_a-k_b)x] + a(x)k_b \sin((k_a-k_b)x) \tag{52a}$$

if we take the real part of eq. (40), or

$$\Delta_b(x) = c[a'(x)\sin[(k_a-k_b)x] + a(x)k_b \cos((k_a-k_b)x) \tag{52b}$$

if we take the imaginary part of eq. (40). The realizable worst-case error function will be the one which produces the largest error. For errors at the peak of the beam $k_{ax} = k_b$, and the two possible functions are $a_b'(x)$ and $a_b(x)k_b$. For steering angles greater than

$$\theta_b \geq \sin^{-1}\left(\frac{\lambda}{2L_x}\right) \tag{53}$$

the second term is predominant and will therefore produce the larger error. For errors in regions off the main beam, the second term is also larger, but in this case is multiplied by the cosine term. The worst-case position error for the beam-steered case is then

$$\Delta_b(x) = c\ a(x)\ k_b \cos((k_b-k_a)x). \tag{54}$$

The three examples we have looked at are typical of most real situations for narrow beam antennas and point out three main features:

1. Except for the restriction that the position error must be real, the worst case errors are reasonable functions and can be realized in an actual situation.
2. The position errors which produce a maximum error in one given direction are periodic functions with a low frequency modulation.
3. Because of the role of periodic error functions, a knowledge of the spectrum of the position error on an actual system would be more useful that just the maximum value of the error.

Now that we have determined the form of the worst case error and found that it is one that could reasonably occur, we need to find the magnitude of the error for the various types of patterns and beam positions. Using eq. (34) and writing the convolution and dot product out in complete form we obtain

$$\Delta D(\underline{K}) = i \int \left(D(\underline{L})\underline{L}\right) \cdot \underline{F}(\underline{K}-\underline{L})\, d\underline{L} \tag{55a}$$

$$= i \int [D(\underline{L})\ell_x F_x(K-L) + D(\underline{L})\ell_y F_y(\underline{K}-\underline{L})]\, d\ell_x d\ell_y \tag{55b}$$

where $\underline{L}$, $\ell_x$ and $\ell_y$ are used as the dummy variables in the integration to replace $\underline{K}$, $k_x$ and $k_y$, and

$$\underline{F}(\underline{K}-\underline{L}) = F_x(\underline{K}-\underline{L})\underline{e}_x + F_y(\underline{K}-\underline{L})\underline{e}_y. \tag{56}$$

If we now use the Schwarz inequality on eq. (55b) and note that the integral of $|F(\underline{K}-\underline{L})|^2$ is the same as the integral of $|F(\underline{L})|^2$ then eq. (55b) becomes

$$|\Delta D(\underline{K})|^2 \leq \int |D(\underline{L})\ell_x|^2 \, d\underline{L} \int |F_x(L)|^2 \, d\underline{L} + \int |D(\underline{L})\ell_y|^2 \, d\underline{L} \int |F_y(\underline{L})|^2 \, d\underline{L} \quad (57)$$

and since $F_x(\underline{L})$ and $F_y(\underline{L})$ are the Fourier transforms of the position error functions, (see. eq. (35)), we can use Rayleigh's theorem [14] to obtain

$$\int |F_x(L)|^2 \, dL = \frac{1}{4\pi^2} \int |\Delta x(\underline{P})|^2 \, d\underline{P} = \frac{L_x L_y \sigma_x^2}{4\pi^2} \quad (58a)$$

$$\int |F_y(L)|^2 \, dL = \frac{1}{4\pi^2} \int |\Delta y(\underline{P})|^2 \, d\underline{P} = \frac{L_x L_y \sigma_y^2}{4\pi^2} \quad (58b)$$

In general, the integration in eq. (55) is over all values of $\ell_x$ and $\ell_y$, but for narrow beam antennas and the periodic error functions being considered, both $D(\underline{K})$ and $F(\underline{K})$ will be narrow band functions having significant maxima at one or at most two values of $\underline{L}$. The significant part of the integral will be due to the integration over the main beam of $D(\underline{K})$ and the maximum value will occur when maxima of the two functions are coincident. For the problem under consideration, we may therefore limit the integration in eq. (55) to the main beam of the antenna.

To further evaluate eq. (55) we must assume some form for $D(\underline{K})$ or $B(\underline{P})$ and know the direction of the main beam. Since a number of combinations of beam types, steering directions and regions of interest will be investigated, a compact notation is required to distinguish between them. In the general analysis, and when referring to sum patterns, or when the results apply to both sum and difference types, the regular capital "D" will denote the spectrum. The script "$\mathcal{D}$" will be used in other cases to specify a difference pattern. The boresight direction will be specified by $\underline{K}_b$ and the direction in which the error is a maximum will be denoted by $\underline{K}_a$. For example, when discussing the error in the side lobe region for a difference type pattern steered off the z-axis, the pertinent quantities would be $\frac{\mathcal{D}_e(\underline{K}_a)}{D(\underline{K}_b)}$, where the "e" subscript denotes the error-contaminated spectrum. First consider a sum-beam pattern with the main beam at $\underline{K} = 0$ whose main beam can be approximated by the function

$$D(\underline{K}) = D(0) \frac{\sin \psi}{\psi} \frac{\sin \xi}{\xi} \quad (59)$$

where

$$\psi = \alpha k_x \quad \text{and} \quad \xi = \beta k_y \, . \quad (60)$$

The constants $\alpha$ and $\beta$ are chosen such that the approximate function equals the actual pattern at the -3 dB points. The integrals in eq. (57) over the main

beam, to the first zeroes of eq. (59) are

$$\int |D(\underline{K})k_x|^2 \, d\underline{K} = \frac{|D(0)|^2 \, 4\pi^2}{L_x^3 L_y \eta^2} \tag{61a}$$

$$\int |D(\underline{K})k_y|^2 \, d\underline{K} = \frac{|D(0)|^2 \, 4\pi^2}{L_x L_y^3 \eta^2} \tag{61b}$$

where $L_x$ and $L_y$ are the dimensions of the antenna in the x and y-directions, and $\eta$ is the antenna aperture efficiency. Combining eq. (61) with eqs. (57) and (58) we have for the error in D(K)

$$|\Delta D(0)| \leq \frac{|D(0)|}{\eta} \left[ \frac{\sigma_x^2}{L_x^2} + \frac{\sigma_y^2}{L_y^2} \right]^{1/2} . \tag{62}$$

If we assume that $L_x = L_y$, and that $\sigma_x = \sigma_y = \frac{\Delta_m}{\sqrt{2}}$, where $\Delta_m$ is the maximum position error then the error in percent of the on-axis value is

$$\left| \frac{\Delta D(0)}{D(0)} \right|_{\%} \leq \frac{100}{\eta} \left( \frac{\Delta_m}{L} \right) \tag{63a}$$

and the error in dB

$$\left| \frac{D_e(0)}{D(0)} \right|_{dB} \leq \frac{8.7}{\eta} \left( \frac{\Delta_m}{L} \right) . \tag{63b}$$

If the position error is of the form given by eq. (41) with $k_{ax} = 0$ then the equality will hold in eq. (63) and the maximum error will be realized at the peak of the main beam. This is illustrated in figures 14-17 which show the near- and far-field data for a narrow beam antenna. The far-field pattern was computed from the actual measured data, and for the data with a simulated position error similar to eq. (41). The original data and the resulting pattern are shown by the continuous curves in figures 14-16 while the data with position error and its resulting pattern are plotted as the discrete points in the same graphs. Figure 17 is a plot of $|\Delta D(\underline{K})/D(0)|$ in percent and shows the maximum occurring at $\theta = 0$ which corresponds to $k_x = 0$. For this simulation $\Delta_m = 0.02\lambda$, $L_x = 25\lambda$, and $\eta = 0.5$. Since the simulation is for one-dimensional data, eq. (63) is modified slightly for this case, and predicts a maximum error of 0.20%. This and similar simulations for other antennas have shown that the approximations used to derive eq. (63) are quite good and that it does in fact give an upper bound for the error in $D(\underline{K})$.

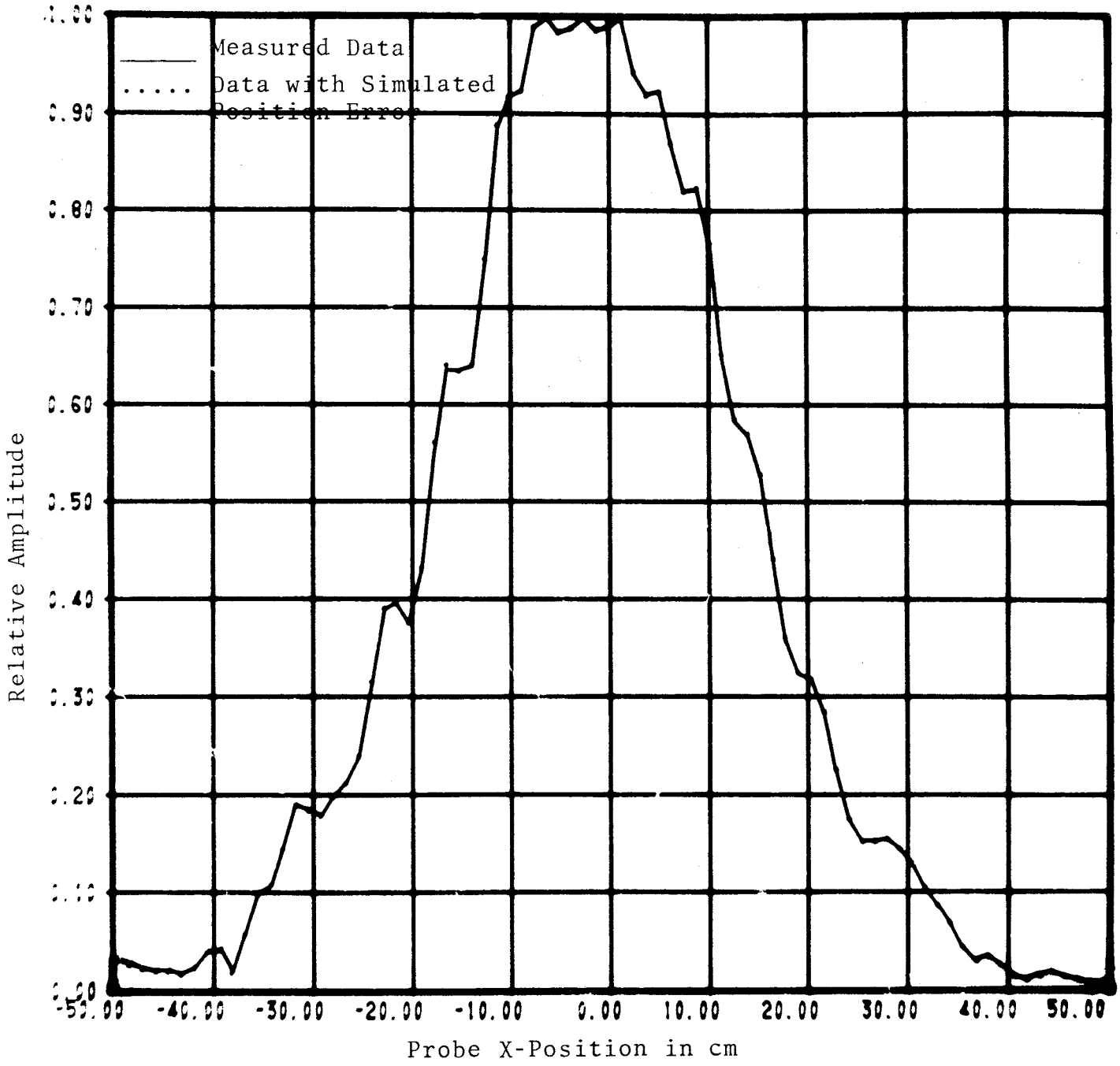


Figure 14. Near-Field Amplitude Along Centerline Y = 0 with Simulated Position Error.

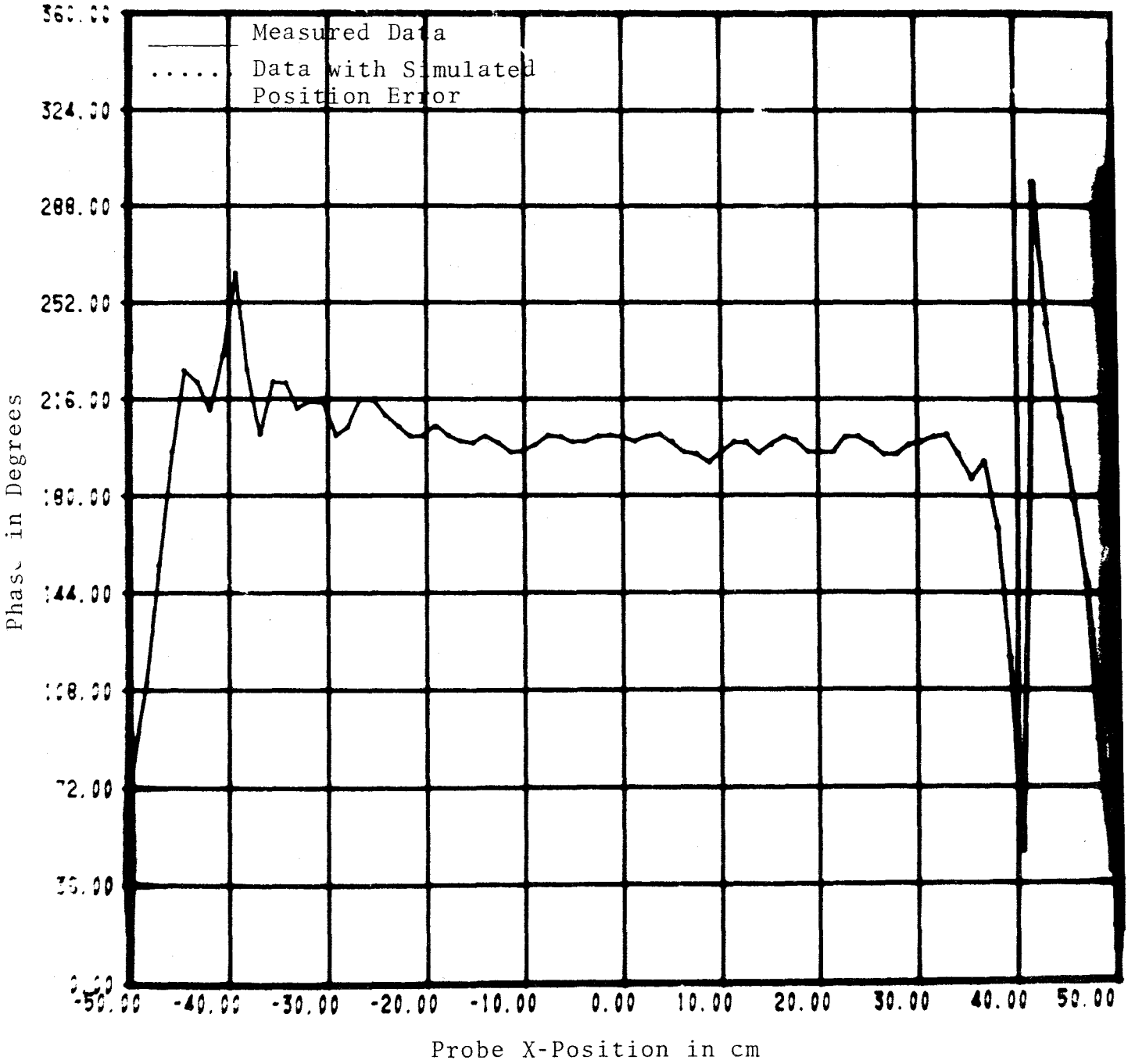


Figure 15. Near-Field Phase Along the Centerline Y = 0, $\Delta_{mx} = 0.02\lambda$.

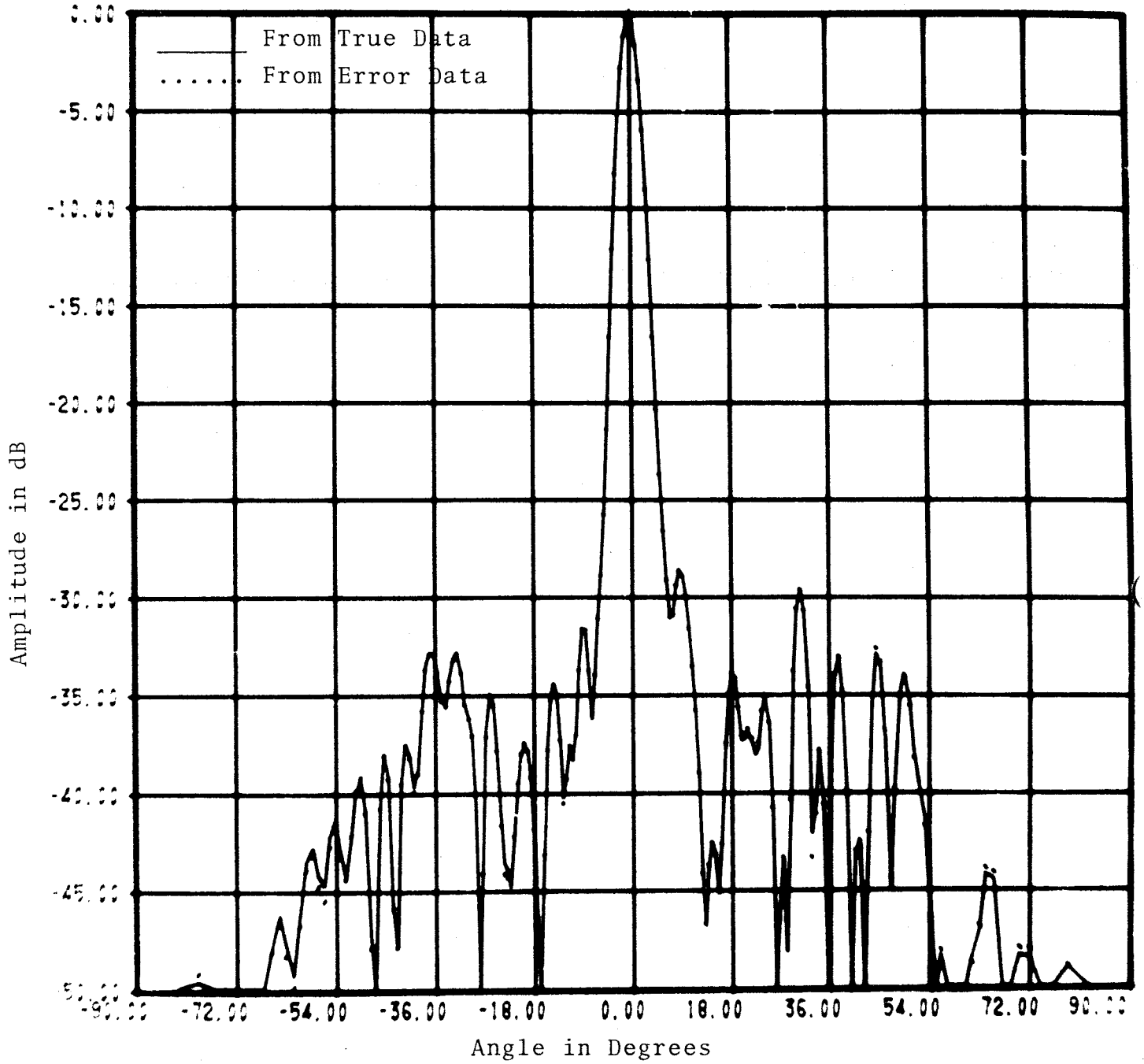


Figure 16. Far-Field Pattern for True Data and x-Position Error Data, $\Delta_{mx} = 0.02\lambda$.

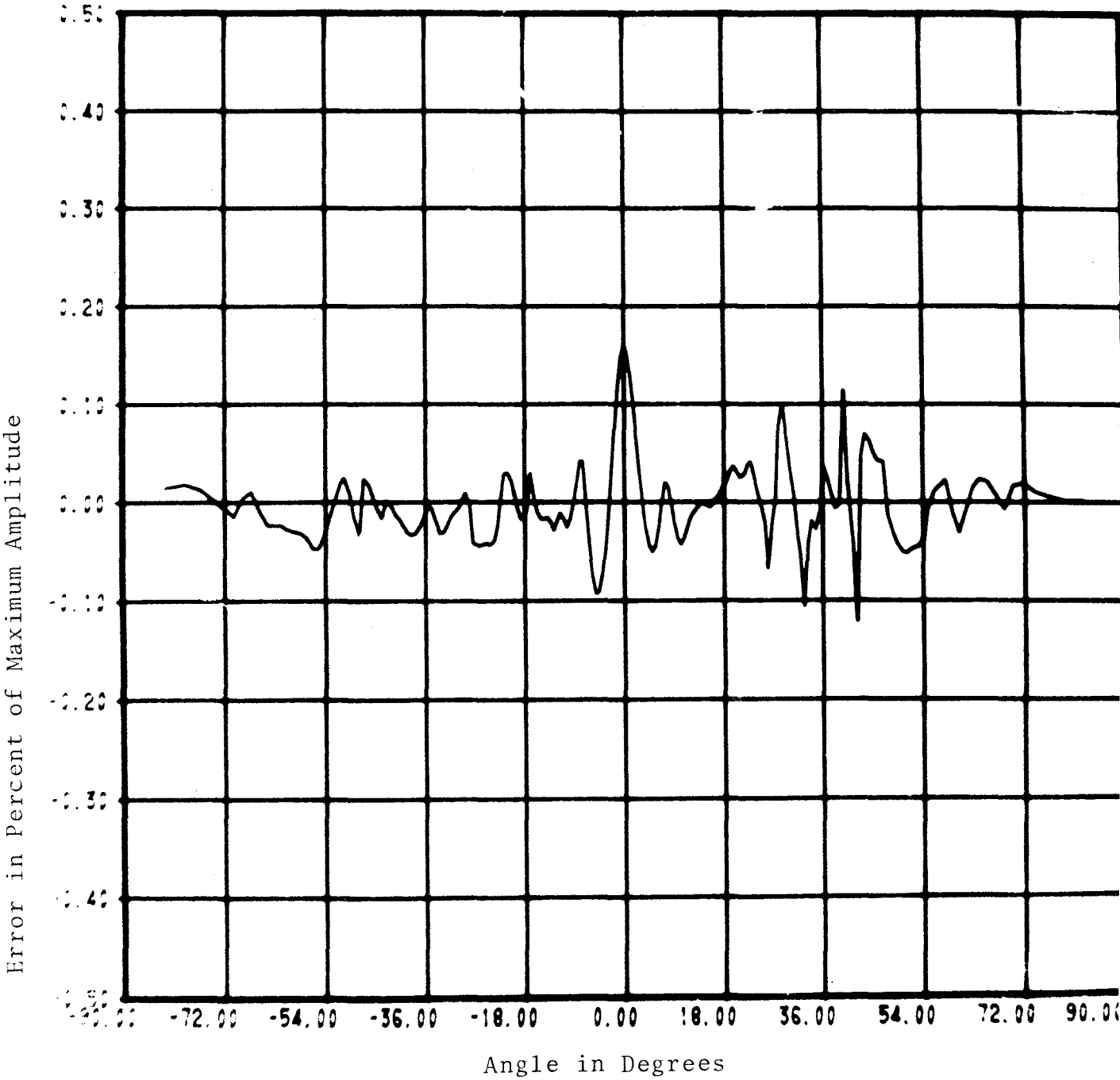


Figure 17. Error in Far-Field Pattern Due to x-Position Error, $\Delta_{mx} = 0.02\lambda$.

If $k_{ax} \neq 0$ in eq. (41), the maximum error in $D(\underline{K})$ will occur at $k_x = \pm k_{ax}$ rather than at $k_x = 0$ with one half the amplitude given by eq. (63). The factor of one half results from the requirement that the position error be a real function, and the $\cos(k_{ax}x)$ factor produces two sidebands at $\pm k_{ax}$ with one half the amplitude of the zero frequency component. In this case the error in a sidelobe is given by

$$\left|\frac{\Delta D(\underline{K}_a)}{D(\underline{K}_a)}\right|_{\%} \leq \left|\frac{D(0)}{D(\underline{K}_a)}\right| \quad 50 \quad \left(\frac{\Delta_m}{L}\right) \tag{64a}$$

$$\left|\frac{D_e(\underline{K}_a)}{D(\underline{K}_a)}\right|_{dB} \leq 4.3 \left|\frac{D(0)}{D(\underline{K}_a)}\right| \left(\frac{\Delta_m}{L}\right). \tag{64b}$$

For a monopulse difference pattern with the null at $\underline{K} = 0$, the analysis leads to essentially the same result. While the shape of the pattern is different, the integral of $|D(\underline{K})\underline{K}|^2$ over the main beam is very nearly the same. The major change in the result is that the D(0) in eqs. (63) and (64) refers to the peak of the sum pattern rather than the difference pattern minimum.

If we now look at the case where the beam is steered away from the z-axis, expressions similar to eqs. (63) and (64) are easily obtained. Assume that the peak of a sum pattern is steered to $\underline{K} = \underline{K}_b \neq 0$. In this case $\underline{K}$ is essentially constant over the main beam integration and can therefore be taken outside the integral. With this approximation, eqs. (31) and (36) become

$$\nabla B_s(\underline{P}) \cong i\underline{K}_b B_s(\underline{P}) \tag{65}$$

$$\Delta D(\underline{K}) = \frac{-ie^{i\gamma d}\ \underline{K}_b}{4\pi^2 F A_n} \int \left(B_s(\underline{P}) e^{-i\underline{K}\cdot\underline{P}}\right) \cdot \underline{\Delta}(\underline{P})\ d\underline{P}. \tag{66}$$

For errors on the peak of the main beam, $B_s(\underline{P})$ can be approximated by

$$B_s(\underline{P}) \cong a_s(\underline{P}) e^{i\underline{K}_b\cdot\underline{P}} \tag{67}$$

and eq. (66) becomes

$$\Delta D(K_b) = \frac{ie^{i\gamma d}\ \underline{K}_b}{4\pi^2 F A_n} \cdot \int a_s(\underline{P})\underline{\Delta}(\underline{P})\ d\underline{P}. \tag{68}$$

We have previously shown (see eq. 54) that the position error function which will produce the maximum error in $D(\underline{K}_a)$ when $\underline{K}_a = \underline{K}_b$ is

$$\underline{\Delta}(\underline{P}) = c\ a_s(\underline{P})\ \underline{K}_b. \tag{69}$$

We have also shown that a constant position error will not produce any error in the amplitude of $D(\underline{K})$ and so we may add a constant U to eq. (69) without changing its effect. Substituting this modified error function into eq. (68) we obtain

$$\Delta D_s(\underline{K}_a) = \frac{ie^{i\gamma d}\ \underline{K}_a}{4\pi^2 F A_n}\left(c\int [a_s(\underline{P})]^2 d\underline{P} + U\int a_s(\underline{P})\ d\underline{P}\right). \tag{70}$$

For the sum pattern, $a_s(\underline{P})$ is positive for all values of $\underline{P}$ and both integrals will be positive. The constant U may therefore be chosen to make $|\Delta D_s(K_a)| = 0$, which indicates that for this case the first term in the Taylor series expansion is not sufficient to represent the error, and the second term must be included. When the second term is used we obtain

$$\Delta D(\underline{K}_b) = \frac{-e^{i\gamma d}\ |\underline{K}_b|^2}{2\pi^2 F A_n}\int a_s(\underline{P})\ |\underline{\Delta}(\underline{P})|^2\ d\underline{P} \tag{71}$$

and now since both factors in the integrand are positive, the integral will not be zero. To evaluate the error, we use a form similar to eq. (34) which results from the second term in the expansion.

$$\Delta D(\underline{K}_b) = -|\underline{K}_b|^2\ [D(\underline{K}) * |\underline{F}(\underline{K})|^2] \tag{72}$$

Using the Schwarz inequality and Rayleigh's theorem again as before, we obtain

$$|\Delta D(\underline{K}_b)|^2 \leq \frac{|\underline{K}_b|^4}{4\pi^2}\int |D(\underline{K})|^2\ d\underline{K}\int |\underline{\Delta}(\underline{P})|^4\ d\underline{P}. \tag{73}$$

Using the earlier approximations (see eq. (59)) for the main beam this becomes

$$\left|\frac{\Delta D(\underline{K}_b)}{D(\underline{K}_b)}\right|_{\%} \leq \frac{100|\underline{K}_b|^2\ |\Delta_{max}|^2}{\sqrt{\eta}}, \tag{74a}$$

and for the error in dB

$$\left|\frac{D_e(\underline{K}_b)}{D(\underline{K}_b)}\right|_{dB} \leq \frac{8.7|\underline{K}_b|^2\ |\Delta_{max}|^2}{\sqrt{\eta}}, \tag{74b}$$

where $|\Delta_{max}|^2$ is the largest value of $|\underline{\Delta}(\underline{P})|^2$.

For a monopulse difference pattern steered to $\underline{K}_a$, the near-field amplitude is an odd function and therefore the second integral in eq. (70) is nearly zero. The error in $\mathcal{D}(\underline{K}_b)$ cannot be made zero by the proper choice of the constant U, and therefore the first term in the expansion is the significant one. For the monopulse type pattern, the position error which is

proportional to $a_d(\underline{P})$ affects the far-field pattern in two ways. First there is an effective linear term in $a_d(\underline{P})$ which shifts the entire pattern by a small amount, and there is also a change in the shape of the pattern. The analysis for this case is very similar to the one for the effects of z-errors on a difference pattern centered on the z-axis which will be discussed in the following section. The results are essentially the same, and so we will defer a discussion of the analysis to the next section. The results show that for the present case of a monopulse difference pattern steered to $\underline{K} = \underline{K}_b \neq 0$, the error in the depth of the minimum at $\underline{K}_b + \underline{\varepsilon}$ is

$$\left|\frac{\mathcal{D}_e(K_b+\varepsilon)}{\mathcal{D}_e(K_b)}\right|_{dB} \leq \frac{|\underline{K}_b|\ \Delta_{max}}{2}\left|\frac{D(\underline{K}_b)}{\mathcal{D}(K_b)}\right| Q \tag{75}$$

where $\underline{K}_b + \underline{\varepsilon}$ is the position of the minimum for the error corrupted spectrum, and Q is equal to the difference in dB of the far-field maxima for the difference pattern.

For either a sum or difference pattern the maximum error in direction off the main beam is given by the same equation. For the beam steering conditions the error function which produced the maximum error in the side-lobe region is given by eq. (54) which for the two dimensional case is

$$\underline{\Delta}_b(\underline{P}) = \Delta_{mx} a(x)\ \sin[(k_{xa}-k_{xb})x]\underline{e}_x + \Delta_{my} a(y)\ \sin[(k_{ya}-k_{yb})y]\underline{e}_y \tag{76}$$

The spectrum of $\underline{\Delta}_b(\underline{P})$ is composed of $\frac{\sin k_x}{k_x}$ type functions whose maxima occur at $\pm(k_{xa}-k_{xb})$ and similar functions in the $k_y$ direction with maxima at $\pm(k_{ya}-k_{yb})$. The width of the "main beam" of these functions will be approximately 1/4 the width of the antenna pattern, and so in the convolution of eq. (55) the net effect is the same as if they were delta functions with amplitudes of $\frac{\Delta_{mx}}{4}$ and $\frac{\Delta_{my}}{4}$. The four maxima in the error $\Delta D(\underline{K})$ will occur at

$$\underline{K} = \begin{cases} (k_{xa}, & k_{ya}) \\ (k_{xa}, & k_{yb}-(k_{ya}-k_{yb})) \\ (k_{xb}-(k_{xa}-k_{xb}), & k_{ya}) \\ (k_{xb}-(k_{xa}-k_{xb}), & k_{yb}-(k_{ya}-k_{yb})) \end{cases} . \tag{77}$$

The amplitude of the error in each of these directions in percent and dB is obtained from the convolution of $D(\underline{K})$ with the delta functions.

$$\left|\frac{\Delta D(\underline{K}_a)}{D(K_a)}\right|_{\%} \leq 25\left|\frac{D(K_b)}{D(K_a)}\right| (k_{xb}\Delta_{mx} + k_{yb}\Delta_{my}) \tag{78}$$

$$\left|\frac{D_e(\underline{K}_a)}{D(K_a)}\right|_{dB} \leq 2.2\left|\frac{D(0)}{D(\underline{K}_a)}\right| (k_{xb}\Delta_{mx} + k_{yb}\Delta_{my}) \tag{79}$$

Under the conditions that $\Delta_{mx} \cong \Delta_{my}$, and approximating $k_{xa} + k_{ya} \cong |\underline{K}_a|$ these become

$$\left|\frac{\Delta D(\underline{K}_a)}{D(0)}\right|_{\%} \leq 25|\underline{K}_b|\ \Delta_m \tag{80}$$

$$\left|\frac{D_e(\underline{K}_a)}{D(\underline{K}_a)}\right|_{dB} \leq \left|\frac{D(0)}{D(\underline{K})}\right| 2.2|\underline{K}_b|\ \Delta_m. \tag{81}$$

The key equations of this section can be put in terms of the angles of the antenna coordinate system by use of the relationships

$$|\underline{K}_a| = k \sin\theta_a = \frac{2\pi}{\lambda} \sin\theta_a \tag{82}$$

$$|\underline{K}_a| = k\sqrt{(1-\cos^2 A_a \cos^2 E_a)} \tag{83}$$

where $\theta$ is the polar angle between the propagation vector $\underline{k}_a$ and the z-axis. The main results are summarized below for the various cases.

1. Main beam on the z-axis,

a. Main beam error Sum pattern
$$\left|\frac{D_e(0)}{D(0)}\right|_{dB} \leq \frac{8.7}{\eta}\left(\frac{\Delta_m}{L}\right) \tag{84}$$

b. Main beam error Difference pattern
$$\left|\frac{\mathcal{D}_e(0)}{\mathcal{D}(0)}\right|_{dB} \leq \frac{8.7}{\eta}\left|\frac{D(0)}{\mathcal{D}(0)}\right|\left(\frac{\Delta_m}{L}\right) \tag{85}$$

c. Sidelobe error
$$\left|\frac{D_e(\underline{K}_a)}{D(\underline{K}_a)}\right|_{dB} \leq 4.3\left|\frac{D(0)}{D(\underline{K}_a)}\right|\left(\frac{\Delta_m}{L}\right) \tag{86}$$

2. Main beam steered to $\underline{K}_b$, $A_b$, $E_b$, $\theta_b$

a. Main beam error Sum pattern
$$\left|\frac{D_e(\underline{K}_b)}{D(\underline{K}_b)}\right|_{dB} \leq \frac{344}{\sqrt{\eta}}\left(\frac{\Delta_m}{\lambda}\right)^2 \sin^2\theta_b \tag{87}$$

b. Main beam error Difference pattern
$$\left|\frac{\mathcal{D}_e(\underline{K}_b+\underline{\varepsilon})}{\mathcal{D}(\underline{K}_b)}\right|_{dB} \leq 3Q\left|\frac{D(K_b)}{\mathcal{D}(K_b)}\right|\left(\frac{\Delta_m}{\lambda}\right)\sin\theta_b \tag{88}$$

c. Sidelobe error
$$\left|\frac{D_e(\underline{K}_a)}{D\ (\underline{K}_a)}\right|_{dB} \leq 13.5\left|\frac{D(K_b)}{D(\underline{K}_a)}\right|\left(\frac{\Delta_m}{\lambda}\right)\sin\theta_b \tag{89}$$

To illustrate the important features of the results for the various cases, let us consider an antenna with a square aperture $L_x = L_y = 50\lambda$, and a 50% aperture efficiency. Table 3 below then gives the maximum error due to x-y position errors for the various cases.

Table 3. Examples of Errors

| Type Pattern | Direction of Main Beam | | Region Where Maximum Error Occurs | | $\frac{\Delta_m}{\lambda}$ | Error in dB |
|---|---|---|---|---|---|---|
| | Azimuth | Elevation | Pattern Character | Relative Amp(dB) | | |
| Sum | 0 | 0 | Peak | 0 | 0.02 | 0.007 |
| Difference | 0 | 0 | Difference Null | -20 | 0.02 | 0.07 |
| Difference | 0 | 0 | Difference Null | -30 | 0.02 | 0.22 |
| Difference | 0 | 0 | Difference Null | -40 | 0.02 | 0.79 |
| Sum or Difference | 0 | 0 | Sidelobe | -20.0 | 0.02 | 0.02 |
| Sum or Difference | 0 | 0 | Sidelobe | -30.0 | 0.02 | 0.05 |
| Sum or Difference | 0 | 0 | Sidelobe | -40.0 | 0.02 | 0.17 |
| Sum | 30° | 30° | Peak | 0 | 0.02 | 0.12 |
| Sum | 60° | 40° | Peak | 0 | 0.02 | 0.23 |
| Difference | 60° | 40° | Difference Null | -20 | 0.02 | 0.54 |
| Difference | 60° | 40° | Difference Null | -30 | 0.02 | 1.62 |
| Difference | 60° | 40° | Difference Null | -40 | 0.02 | 5.40 |
| Sum or Difference | 60° | 40° | Sidelobe | -20 | 0.02 | 2.5 |
| Sum or Difference | 60° | 40° | Sidelobe | -30 | 0.02 | 7.5 |
| Sum or Difference | 60° | 40° | Sidelobe | -40 | 0.02 | 24.9 |

The predicted errors in table 3 are very close to the results of the error simulation with one-dimensional data in all cases.

The sidelobe errors for off-axis steering are definitely the most serious and are the ones to consider in designing a measurement system. It must be remembered that these are worst case type errors and result when there is a very special position error which concentrates all of its effect in one or a few directions. It is evident in figure 18 that the error is very large in two directions, but quite small in all other directions. Also it is unlikely that the error function would be a single frequency sinusoid but more likely that the error would be composed of a number of frequency components with much smaller amplitudes than $\Delta_m$. In actual practice then, through careful design and measurement, the sidelobe errors as well as those for other parameters due to x-y position error will be much less than the upper bounds illustrated in table 3.

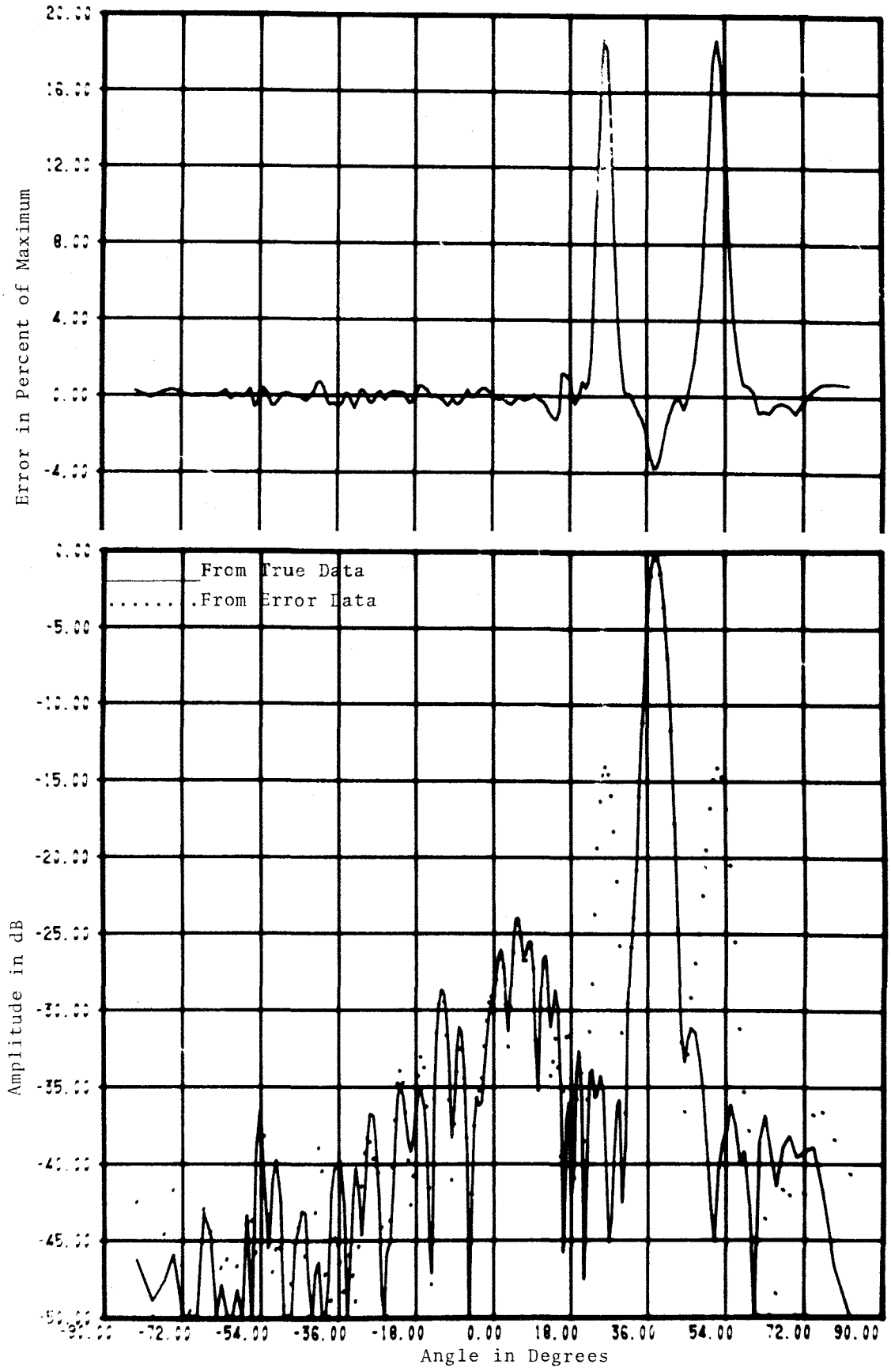


Figure 18. Sidelobe Error for Steered Beam $\Delta_{mx} = 0.10\lambda$.

### 3.1.2 Probe z-Position Errors

The analysis of z-position errors follows very similar lines to the last section for x-y errors and many of the results of the last section can be used with only slight modification. In this case we assume that the probe is at the correct x-y position, but there is a small error in its z-position given by

$$z' = d + \Delta z(\underline{P}), \tag{90}$$

and the change in the measured data is

$$B(\underline{P},z') = B(\underline{P},d) + \frac{\partial B(\underline{P},z)}{\partial z}\,\Delta z(\underline{P}). \tag{91}$$

Since we are looking at z-position errors, we have made the dependence of B upon z explicit. The partial derivative can be determined from eq. (25a) in the same way that $\nabla B(\underline{P})$ was obtained to give

$$\frac{\partial B(\underline{P},z)}{\partial z} = iFA \int \gamma(\underline{K}) D(\underline{K}) e^{i\gamma d}\, e^{i\underline{K}\cdot\underline{P}}\, d\underline{K}. \tag{92}$$

For the narrow beam antennas under study, $\gamma(\underline{K})$ will be essentially constant over the significant part of the integral in eq. (92) and can be taken outside the integral. The z-derivative of $B(\underline{P},z)$ in terms of general amplitude and phase functions and from eq. (92) is then

$$\frac{\partial B(\underline{P},z)}{\partial z} = a'(\underline{P},z)e^{i\phi(\underline{P},z)} + i\phi'(\underline{P},z)\, B(\underline{P},z) \cong i\gamma(\underline{K}_b)\, B(\underline{P},z). \tag{93}$$

This expresses the facts which are observed in the near-field measurements that

$$a'(\underline{P},z) \cong 0, \tag{94a}$$

and

$$\phi'(\underline{P},z) \cong \gamma(\underline{K}_b) = \frac{2\pi}{\lambda}\cos\theta. \tag{94b}$$

That is, that the amplitude change is very small for z-motion of the probe, while the phase change is large. Using eqs. (91), (92), and (25a), and the convolution theorem, we obtain the two forms of the error equation for z-errors which correspond to eqs. (34) and (36)

$$\Delta D(\underline{K}) = i[\gamma(\underline{K})\, D(\underline{K})] * H(\underline{K}) \tag{95}$$

$$\Delta D(\underline{K}) = \frac{e^{i\gamma d}}{4\pi^2 FA_n} \int \left[\frac{\partial B(\underline{P},z)}{\partial z}\, e^{-i\underline{K}\cdot\underline{P}}\right] \Delta z(\underline{P})\, d\underline{P}, \tag{96}$$

where $H(\underline{K})$ is the spectrum of the error function

$$H(\underline{K}) = \frac{1}{4\pi^2} \int \Delta z(\underline{P}) e^{-i\underline{K}\cdot\underline{P}}\, d\underline{P} = \mathcal{F}[\Delta z(\underline{P})]. \tag{97}$$

Before proceeding to evaluate eqs. (95) or (96) for the various cases, two special z-position errors should be considered. The first is one where $\Delta z(\underline{P})$ = constant = $\Delta d$. Since d does not appear in the integrand of eq. (25b), a position error of this type will not produce any error in the gain or relative pattern. The only effect it will have is to uniformly change the phase of the far-field by the amount $e^{i\gamma\Delta d}$. Therefore, $|\Delta D(\underline{K})| = 0$ when $\Delta z(\underline{P})$ = constant, and

$$\Delta D_1(\underline{K}) = \Delta D_2(\underline{K}) \tag{98}$$

when

$$\Delta z_2(P) = \Delta z_1(\underline{P}) + \text{constant}, \tag{99}$$

where $\Delta D_1(\underline{K})$ and $\Delta D_2(\underline{K})$ are the errors resulting from $\Delta z_1(\underline{P})$ and $\Delta z_2(\underline{P})$ respectively. This means that we can add a small arbitrary constant to a given z-position error function without changing its effect on the far-field pattern or gain. This fact will be useful in some of the following analyses.

The second special error is one which is linear in $\underline{P}$ and given by the relationship

$$\Delta z(\underline{P}) = \alpha x + \beta y. \tag{100}$$

This error would result from a rotational misalignment of the test antenna with respect to the measurement plane and results in a shift of the entire pattern by the angles

$$\Delta A = \arctan \alpha, \quad \Delta E = \arctan \beta. \tag{101}$$

The relative shape of the pattern is not changed and the only error is in our knowledge of the direction angles to a specific part of the pattern, such as at the peak or null of the main beam. Therefore when analyzing the effect of a given error function, both the constant and linear terms should be removed before determining its effect on the gain or relative pattern.

The functional form of $\Delta z(\underline{P})$ which will produce the maximum error at $\underline{K} = \underline{K}_a$ is, as before, proportional to the complex conjugate of the quantity in the brackets of eq. (96). Since $\Delta z(\underline{P})$ must be a real function, the maximum realizable condition occurs where $\Delta z(\underline{P})$ is proportional to either the real or imaginary parts of the bracketed expression.

From eqs. (93) and (96), the worst case error function is then

$$\Delta z(\underline{P}) = \delta_m a(\underline{P},z) \sin [\phi(\underline{P},z) - \underline{K}_a \cdot \underline{P}] \tag{102}$$

if we use the real part, and

$$\Delta z(\underline{P}) = \delta_m a(\underline{P},z) \cos [\phi(\underline{P},z) - \underline{K}_a \cdot \underline{P}] \tag{103}$$

if we use the imaginary part. In both cases, $\delta_m$ is the maximum error in the z-position, and the proportionality constant has been taken as $\delta_m/\gamma$ so that the maximum value of the error will be attained when $a(\underline{P},z) = 1.0$.

For the case where the main beam or difference null is centered on the z-axis, the error at $\underline{K}_b = \underline{K}_a = 0$ is given by

$$\Delta D(0) = \frac{ie^{i\gamma d}k}{4\pi^2 FA_n} \int B(\underline{P})\ \Delta z(\underline{P})\ d\underline{P}. \tag{104}$$

An arbitrary change in the reference plane by a constant amount will not cause any error in the far-field pattern since we can chose any reference plane on which to make the measurements. If we change the reference plane by a constant amount to obtain a new error function.

$$\Delta z_2(\underline{P}) = \Delta z_1(\underline{P}) + C \tag{105}$$

then the resultant error at $K_a = 0$ is given by

$$\Delta D(0) = \frac{ie^{i\gamma d}k}{4\pi^2 FA_n} \left( \int B(\underline{P},z)\Delta z(\underline{P})\ d\underline{P} + C \int B(\underline{P},z)\ d\underline{P} \right). \tag{106}$$

For a sum pattern the second integral in eq. (106) will be positive, and we can therefore choose C to make $\Delta D(0) = 0$. This result is similar to the case for the effect of x-y errors on a steered main beam, and indicates that the first order term is not sufficient and higher order terms must be used. When we use the second order term the on-axis error becomes

$$\Delta D(0) = \frac{e^{i\gamma d}}{2\pi^2 FA_n} \int \frac{\partial^2 B(P,z)}{\partial z^2} [\Delta z(\underline{P})]^2\ d\underline{P} \tag{107}$$

$$= -\frac{e^{i\gamma d}k^2}{2\pi^2 FA_n} \int B(\underline{P})[\Delta z(P)]^2\ d\underline{P}. \tag{108}$$

For a sum pattern, both factors in the integrand will be positive for all values of $\underline{P}$, and the error cannot be reduced to zero by an arbitrary shift in the measurement plane. The error resulting from the second order term may now be evaluated by using a form similar to eqs. (95) and (72)

$$\Delta D(0) = -k^2[D(\underline{K}) * |H(\underline{K})|^2] \tag{109}$$

Using the Schwarz inequality and Rayleigh's theorem on the above expression with the earlier approximation for the main beam, we obtain

$$\left|\frac{\Delta D(0)}{D(0)}\right|_{\%} \leq \frac{493}{\sqrt{n}} \left(\frac{\delta_m}{\lambda}\right)^2 \tag{110}$$

$$\left|\frac{D_e(0)}{D(0)}\right|_{dB} \leq \frac{43}{\sqrt{n}} \left(\frac{\delta_m}{\lambda}\right)^2. \tag{111}$$

In the following discussion concerning monopulse type patterns, it will be helpful to refer to the results of the error simulation to illustrate the steps in the analysis. The pattern under discussion is similar to the one shown in figure 19, and we want to determine the effects of z-position errors on the position and depth of the minimum in the boresight direction. Let us assume that the pattern shown in figure 19 is for the principle plane, $k_y = 0$, and that the near-field amplitude and phase along the line $y = 0$ are similar to those shown in figure 20. In the error simulation program, the measured data shown in figure 20 is stored in the computer and the far-field pattern is computed using these data and eq. (25b). These input data and the resulting far-field are considered to be the "true" values with no z-position errors present. We next modify the input data by changing the amplitude and/or phase in a way which represents the effects of the worst case z-position error. The far-field is again computed using the modified data and compared to the original results to determine the effects of the simulated errors. This is repeated using different values of $\delta_m$ and near-field data from other antennas.

In the present case for $\underline{K}_a = \underline{K}_b = 0$, eq. (103) gives the worst-case error function as

$$\Delta z(\underline{P}) = \delta_m \, a(\underline{P}) \cos(\phi(\underline{P},z)) \tag{112}$$

and from eqs. (91) and (94) the modified data are

$$a_e(\underline{P}) = a(\underline{P}) \tag{113a}$$

$$\phi_e(\underline{P},z) = \phi(\underline{P},z) + k\delta_m a(\underline{P}) \cos(\phi(P,z)) \tag{113b}$$

where $a_e$ and $\phi_e$ are the modified amplitude and phase functions. When this change is made in the input data, the simulated phase error resulting from the z-position error is shown in figure 21. This phase error has two effects on the far-field pattern as shown in figure 22. The entire pattern has been shifted and there is also some change in the shape of the pattern. The shift complicates both the mathematical analysis and the simulation when trying to determine the change in the depth of the minimum. For in the analysis we must compare $\mathcal{D}(0)$ with $\mathcal{D}_e(0+\underline{\varepsilon})$ since the minimum of the error pattern is at $\underline{K} = \underline{\varepsilon}$ and since the pattern is so sharp in this region, we must know quite closely how much shift is introduced by a given error $\delta_m$. In the simulation, a problem arises because we do not have continuous data, since the digital transformation provides far-field values at discrete, equally-spaced points as shown by the error pattern in figure 22. (In the "true" pattern the points have been connected by straight-line interpolation to distinguish between the curves.) A data point may not occur exactly at $\underline{K} = \underline{\varepsilon}$, and due to the sharpness of the curve, comparison of a point which is not at $\underline{\varepsilon}$ with the original minimum may be misleading.

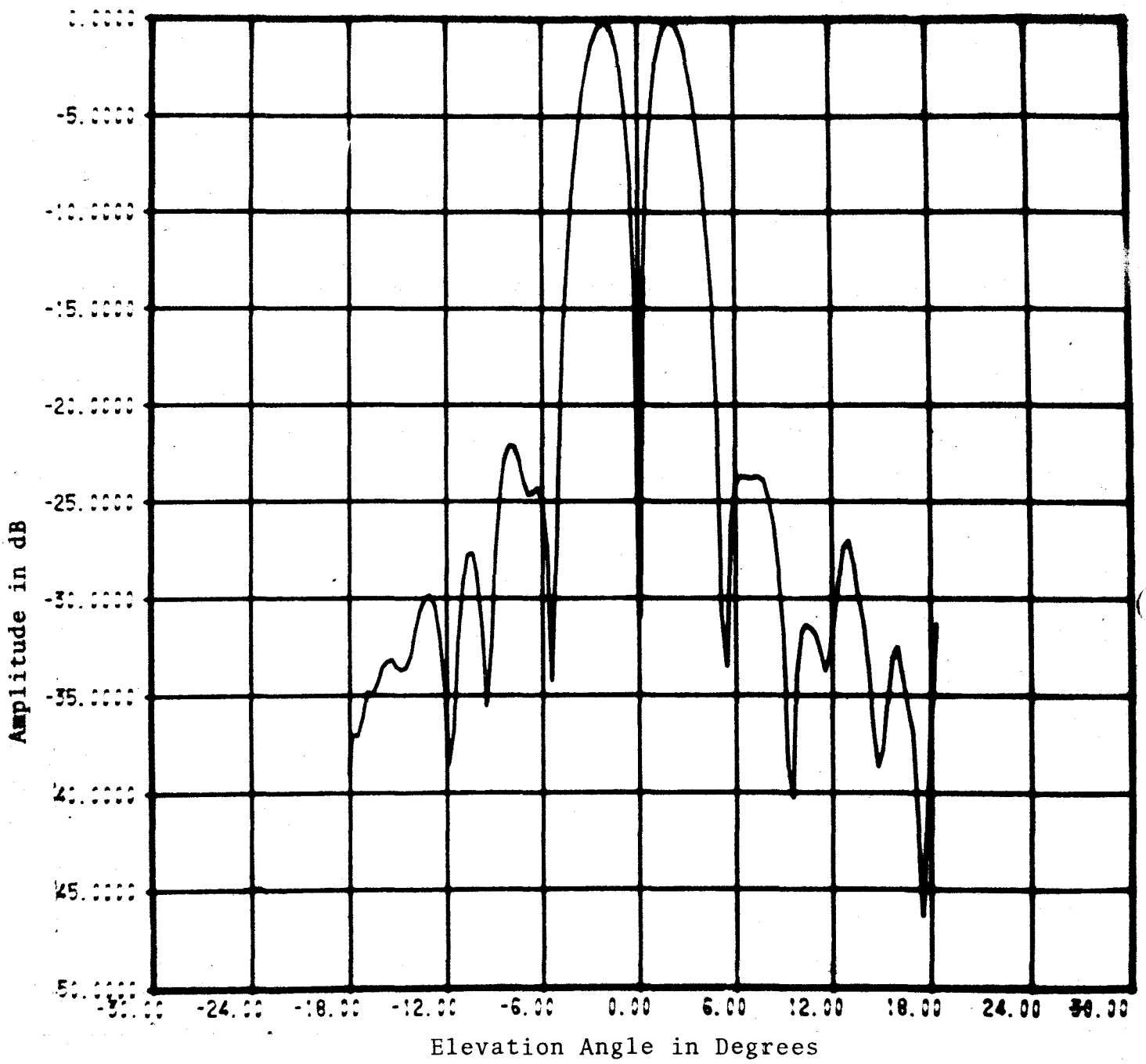


Figure 19. Far-Field Amplitude for Monopulse Difference Pattern Obtained from Near-Field Data.

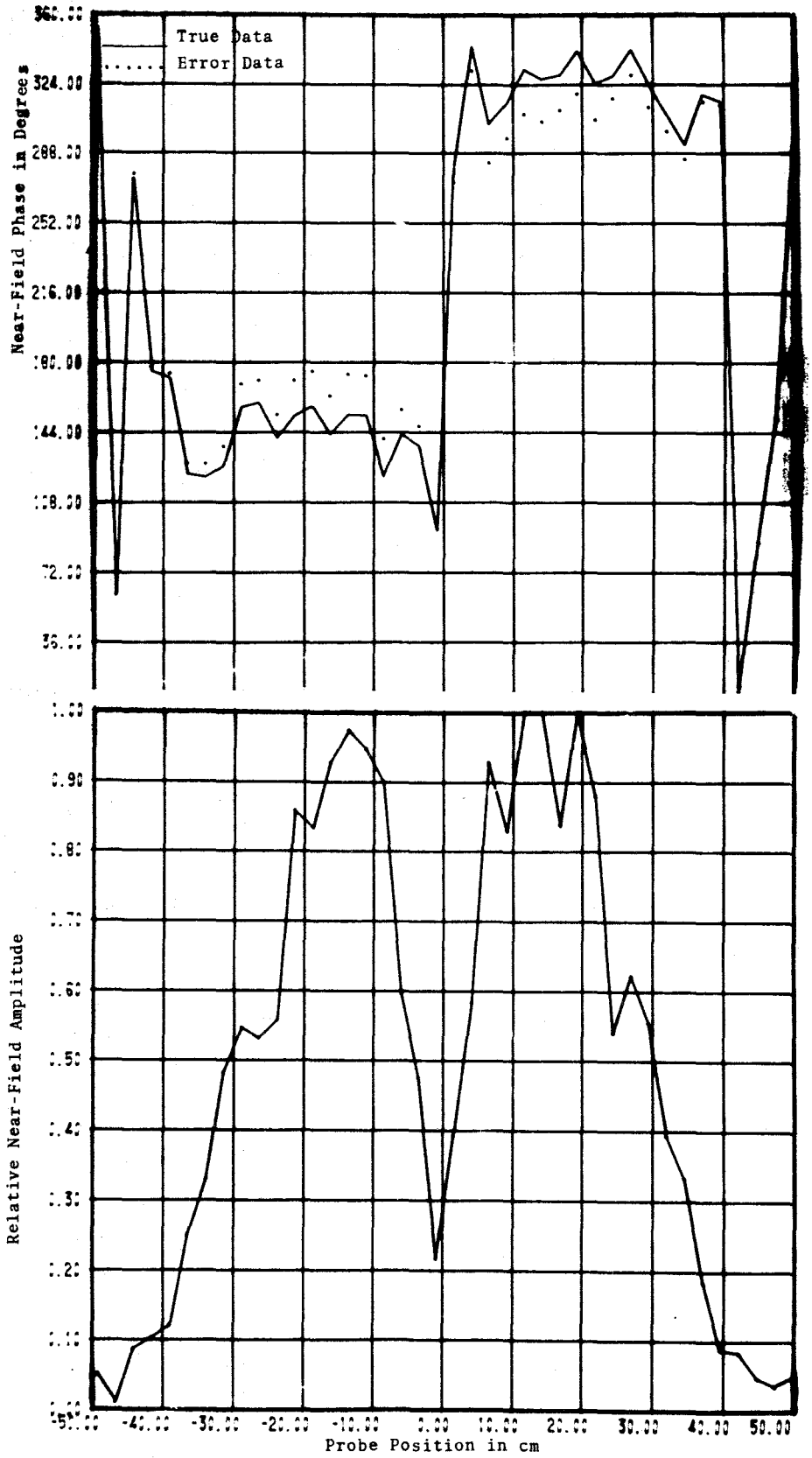


Figure 20. Near Field Data for Monopulse Difference Type Pattern.

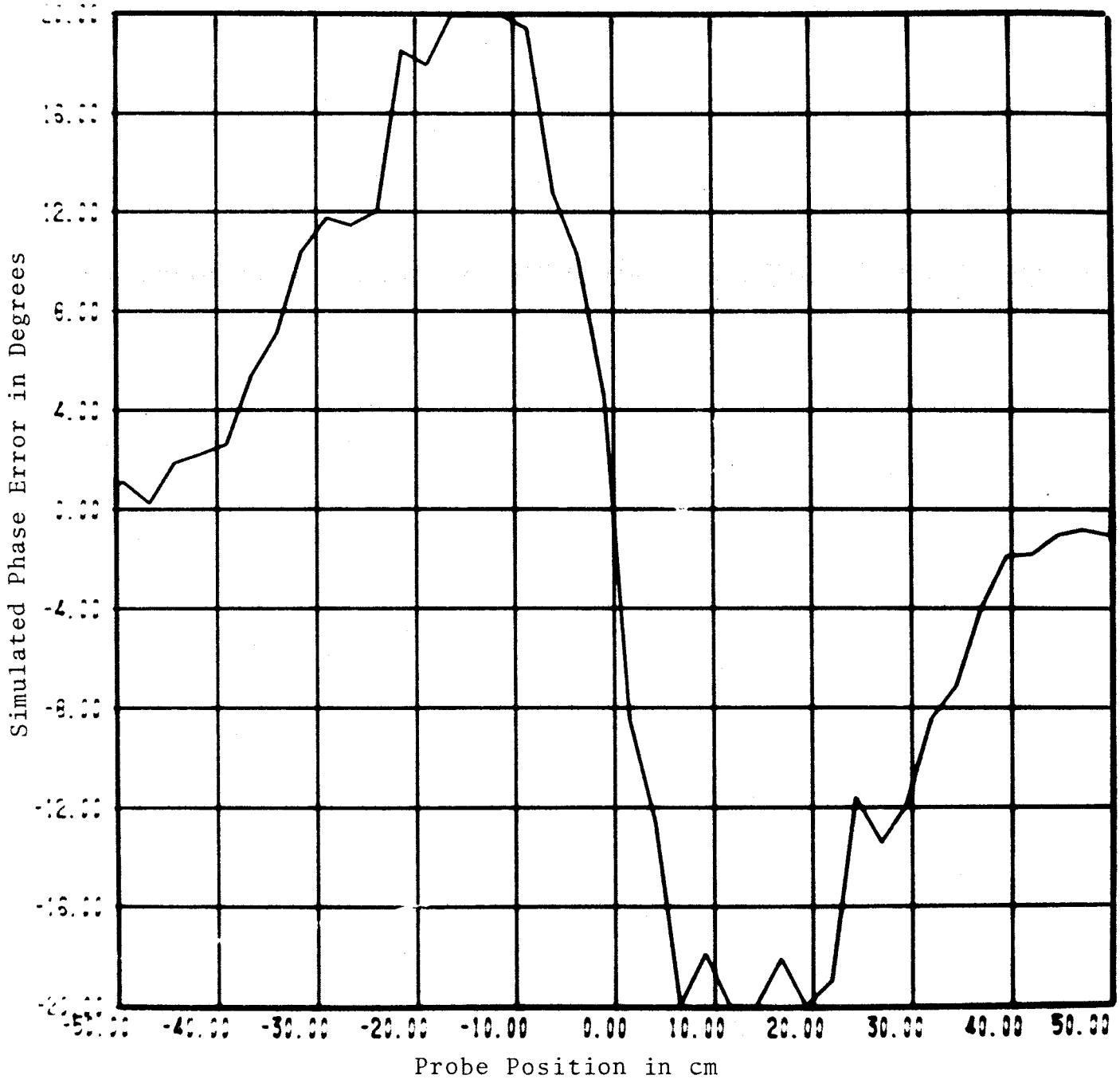


Figure 21. Near-Field Phase Error Resulting From Simulated Worst-Case Z-Position Error.

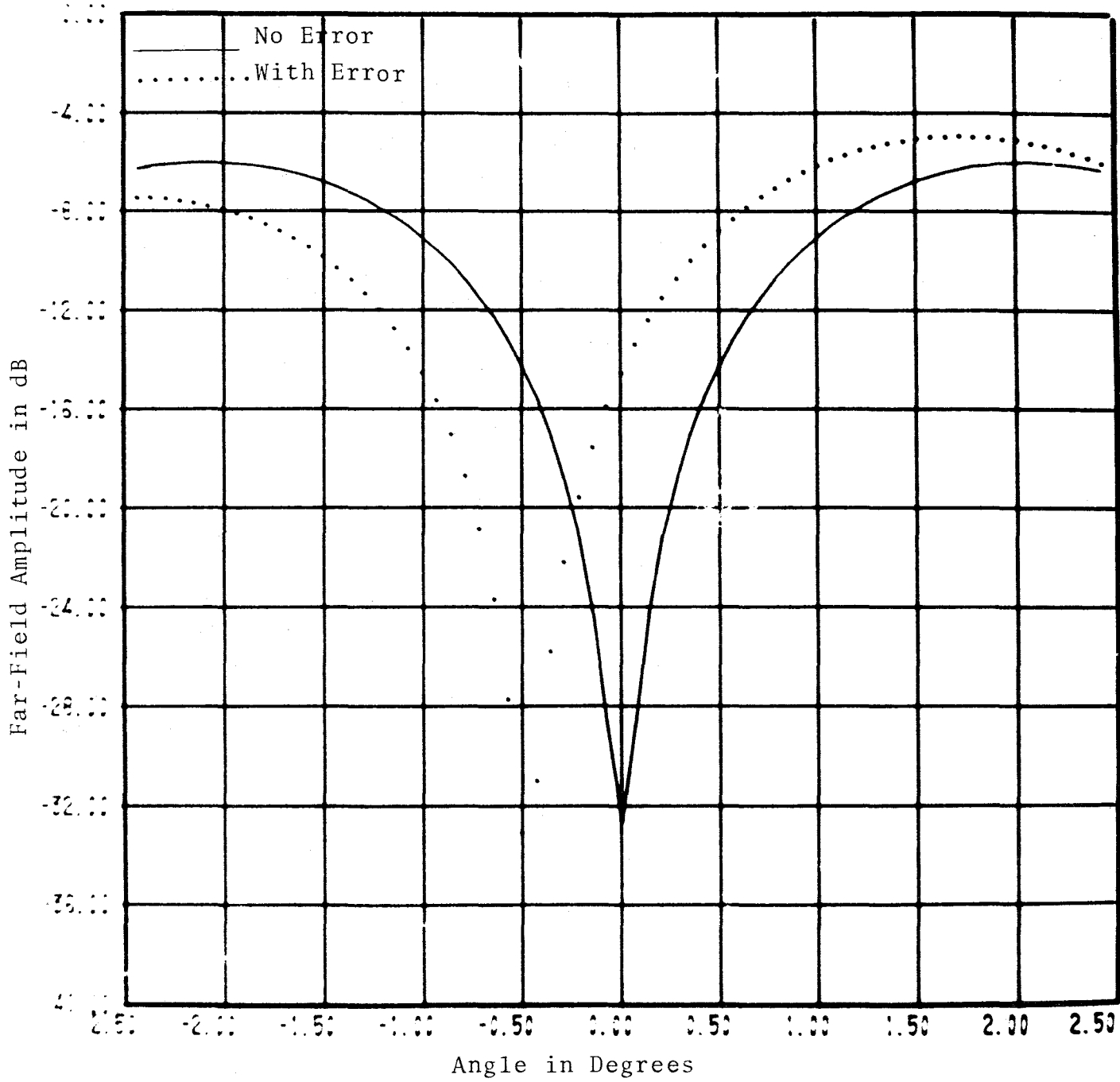


Figure 22. Monopulse Difference Minimum With and Without Simulated Worst-Case Z-Position Error.

To overcome this difficulty in the simulation, a linear phase correction is applied to the near-field data along with the simulated z-position error to shift the minimum back to $\underline{K} = 0$. The modified phase is then given by

$$\phi_e(\underline{P},z) = \phi(\underline{P},z) + \delta_m k\, a(\underline{P}) \cos(\phi(\underline{P},z)) - \alpha x. \tag{114}$$

The value of $\alpha$ is chosen to make the minimum of the error pattern occur at $\underline{K} = 0$, and this sometimes requires multiple runs to find the correct value. The result of this modification to the phase error on the error spectrum is shown in figure 23, and it is apparent that now we can compare the two curves point by point to find the change in the minimum depth or sidelobe level.

We have previously shown that the linear phase correction used here will not change the shape of the pattern, and so this does not alter the results. In effect, we have removed whatever linear term there is in the position error by the above technique and can now analyze the effect of the remainder of the error function. This approach has the added benefit that we obtain an approximate empirical relationship between the maximum position error and shift in the boresight direction which will be of value in the analysis.

Table 4 below summarizes the results of the z-position error simulation on two monopulse antennas. Two sets of data were used for both antennas. The first was the actual measured data and in the second, the amplitude for $x \geq 0$ was modified to make it more nearly equal to the amplitude for $x < 0$. This amplitude modification resulted in a lower minimum in the boresight direction and demonstrated the dependence of the error on the magnitude of the minimum. The modified near-field data and the resulting far-field pattern for one antenna are shown in figures 24 and 25 (compare with figures 20 and 22).

It is apparent from Table 4 that the error in the depth of the monopulse difference minimum is linearly proportional to the maximum position error $\delta_m$, and inversely proportional to the magnitude of the minimum. Furthermore, the shift in the boresight direction is also linear in $\delta_m$.

$$\left|\frac{\mathcal{D}_e(0)}{\mathcal{D}(0)}\right| = C_1 \left|\frac{D(0)}{\mathcal{D}(0)}\right| \delta_m \tag{115}$$

$$\Delta A = C_2\, \delta_m$$

It is also evident that $C_1$ is not the same for the two antennas, and the simulation does not give much indication why they are different or what antenna characteristic determines the magnitude of $C_1$. To determine these factors, the mathematical analysis must be used.

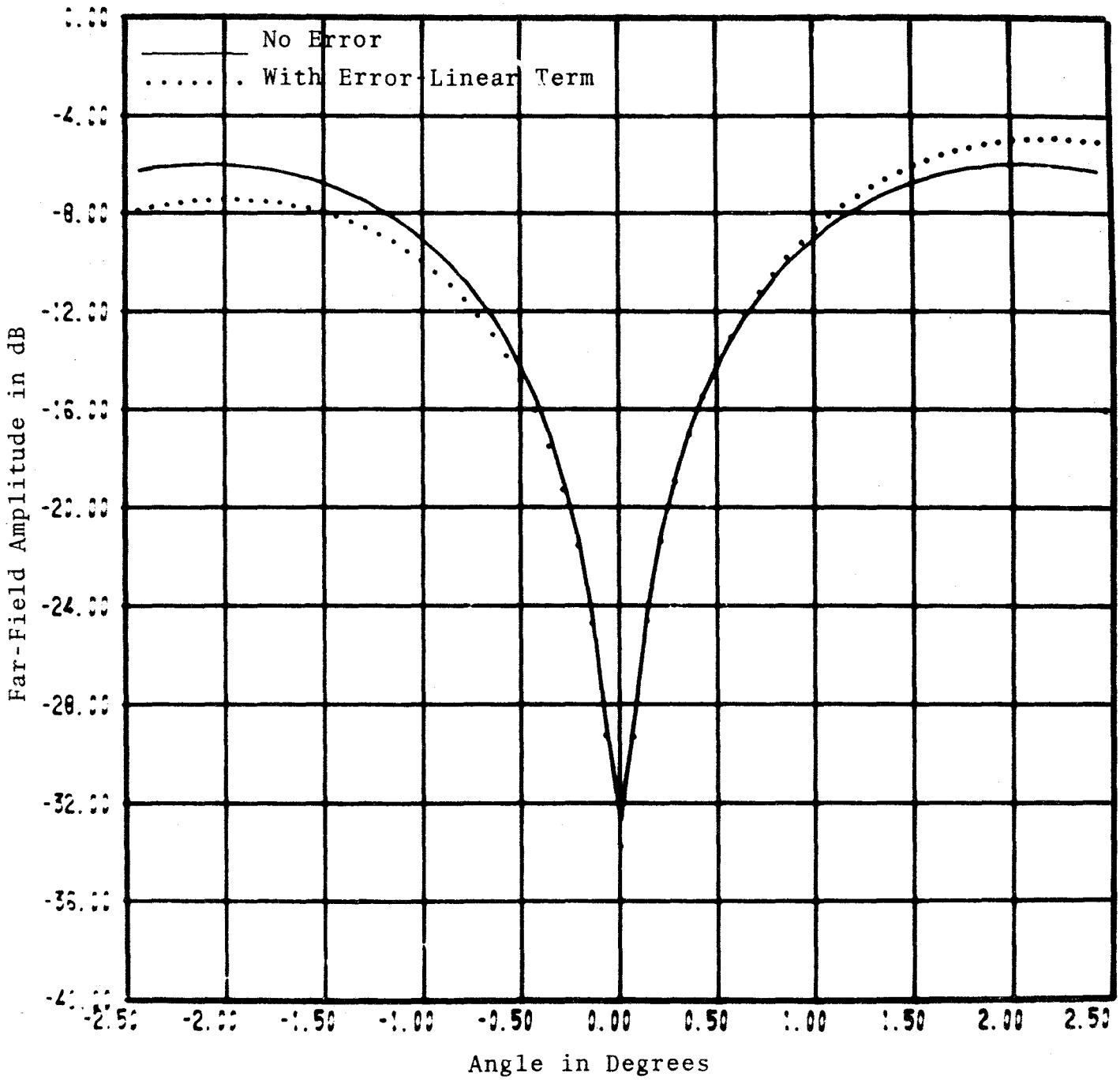


Figure 23. Monopulse Difference Minimum Without Error and With Worst-Case Z-Position Error Minus Linear Term.

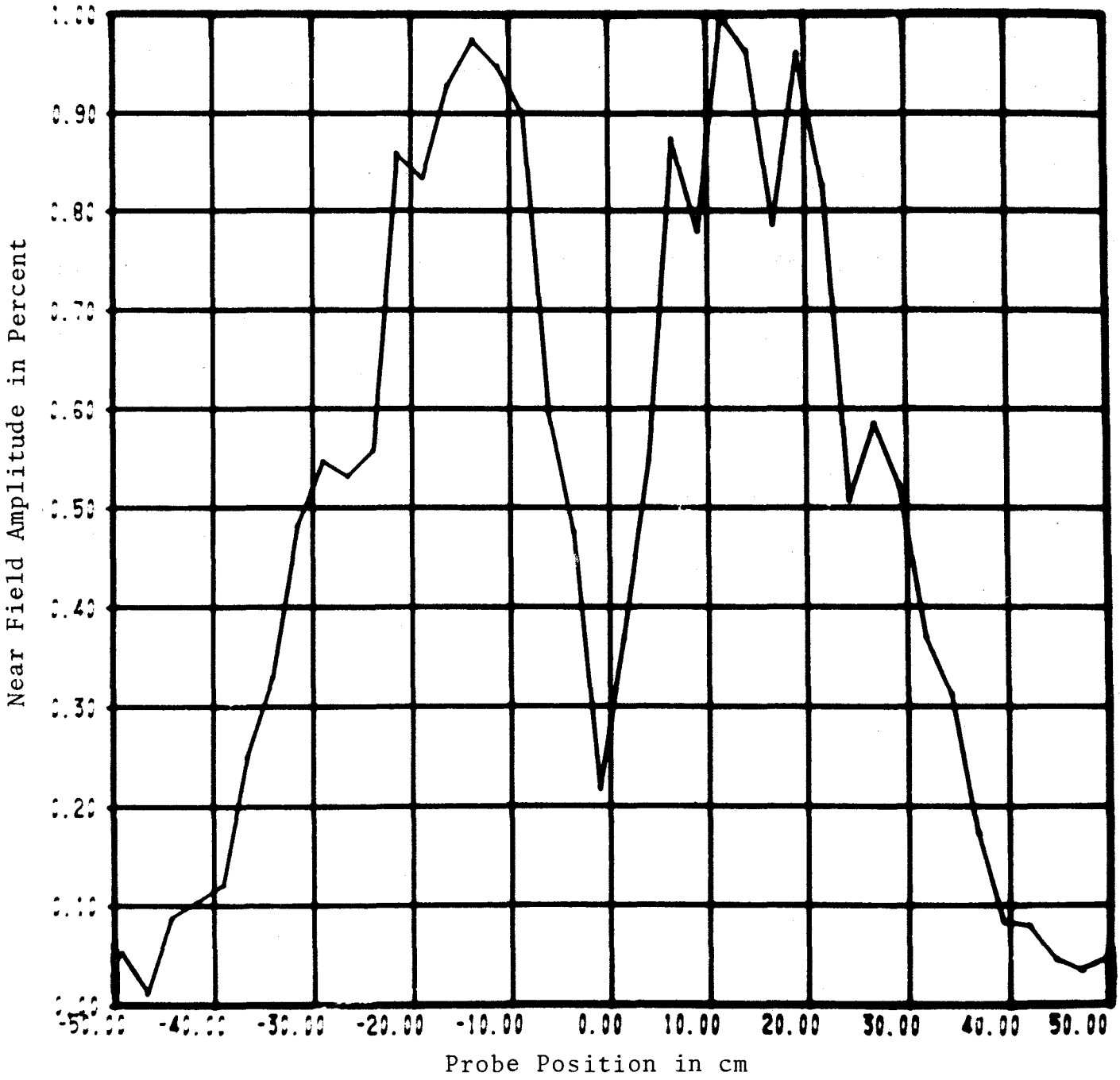


Figure 24. Modified Near Field Amplitude to Produce Lower Far-Field Difference Minimum.

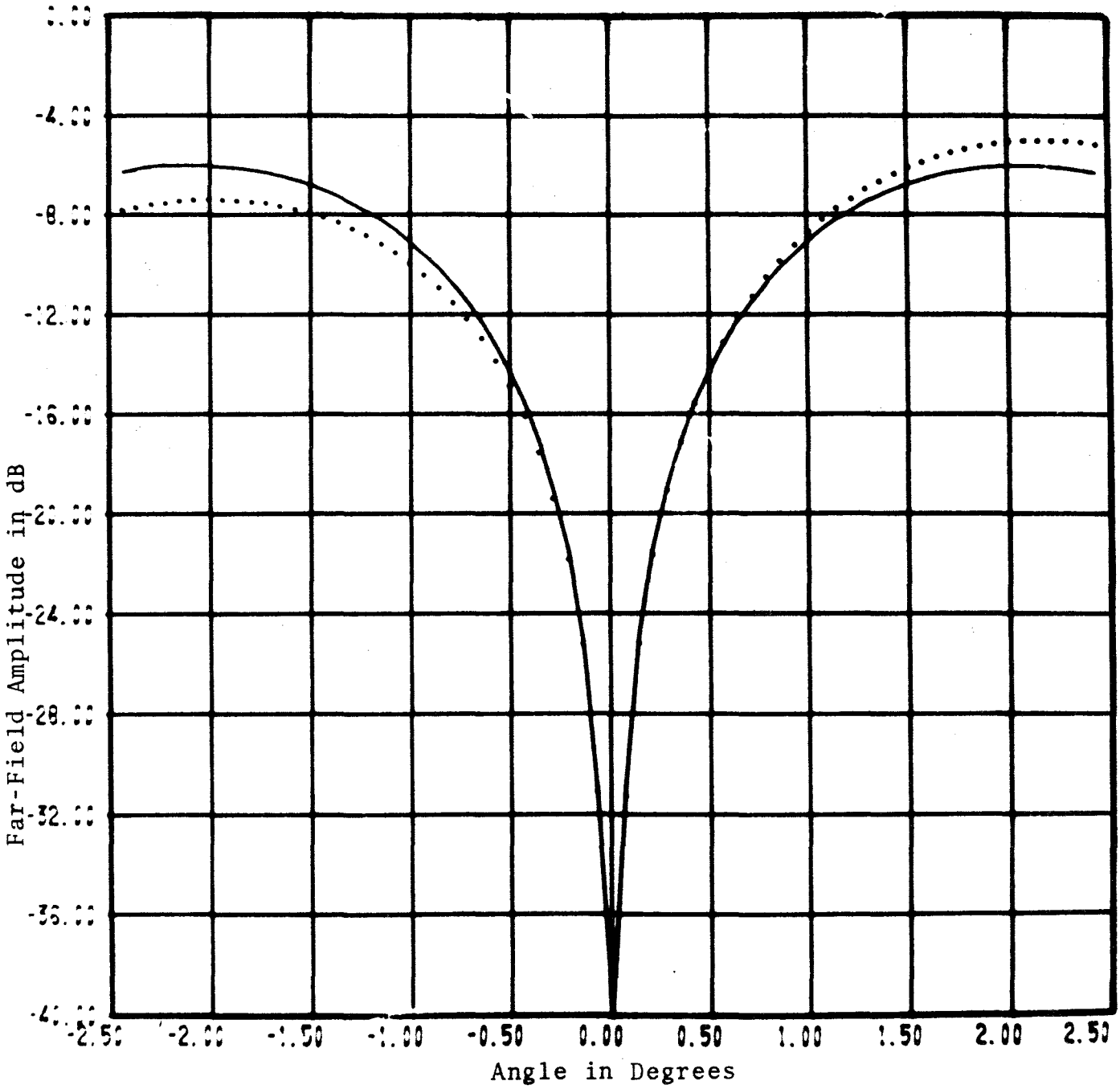


Figure 25. Monopulse Difference Minimum Resulting From Modified Near-Field Amplitude.

Table 4. Summary of Results from z-Error Simulation

| Antenna | f | True Minimum (dB) | Maximum z-Position Error | Change in Minimum (dB) | Shift in Minimum (deg) |
|---|---|---|---|---|---|
| Constrained lens | 9.2 | -30.7 | 0.02λ | -0.3 | -0.16 |
| | | | 0.04λ | -0.5 | -0.31 |
| | | | 0.06λ | -0.7 | -0.47 |
| Constrained lens (Modified Amplitude) | 9.2 | -49.6 | 0.02λ | -2.7 | -0.16 |
| | | | 0.04λ | -6.3 | -0.31 |
| | | | 0.06λ | -10.2 | -0.47 |
| Volphase | 8.4 | -23.8 | 0.02λ | -0.4 | -0.15 |
| | | | 0.04λ | -0.7 | -0.31 |
| | | | 0.06λ | -1.0 | -0.46 |
| Volphase (Modified Amplitude) | 8.4 | -35.4 | 0.02λ | -1.4 | -0.15 |
| | | | 0.04λ | -2.8 | -0.31 |
| | | | 0.06λ | -4.00 | -0.46 |

Let us approximate the essential features for the azimuthal difference mode near-field by

$$B(\underline{P},z) = f(x)\, g(y) \tag{116}$$

where

$$f(x) = \begin{cases} -\sin^2\left(\frac{2\pi x}{L_x}\right) & x \leq 0 \\ \alpha \sin^2\left(\frac{2\pi x}{L_x}\right) e^{iq} & x > 0 \end{cases} \tag{117}$$

$$g(y) = \cos^2\left(\frac{\pi y}{L_y}\right) \tag{118}$$

The constants $\alpha$ and q will determine the departure from a perfect difference pattern, with $\alpha$ being nearly unity and q being close to zero. It can be shown that $\alpha$ will determine the depth of the minimum, and q will determine the symmetry of the far-field pattern. Let us further assume that in measuring the above near-field, there is a worst-case z-position error as given by eq. (103), and that due to this error, the apparent position of the difference minimum is at $k_x = \varepsilon$, $k_y = 0$. The value of $\mathcal{V}_e(\varepsilon,0)$ is then

$$\mathcal{V}_e(\varepsilon,0) = \frac{e^{-i\gamma d}}{4\pi^2 F A_n} \int g(y)dy \int f(x)\, e^{i[k\delta_m a(x) - \varepsilon x]}\, dx \tag{119}$$

$$= I_y \frac{1}{2\pi} \int f(x)[1 + i(k\delta_m a(x) - \varepsilon x)]\, dx \tag{120}$$

where $I_y$ is the integral involving $g(y)$, and $a(x)$ is the amplitude function for $f(x)$. The second order terms in the approximation of the complex exponential have been dropped since they are even functions, $f(x)$ is very nearly odd, and the integral of their product is small compared to the retained terms which appear in eq. (120). The remaining terms produce three integrals, the first of which when multiplied by $I_y$ yields the true far-field minimum $\mathcal{D}(0)$. The error in $\mathcal{D}$ is then

$$\Delta\mathcal{D}(0) = \mathcal{D}_e(\varepsilon,0) - \mathcal{D}(0) = \frac{i}{2\pi} (I_{x1}-I_{x2})\ I_y \tag{121}$$

where

$$I_{x1} = k\delta_m \int f(x)\ a(x)\ dx \tag{122}$$

$$I_{x2} = \varepsilon \int x\ f(x)\ dx \tag{123}$$

Using the assumed form for $f(x)$, $I_{x1}$, $I_{x2}$, and $I_y$ can be evaluated to give

$$I_{x1} = \frac{3L_x k\delta_m}{16} (1+\alpha^2+i\alpha^2 q), \tag{124a}$$

$$I_{x2} = \frac{L_x^2\varepsilon}{16} (1+\alpha+i\alpha q). \tag{124b}$$

$$I_y = \frac{L_y}{4\pi}\ \frac{e^{-i\gamma d}}{FA_n} \tag{124c}$$

Combining these terms, the error is then

$$\Delta\mathcal{D}(0) = \frac{3L_xL_y\delta_m}{64\pi\lambda FA_n} \left[\alpha q\left(\frac{\beta}{3}-\alpha\right) + i\left((1+\alpha^2) - \frac{\beta}{3}(1+\alpha)\right)\right] \tag{125}$$

where we have used the relation

$$\varepsilon = \frac{2\pi}{\lambda}\frac{dz}{dx} = \frac{2\pi}{\lambda}\beta\frac{\delta_m}{L_x}. \tag{126}$$

Under certain special conditions, either the real or imaginary terms may be zero, but since an upper bound is desired, these cases will not be considered. The results of the error simulation indicate that generally the two terms will be of about the same magnitude, but the real term has the major effect on the change in the null depth. This is because $\mathcal{D}(0)$ is real for the assumed near-field distribution, and therefore, in phase with the real part of eq. (125). For a more general distribution, the real part of eq. (125) will still be in phase with $\mathcal{D}(0)$ and therefore produces more of a change in the null

depth than the imaginary term. The change in the boresight minimum is then

$$\left|\frac{\mathcal{D}_e(\underline{\varepsilon})}{\mathcal{D}(0)}\right|_{dB} \leq \frac{20.2\ \delta_m\ \alpha q}{\lambda}\left(\frac{\beta}{3} - \alpha\right)\left|\frac{D(0)}{\mathcal{D}(0)}\right|. \tag{127}$$

The dependence upon q in eq. (127) is consistent with the results of the simulation, but the simulation does not show the dependence upon $\alpha$. Since $\beta \simeq 2.5$ to 3.2 and $\alpha \simeq 0.94$ to 1.2, it appears that a more realistic expression is obtained by setting the factor $\alpha(\beta/3 - \alpha)$ equal to 0.5 to give

$$\left|\frac{\mathcal{D}_e(\underline{\varepsilon})}{\mathcal{D}(0)}\right|_{dB} \leq 10.1q\left|\frac{D(0)}{\mathcal{D}(0)}\right|\left(\frac{\delta_m}{\lambda}\right). \tag{128}$$

Also from the simulation it is apparent that q determines the symmetry of the difference pattern, and we can estimate q from the ratio in the maxima on each side of the boresight minima. If we denote the ratio of these maxima in dB by Q, then q in radians is approximately

$$q \cong \frac{Q}{3},$$

and the error equation in terms of far-field parameters is

$$\left|\frac{\mathcal{D}_e(\underline{\varepsilon})}{\mathcal{D}(0)}\right|_{dB} \leq 3.4Q\left|\frac{D(0)}{\mathcal{D}(0)}\right|\left(\frac{\delta_m}{\lambda}\right). \tag{129}$$

For errors in regions off the main beam, the results are essentially the same for sum and difference patterns and are similar to the case for x-y position errors when the beam is steered off axis. The worst-case z-position error is given by eq. (102) or (103) with $\underline{K}_a \neq 0$ and is therefore equal to the amplitude modulated by a periodic function. The error in a sidelobe at $\underline{K}_a$ is obtained from eq. (95) where $H(\underline{K})$ is approximated by delta functions at the combinations of $\pm k_{xa}$ and $\pm k_{ya}$ given in eq. (77). The magnitude of these delta functions is $\delta_m/4$, due to one factor of 1/2 which arises from the fact that the error function produces two sidebands, and another factor of approximately 1/2 because the variations in z should be measured from the average value and not the minimum value. The resulting error expression is

$$\left|\frac{D_e(\underline{K}_a)}{D(\underline{K}_a)}\right|_{dB} \leq 13.5\left|\frac{D(0)}{D(K_a)}\right|\left(\frac{\delta_m}{\lambda}\right). \tag{130}$$

When the beam is steered away from the z-axis, the only change in the analysis is that gamma is not equal to k but is now

$$\gamma(\underline{K}_b) = k\sqrt{1 - (K_b/k)^2} = k\cos\theta_b. \tag{131}$$

Equations (111), (129), and (130) may then be generalized to any steering direction by using eq. (131) in place of k and $\underline{K}_b$ in place of 0 to give for a sum pattern,

$$\left|\frac{D_e(\underline{K}_b)}{D(\underline{K}_b)}\right|_{dB} \leq \frac{43}{\sqrt{\eta}} \left(\frac{\delta_m}{\lambda}\right)^2 \cos^2\theta_b \tag{132}$$

for the difference minimum,

$$\left|\frac{\mathcal{D}_e(\underline{K}_b+\underline{\varepsilon})}{\mathcal{D}(\underline{K}_b)}\right|_{dB} \leq 3.4Q\left|\frac{D(\underline{K}_b)}{\mathcal{D}(\underline{K}_b)}\right| \left(\frac{\delta_m}{\lambda}\right) \cos\theta_b \tag{133}$$

and for a sidelobe on either type pattern,

$$\left|\frac{D_e(\underline{K}_a)}{D(\underline{K}_a)}\right|_{dB} \leq 13.5\left|\frac{D(\underline{K}_b)}{D(\underline{K}_a)}\right| \left(\frac{\delta_m}{\lambda}\right) \cos\theta_b. \tag{134}$$

### 3.1.3 Instrumentation Errors in Measured Amplitude and Phase

In the last two sections it has been shown that position errors result in incorrect values for the amplitude and/or phase and therefore produce errors in the computed far-field parameters. In this section the electronic equipment used to measure and record the probe output will be treated to determine the types and magnitudes of errors which they produce.

The main subject for study is the RF receiver which detects the probe output at the operating frequency and converts the measured signal to a lower frequency where the amplitude and phase are measured. Ideally the conversion and the measurement are linear, and the receiver output is directly proportional to the probe output $B(\underline{P})$. In fact there are nonlinearities present due to such things as mixer non-linearity, interference and noise signals within the receiver, sensitivity and linearity of detectors and resolution of digitizers. Their combined effects may be represented by the relation

$$B_e(\underline{P}) = \nu(a,\phi)\ B(\underline{P}) \tag{135}$$

where $B(\underline{P})$ is the true probe output, $B_e(\underline{P})$ is the receiver output, and $\nu(a,\phi)$ represents the receiver response which is in general a function of the amplitude a and the phase $\phi$. Certain special cases of $\nu(a,\phi)$ have already been treated in the position error section, because the worst-case position errors were usually function of a and $\phi$ also, and produced errors in $B(\underline{P})$. For instance, the worst-case z-error resulted in a phase error given by

$$\Delta\phi(a,\phi) = k\ \delta_m\ a(\underline{P})\ \cos\ (\phi(\underline{P})) \tag{136}$$

and produced errors in the far-field given by eq. (132), (133), and (134), and the worst case x-y error for the main beam on-axis resulted in an amplitude error given by eq. (30) and (40)

$$\Delta a(a,\phi) \propto \nabla a(\underline{P}) \cdot \nabla a(\underline{P}) \tag{137}$$

which led to the results in eqs. (84), (85), and (86). These results are of value, but may not represent the upper bound type errors which are the object of this analysis.

To obtain expressions for the errors in $D(\underline{K})$ we substitute eq. (135) into (25b) and employ the Schwarz inequality to show that the change in $D(\underline{K})$ will be a maximum at $\underline{K} = \underline{K}_a$ if

$$\nu(a,\phi) \propto \left[B(\underline{P})e^{-i\underline{K}_a \cdot \underline{P}}\right]^* . \tag{138}$$

This implies an unrealistically large error in both the near and far-fields, for it would mean that

$$a_e(\underline{P}) = [a(\underline{P})]^2 \tag{139}$$

and for instance where $a(\underline{P}) = -20$ dB, the measured value would be -40 dB. A 20 dB error at this level is completely unreasonable. Equation (139) does suggest a form for the amplitude error which is consistent with observations however and given by

$$a_e(P) = [1 + (a(\underline{P}) - 1)\mu]\, a(\underline{P}). \tag{140}$$

This is similar to eq. (139) because the error is zero when $a(x) = 1$, increases as $a(x)$ decreases, and is identical to eq. (139) if $\mu = 1$. When $\mu$ is small, the error has the same form as the worst case type, but is still realistic.

When the above type of error is applied to the measured data in the error simulation program, it resembles quite closely the scale error described at the beginning of section 3.1.1 and formulated in eqs. (28) and (29). As seen in figure 26, the effect is to decrease the apparent size of the aperture, which will reduce the far-field gain and increase the beam width. Since eq. (29) gives an exact formulation for the effect of the scale error, the effect of the above amplitude error will also be known if we can obtain a relation between $\mu$ and $\alpha$. Such a relation was derived from the results of the simulation, and showed that for a variety of antenna types,

$$\alpha \cong 1 + 0.35\mu. \tag{141}$$

When the amplitude function in the y-direction and its error are included, the error at $\underline{K}_a = \underline{K}_b$ is then

$$\left|\frac{D_e(K_b)}{D(K_b)}\right|_{dB} \leq 6.0\mu \tag{142}$$

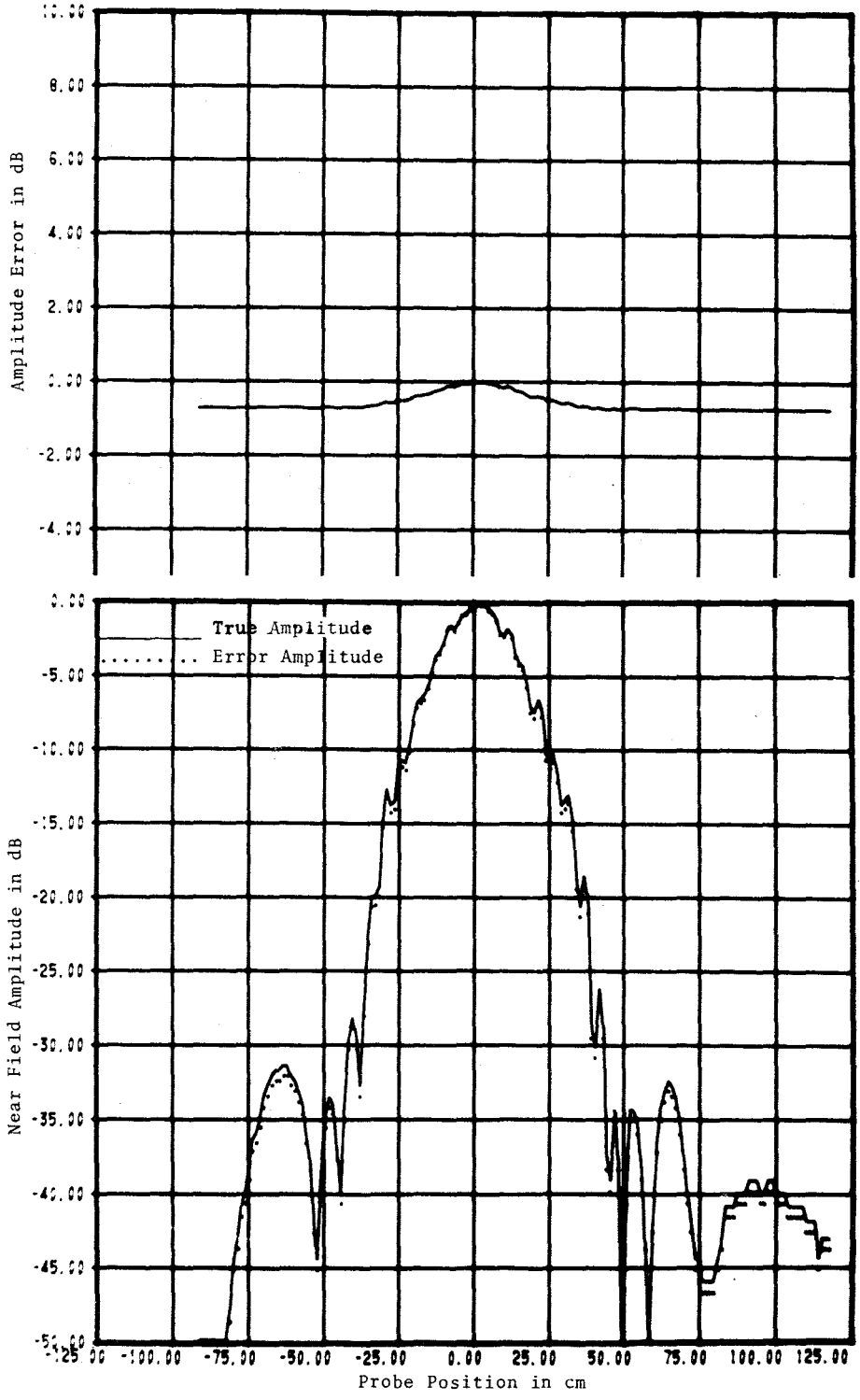


Figure 26. Near-Field Amplitude with Non-Linear Amplitude Error.

This result is valid for either a sum or difference type pattern and includes the case when the beam is along or steered off the z-axis. If $\mu$ is not a constant, but is a periodic function of the amplitude and therefore a function of x and y, the maximum error will occur in directions other than boresight with the magnitude

$$\left|\frac{D_e(\underline{K}_a)}{D(\underline{K}_a)}\right| = 3.0\left|\frac{D(\underline{K}_b)}{D(\underline{K}_a)}\right| \mu . \tag{143}$$

These two types of errors are illustrated in figures 26-29 which show samples of the results of the error simulation for amplitude errors. As in the case of position errors, the periodic amplitude error causes the largest effect on the far-field pattern, since most of its effect is concentrated in directions where the far-field amplitude is low.

Figures 30 and 31 show the amplitude error as a function of amplitude in dB and percent for various values of $\mu$. These graphs are helpful in evaluating the error which will result from a given receiver non-linearity. It is evident from eqs. (142) and (143) that the linearity of the receiver must be checked with a calibrated attenuator to verify its accuracy or to derive a correction curve which can be applied to the measured data.

The analysis for instrumentation phase errors has essentially been done in the section on z-position errors. It was found there that for small z-motion of the probe, only the phase of the measured signal changed, and so the errors were in fact phase errors. The results of section 3.1.2 therefore can be used here if the substitution

$$\delta_m = \frac{\lambda}{2\pi} \Delta\phi_m$$

is used, where $\Delta\phi_m$ is the maximum phase error. They are summarized here in terms of $\Delta\phi_m$ for reference. For a sum pattern,

$$\left|\frac{D_e(\underline{K}_b)}{D(\underline{K}_b)}\right|_{dB} \leq \frac{43}{\sqrt{\eta}} \left(\frac{\Delta\phi_m}{2\pi}\right)^2 ; \tag{144}$$

for the difference minimum,

$$\left|\frac{\mathcal{D}_e(\underline{K}_b+\underline{\varepsilon})}{\mathcal{D}(\underline{K}_b)}\right|_{dB} \leq 3.4Q\left|\frac{D(\underline{K}_b)}{\mathcal{D}(\underline{K}_b)}\right| \left(\frac{\Delta\phi_m}{2\pi}\right) ; \tag{145}$$

and for a sidelobe on either type,

$$\left|\frac{D_e(\underline{K}_a)}{D(K_a)}\right|_{dB} \leq 13.5\left|\frac{D(\underline{K}_b)}{D(\underline{K}_a)}\right| \left(\frac{\Delta\phi_m}{2\pi}\right) . \tag{146}$$

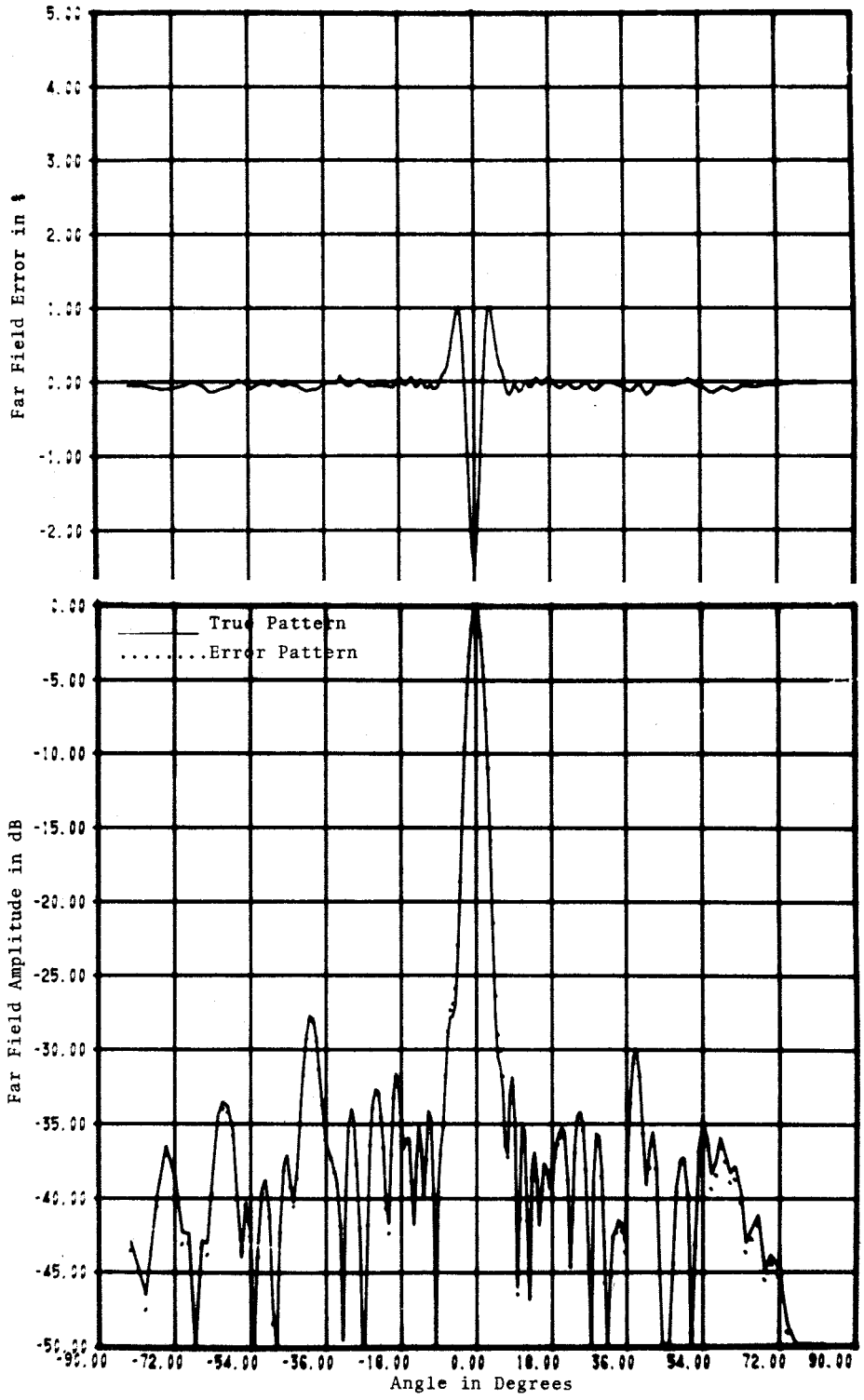


Figure 27. Error in Far-Field Due to Amplitude Non-Linearity.

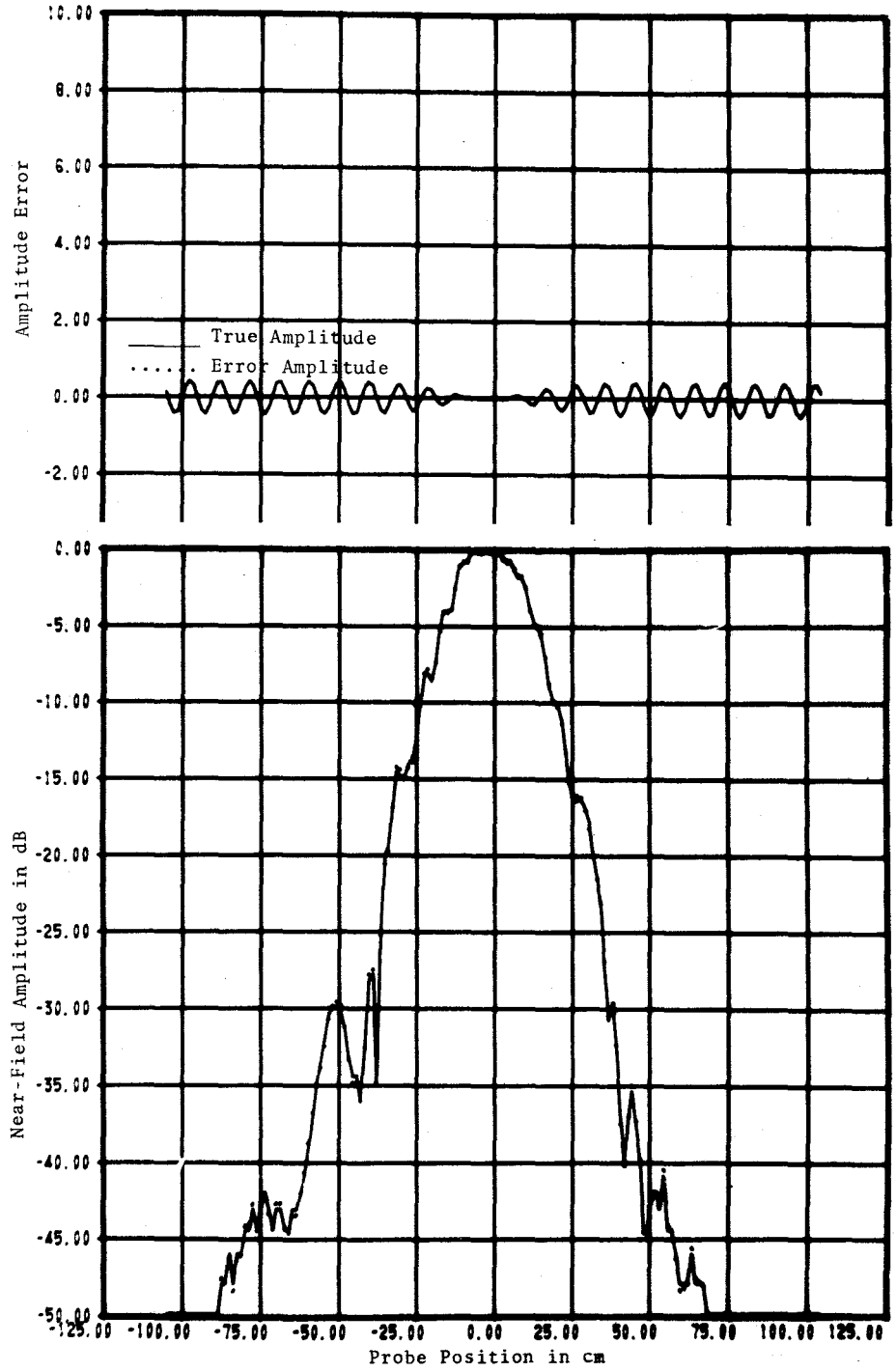


Figure 28. Periodic Non-Linear Amplitude Error.

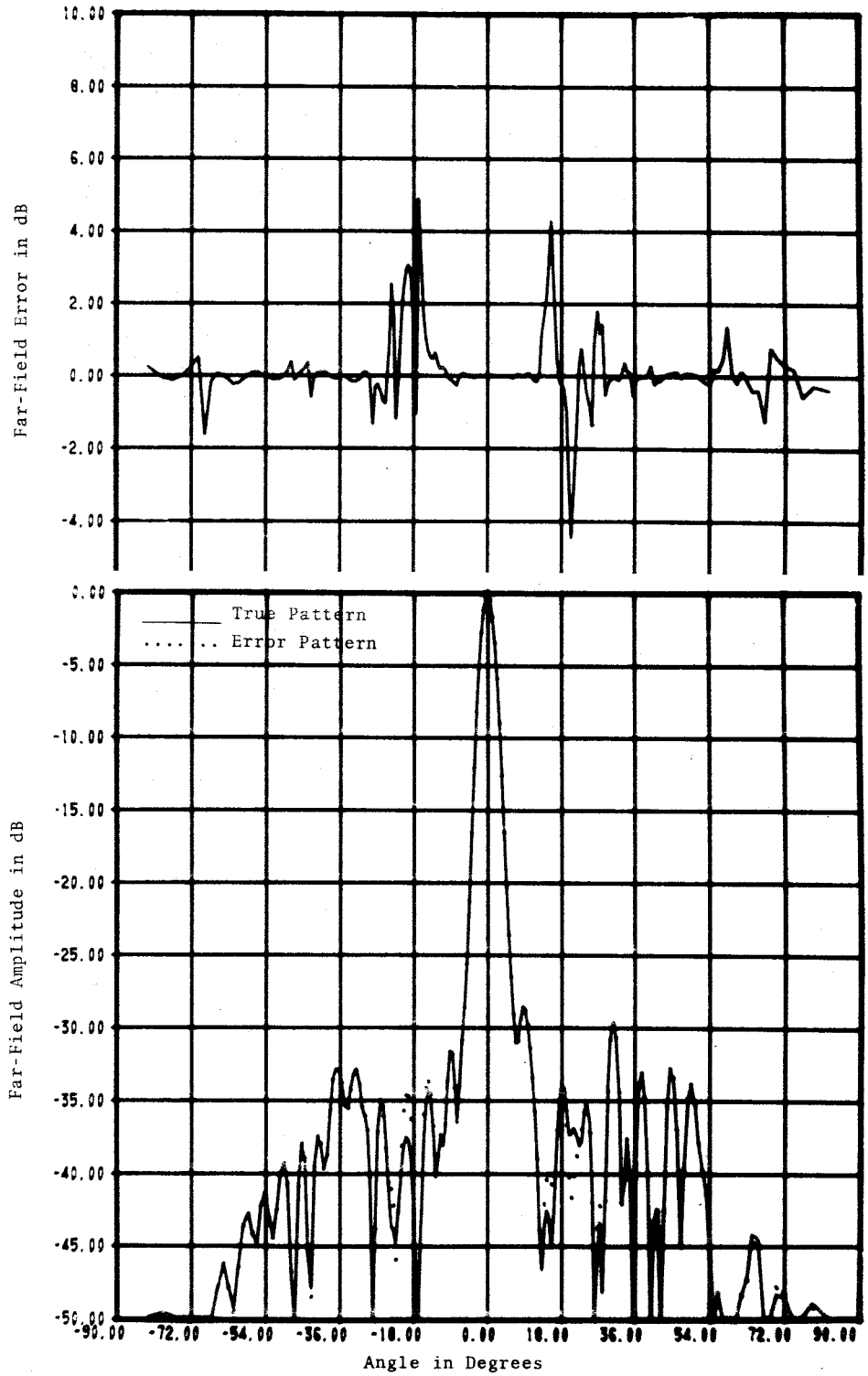


Figure 29. Error in Far-Field Due to Periodic Non-Linear Amplitude Error.

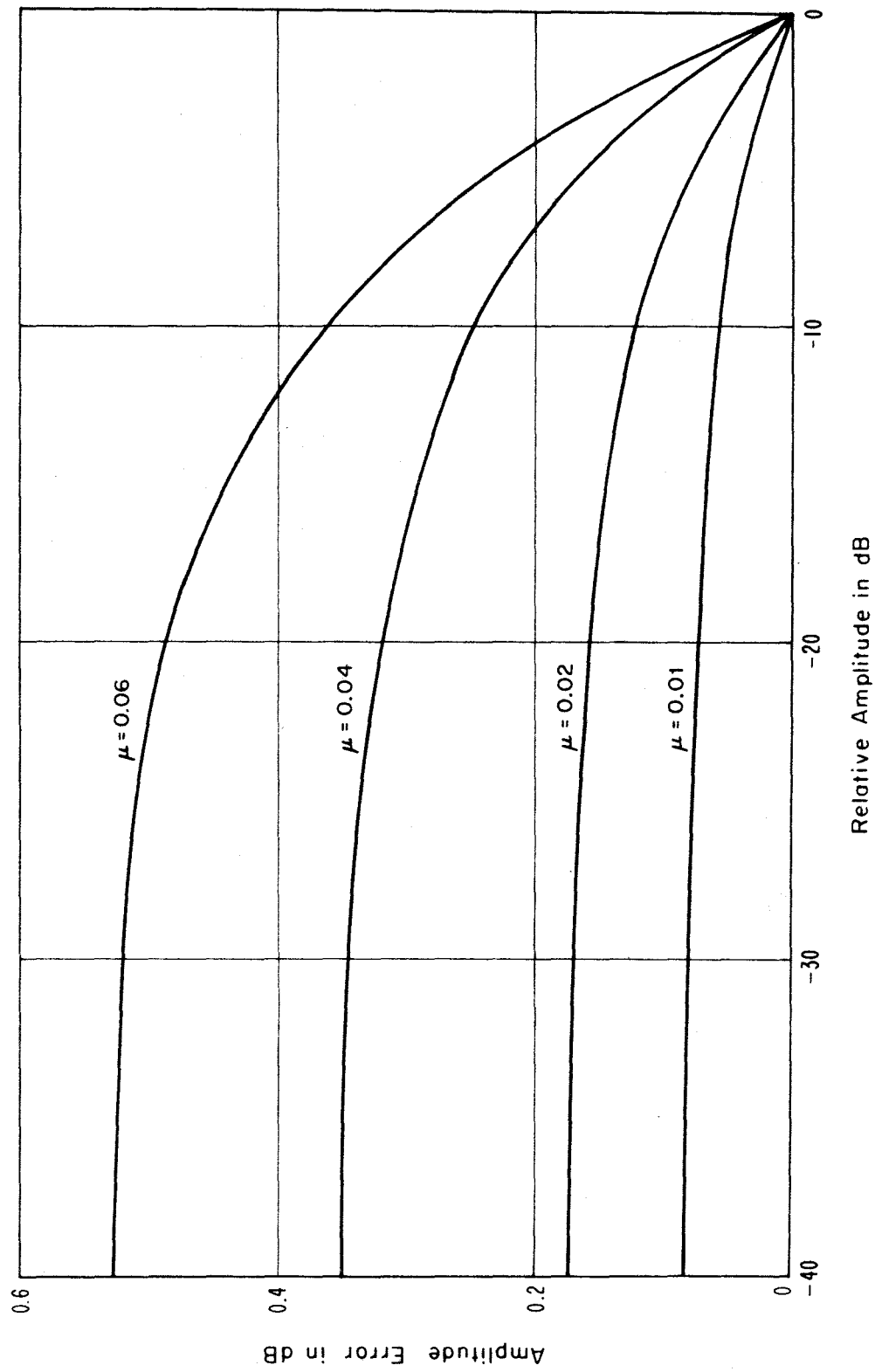


Figure 30. Effect of Receiver Non-Linearity on Measured Data in dB.

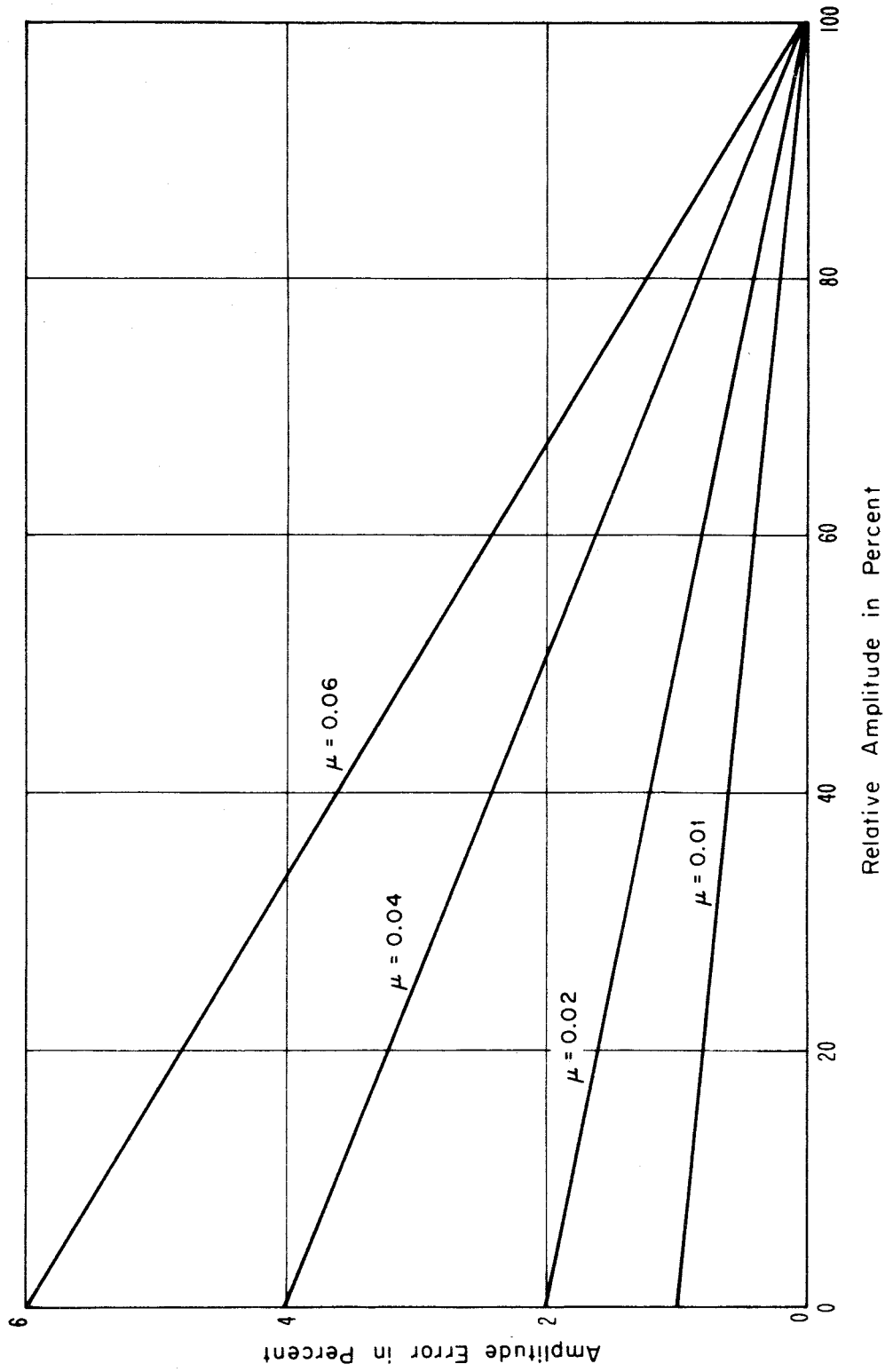


Figure 31. Effect of Receiver Non-Linearity on Measured Amplitude in Percent.

### 3.1.4 Multiple Reflection Errors

It was mentioned in the background material of section 2.0 that multiple reflections between the test antenna and probe are assumed to be negligible. In any actual measurement situation there is a detectable level of reflections, which result in some error in the calculated far-field parameters. The level and effect of multiple reflections are estimated experimentally by taking centerline scans of near-field data on planes which are separated by $\lambda/8$. These scans are transformed to obtain approximate far-field patterns, and the differences in individual scans provide an estimate of the effect which the reflections will have on the complete two-dimensional data. This procedure is described in other references [11] and examples are given.

In the following analysis, equations will be derived which can be used with information obtained from the measurements to further estimate the effect of multiple reflections.

Assume that in the measured probe output, $b_o(\underline{P})$ is the true signal which results from the direct signal, and $m_o(\underline{P})$ is the signal due to the multiple reflections. The total relative output is then

$$B_e(\underline{P}) = B(\underline{P}) + \frac{m_o(\underline{P})}{b_o(P_o)} = B(\underline{P}) + M(\underline{P}) \tag{147}$$

and the resulting far-field spectrum is

$$\begin{aligned} D_e(\underline{K}) &= D(\underline{K}) + \mathcal{F}[M(\underline{P})] \\ &= D(\underline{K}) + J(\underline{K}) \end{aligned} \tag{148}$$

The form of $J(\underline{K})$ will of course depend upon the character of $M(\underline{P})$, and the approximate amplitude and phase functions for $M(\underline{P})$ can be estimated from a series of measurements. To estimate the amplitude functions $a_m(\underline{P})$, the probe is first placed at $\underline{P} = \underline{P}_o$ and the probe output is recorded as the z-separation distance is varied over a distance of a number of wavelengths. Figure 32 is an example of such a measurement and the cyclic variations with a period of approximately $\lambda/2$ are due to the interference between the true and the multiply reflected signals. If we denote the peak to peak variations in dB by w, then the ratio of the two signals denoted by $R_m(\underline{P}_o)$ is

$$R_m(\underline{P}_o) = \left(\frac{\rho-1}{\rho+1}\right), \quad \rho = \log^{-1}(w/20).$$

In general, the amplitude $a_m$ and the phase $\phi_m$ of the interference signal will vary as a function of $\underline{P}$, and this procedure is repeated at a few other points to determine whether $R_m$ is relatively constant, or whether it changes significantly over the scan area. For antennas such as lenses or arrays which do not have diffracting objects such as feeds, subreflectors or struts in the aperture area, the amplitude is generally constant, and an upper bound

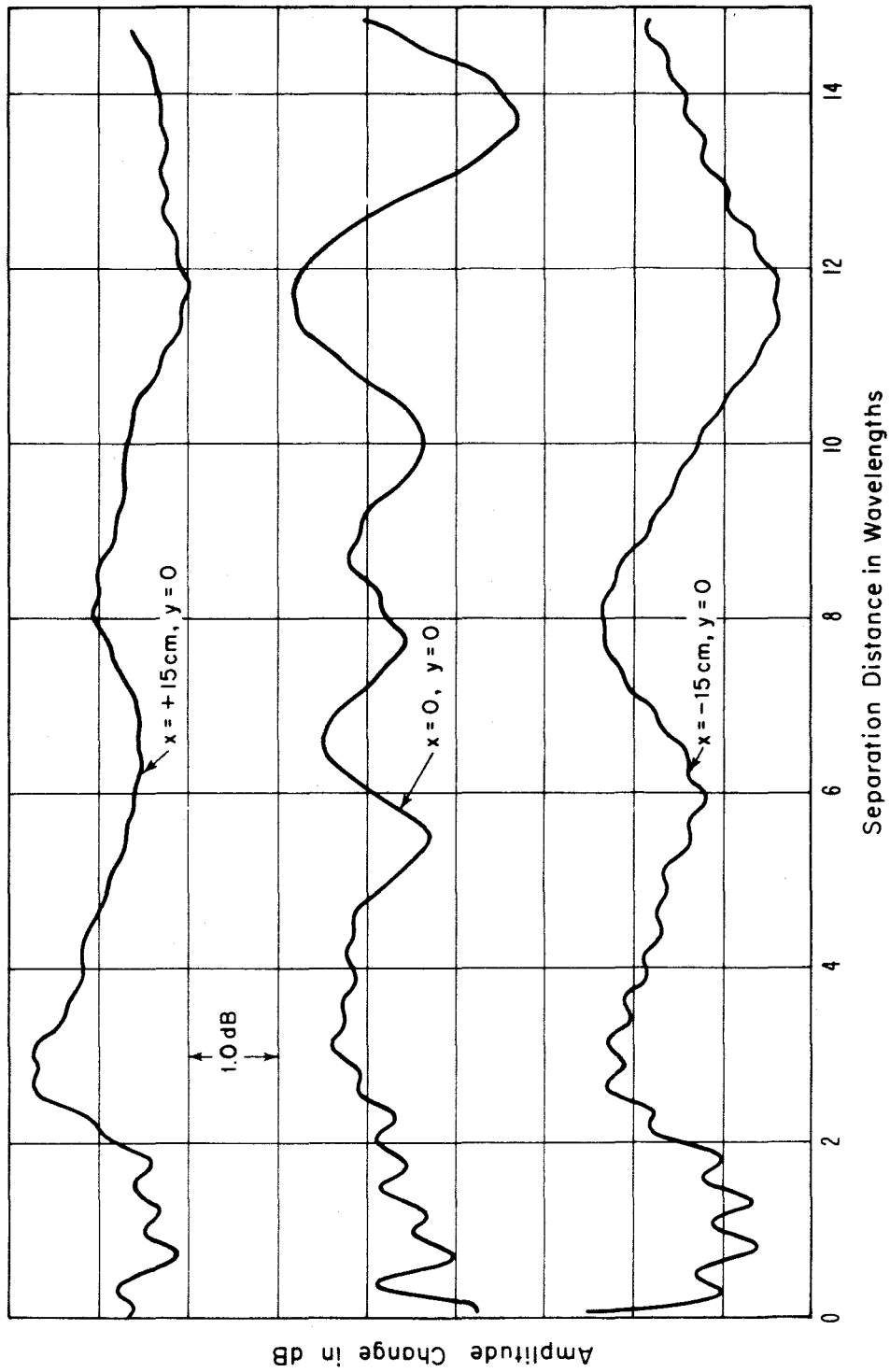


Figure 32. Variation in Near-Field Amplitude as a Function of Separation Distance Illustrating Modulation Due to Multiple Reflections.

can be estimated by taking the largest measured value for $R_m(\underline{P})$. To estimate the phase character of $M(\underline{P})$, two near-field scans are taken along the center lines $y = 0$ at $z = d$ and $z = d + \lambda/4$. The ratio of the data along these two lines is then given by

$$R_m(\underline{P}) = \frac{m(\underline{P}) + b_o(\underline{P})}{m(\underline{P}) - b_o(\underline{P})}$$

$$= \frac{R_m(\underline{P})e^{i(\phi_m(\underline{P})-\phi(\underline{P}))}+1}{R_m(\underline{P})e^{i(\phi_m(\underline{P})-\phi(\underline{P}))}-1}$$

$$\cong -(1 + 2R_m(\underline{P})e^{i\Delta\phi_m} \tag{149}$$

There are two cases which can be easily recognized from graphs of $R_m(\underline{P})$. The first is when $R_m(\underline{P})$ is essentially constant along both x and y centerlines which indicates that

$$M(\underline{P}) = R_m(P_o)\ B(\underline{P}) \tag{150}$$

and therefore

$$J(\underline{K}) = R_m(P_o)\ D(\underline{K}) \tag{151}$$

and the error in any given direction is

$$\left|\frac{D_e(\underline{K})}{D(\underline{K})}\right|_{dB} = w/2. \tag{152}$$

The second case, which is more typical, is illustrated in figure 33 which is a graph of $R_m(x,0)$ and shows a periodic variation which indicates that the phase of the multiple reflection signal is changing fairly rapidly as a function of x. This will shift the peak of the spectrum of $M(\underline{P})$ away from $\underline{K} = 0$, reduce the on-axis error, but increase the error in the sidelobe regions. If the period of the ratio plot in figure 33 is denoted by $T_m$, then the maximum error will occur where

$$k_{xm} = \frac{d\phi_m}{dx} = \frac{\lambda}{T_m} = \frac{2\pi}{\lambda} \sin\theta \tag{153}$$

From similar measurements and calculations along the y-axis, the value of $k_{ym}$ may be determined and the maximum of the interference spectra will occur at $\underline{K} = \underline{K}_m = (k_{xm}, k_{ym})$. The far-field error in any direction is then given by

$$D_e(\underline{K}) = D(\underline{K}) + R_m(\underline{P}_o)\ D(\underline{K}-\underline{K}_m) \tag{154}$$

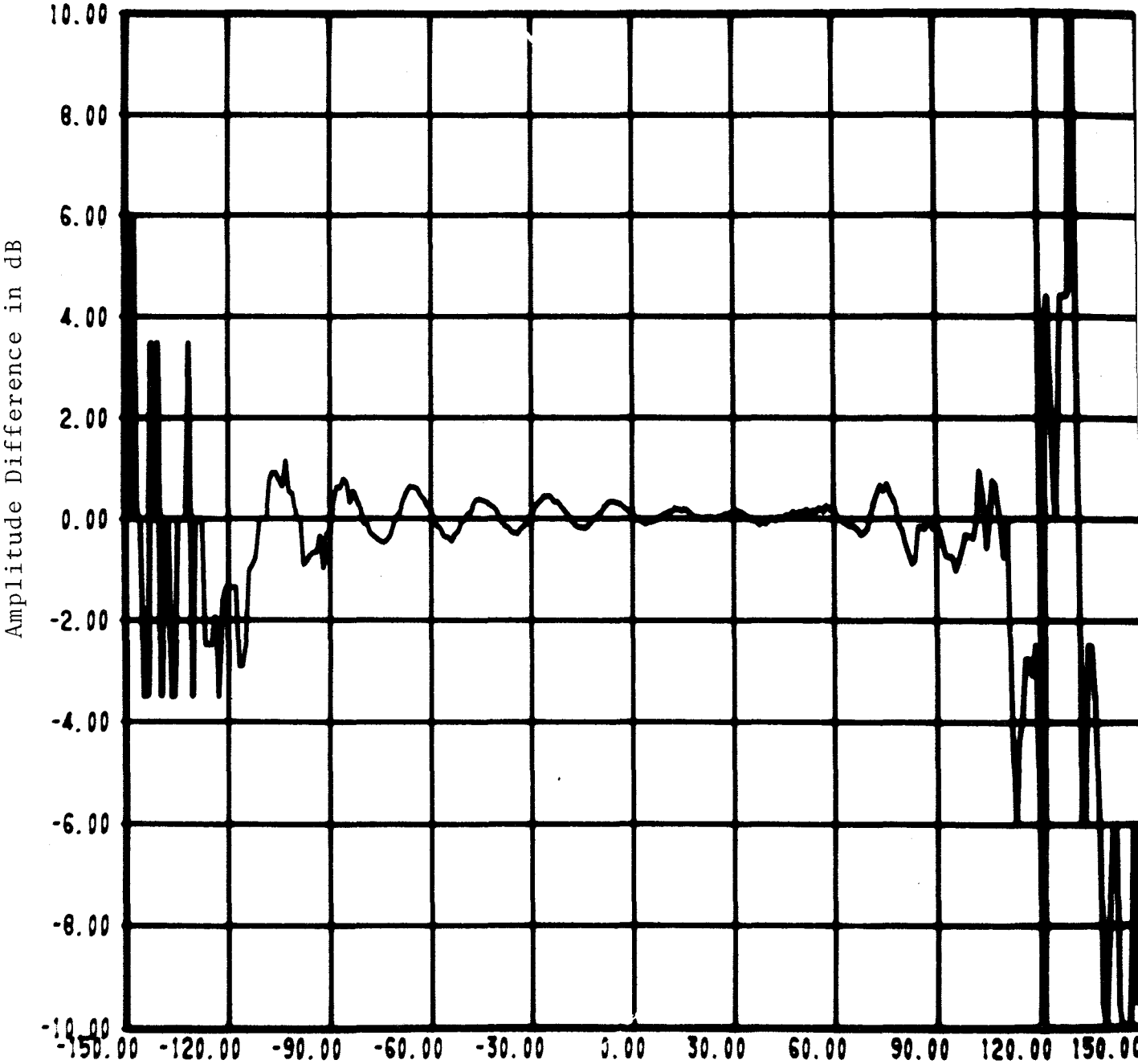


Figure 33. Change in Amplitude for Centerline Scans at z-Distances Separated by $\lambda/8$.

which will be a maximum at $\underline{K} = \underline{K}_m$ where

$$\frac{D_e(K_m)}{D(K_m)} \leq \left|\frac{D(0)}{D(\underline{K}_m)}\right| \quad w/2. \tag{155}$$

A more general case is when there are a number of frequency components present in $R_m(\underline{P})$, and there will then be more than one maxima for the error, but each one will be smaller than given by eq. (155). Equations (152) and (155) therefore respectively represent the two cases where the error is a maximum in the boresight direction and is at a sidelobe.

### 3.1.5 Errors in Gain, Beamwidth and Boresight Direction

In this section, the results of the previous analysis which applies to gain, beamwidth and boresight direction will be summarized. In addition some other sources of error will be included so that the total error in these three quantities may be obtained.

In the previous sections, the study has concentrated upon errors in the measured relative near-field data, $B(\underline{P})$, and expressions have been obtained giving the errors in the relative far-field pattern which they produced. Two other factors are required to calculate the partial gain for one component or the total power gain. These are the gain and polarization of the probe and the magnitude of the normalization constant $A_n = \frac{b_o(P_o)}{a_o}$. To illustrate the role of each of these quantities in the gain calculation, let us assume that the peak of the sum beam is along the z-axis, and $G(0)$ is therefore desired. From eq. (11) this is given in terms of the spherical components of $\underline{s}_{10}(0)$ by

$$G_s(0) = \frac{4\pi\, k^2\, Y_o}{(1-|\Gamma_s|^2)\eta_o}\left(|s_{10A}(0)|^2 + |s_{10E}(0)|^2\right) \tag{156}$$

Let us further assume that the probe is reciprocal and nearly linearly polarized with $|r_{01E}(0)| >> |r_{01A}(0)|$ and eq. (12) may therefore be expressed in terms of the probe gain $G_r(0)$ by

$$G_r = \frac{4\pi k^2 \eta_o}{(1-|\Gamma_r|^2)Y_o}\left(|r_{01A}(0)|^2 + |r_{01E}(0)|^2\right). \tag{157}$$

and in terms of the polarization ratio and $|r_{01E}(0)|^2$ by

$$G_r(0) = \frac{4\pi k^2 \eta_o |r_{o1E}(0)|^2}{(1-|\Gamma_r|^2)Y_o}\left(1 + |\rho_\ell(0)|^2\right). \tag{158}$$

The usual approach to obtaining $G_s(0)$ for the test antenna is to first measure the gain and polarization ratio of the probe in a separate experiment. These known quantities are then used with eq. (158) to obtain the magnitude of $r_{01E}(0)$ given by

$$|r_{01E}(0)| = \left[\frac{(1-|\Gamma_r|^2)Y_o}{4\pi k^2(1-|\rho_{\ell r}(0)|^2)\eta_o} G_r(0)\right]^{1/2} \tag{159}$$

The phase of $r_{01E}(0)$ may be chosen arbitrarily as zero, and the magnitude and phase of the cross component are obtained from eq. (13) as

$$r_{01E}(0) = \rho_{\ell r}(0)\ r_{01E}(0). \tag{160}$$

The next step is to measure the relative near-field data $B'(\underline{P})$ and $B''(\underline{P})$ and then measure the two normalization factors

$$A'_n = \frac{a_o}{b'_o(0)}, \quad A''_n = \frac{a_o}{b''_o(0)}. \tag{161}$$

The usual approach to obtaining these factors is to place the probe at $\underline{P} = 0$, set both the amplitude and phase of the receiver output to zero or some convenient level, and then connect the "generator" and "load" ports, which have been connected to the antennas, directly together. $A'_n$ or $A''_n$, depending upon the orientation of the probe, is then obtained from the change in the amplitude and phase. If the observed amplitude changes associated with $A'_n$ and $A''_n$ respectively are denoted by $a'_n$ and $a''_n$, and the observed phase changes are similarly denoted by $\phi'_n$ and $\phi''_n$ then

$$A'_n = \frac{a_o}{b'_o(0)} = \frac{(1-\Gamma_g\Gamma_\ell)}{(1-\Gamma_g\Gamma_s)}\, a'_n e^{i\phi'_n} \tag{162a}$$

$$A''_n = \frac{a_o}{b''_o(0)} = \frac{(1-\Gamma_g\Gamma_\ell)}{(1-\Gamma_g\Gamma_s)}\, a''_n e^{i\phi''_n} \tag{162b}$$

where $\Gamma_g$ and $\Gamma_\ell$ are the reflection coefficients for the generator and load respectively. With these data, $D'(0)$ and $D''(0)$ are calculated from eqs. (2) and (5).

The next step in the calculations is to use eqs. (6), (7) and (8) to obtain the spherical components of $\underline{s}_{10}(0)$. In the present case where $\underline{K} = 0$ these can be simplified by using the fact that

$$r''_{01A}(0) = r'_{01E}(0), \quad r''_{01E}(0) = -r'_{01A}(0). \tag{163}$$

With these substitutions, the probe correction equations become

$$s_{10A}(0) = \frac{\dfrac{D''(0)}{r'_{01E}(0)} + \dfrac{D'(0)\rho_{\ell r}}{r'_{01E}(0)}}{1 + (\rho_{\ell r}(0))^2} \tag{164a}$$

$$s_{10E}(0) = \frac{\dfrac{D'(0)}{r'_{01E}(0)} - \dfrac{D''(0)\rho_{\ell r}}{r'_{01E}(0)}}{1 + (\rho_{\ell r}(0))^2} . \tag{164b}$$

The final step is to substitute these values of $s_{10A}(0)$ and $s_{10E}(0)$ into eq. (156) to obtain the gain.

A good deal of simplification arises when the probe is linear enough ($|\rho_{\ell r}(0)| < .03$) that for practical purposes $|\rho_{\ell r}(0)|$ may be taken as zero. Further conciseness results when the test antenna is also nearly linearly polarized or the partial gain for one component is desired. In that case the various equations can be combined to give an equation which clearly illustrates the role of each of the measured and calculated quantities.

If we therefore assume that $|\rho_{\ell r}(0)| = |\rho_{\ell s}(0)| = 0$, then eqs. (164), (159), and (156) reduce to

$$|s_{10E}(0)|^2 = \frac{|D'(0)|^2}{|r'_{01E}(0)|^2} \tag{165}$$

$$|r'_{01E}(0)|^2 = \frac{(1-|\Gamma_r|^2)Y_o}{4\pi k^2 \eta_o} G_r(0) \tag{166}$$

$$G_s(0) = \left(\frac{4\pi}{\lambda^2}\right)^2 \left(\frac{|1-\Gamma_\ell\Gamma_r|^2|1-\Gamma_s\Gamma_g|^2}{|1-\Gamma_g\Gamma_\ell|^2(1-|\Gamma_r|^2)(1-|\Gamma_s|^2)}\right) \left(\frac{\left|\int B'(\underline{P})\, dP\right|^2}{|a'_n|^2\, G_r(0)}\right). \tag{167}$$

The four significant factors are then the mismatch term, the normalization amplitude, the gain of the probe, and the magnitude of the integration of the relative near-field data.

For a typical measurement, the gain of the probe is approximately 6 dB with an uncertainty of about 0.1 dB. The magnitude of $a'_n$ is approximately equal to the ratio of gains of the probe and test antenna, and is usually on the order of 20-40 dB with an uncertainty of about 0.05 to 0.10 dB. These uncertainties in $G_r(0)$ and $|a'_n|$ are the major errors in G(0), as will be more apparent when a specific example is considered in the next section.

The errors in beam width can be obtained directly from the analysis of errors in D(0) since the directivity is proportional to $|D(0)|^2$, and also to the product of the beam widths in two orthogonal planes,

$$\theta_E \theta_A \propto |D(0)|^2 \tag{168}$$

where $\theta_E$ and $\theta_A$ are the 3 dB beam widths in the azimuthal and elevation planes respectively. If we assume that $\theta_E = \theta_A = \theta_b$ then the beam width error is given by

$$\Delta\theta_b = \left(\frac{\Delta D(0)}{D(0)}\right) \theta_b . \tag{169}$$

Expressions for $\Delta\theta_b$ due to the various sources of error are easily obtained from the corresponding equations for $\frac{\Delta D(0)}{D(0)}$.

A boresight error means that the apparent position of the peak of the sum pattern or minimum of the difference pattern is shifted slightly from its true position due to errors in the measured near-field data. In terms of the previously used notation,

$$D_e(\underline{K}+\underline{\varepsilon}) = D(\underline{K}), \tag{170}$$

where $\underline{\varepsilon}$ is the boresight error. Substituting $D_e(\underline{K}+\underline{\varepsilon})$ into eq. (25a) the near field data which will produce this kind of error is given by

$$B_e(\underline{P}) = B(\underline{P}) e^{-\underline{\varepsilon}\cdot\underline{P}}. \tag{171}$$

This shows that a linear phase error given by

$$\Delta\phi(\underline{P}) = \varepsilon_x x + \varepsilon_y y \tag{172}$$

will produce the boresight shift. An error in the instrumentation which is linear with position is one possible source of this problem. If the maximum phase error due to instrumentation is denoted by $\Delta\phi_m$ then this could produce a shift in the boresight given by

$$\varepsilon_{xs} = \frac{\Delta\phi_m}{L_x} = \Delta k_x \tag{173}$$

$$\varepsilon_{ys} = \frac{\Delta\phi_m}{L_y} = \Delta k_y . \tag{174}$$

Equations (173) and (174) are valid for a sum pattern but should be modified slightly for a difference pattern. In section 3.1.2 on z-position errors, it was found that for a difference pattern the effective linear term in the worst-case z-position error produced a shift in the position of the boresight null given by

$$\varepsilon_{xd} = \frac{2\pi}{\lambda} \beta \frac{\delta_m}{L_x} = \beta \frac{\Delta\phi_m}{L_x} \tag{175}$$

From the simulation, $\beta$ was found to be approximately equal to 3.0, and so the boresight error for a difference pattern can be about three times as large as for a sum pattern for the same maximum position or instrumentation errors. Since the upper bound errors are desired, we will use the case of a difference pattern and the boresight error will be given by

$$\varepsilon_{xd} = \frac{3\Delta\phi_m}{L_x} = \Delta k_x \tag{176}$$

$$\varepsilon_{yd} = \frac{3\Delta\phi_m}{L_y} = \Delta k_y. \tag{177}$$

By expressing $k_x$ and $k_y$ in terms of the angles A and E, the above expressions can be given in terms of angle changes.

$$k_x = \frac{2\pi}{\lambda} \sin A \cos E \tag{178}$$

$$k_y = \frac{2\pi}{\lambda} \sin E \tag{179}$$

$$\Delta A_\phi = \left( \frac{1}{\cos A \cos E} + \frac{L_x}{L_y} \frac{\tan A \tan E}{\cos E} \right) \frac{3\Delta\phi_m \lambda}{2\pi L_x} \tag{180}$$

$$\Delta E_\phi = \left( \frac{1}{\cos E} \right) \frac{3\Delta\phi_m \lambda}{2\pi L_y} \tag{181}$$

where A and E are the direction angles to the boresight direction. A linear z-position error would also produce this type of change in the far field. If the maximum z-error is $\delta_m$, then for the beam at A, E as above, the phase errors and resultant angle errors are given by,

$$\Delta\phi_{mz} = \frac{6\pi}{\lambda}(\cos A \cos E)\delta_m \tag{182}$$

$$\Delta A_z = \left(1 + \frac{L_x}{L_y} \sin A \sin E\right) \frac{3\delta_m}{L_x} \tag{183}$$

$$\Delta E_z = (\cos A) \frac{3\delta_m}{L_y} \tag{184}$$

Also linear x-y position errors can have this effect with the resulting errors given by

$$\Delta\phi_{mx} = k_x \Delta_{mx} = \frac{6\pi}{\lambda}(\sin A \cos E)\Delta_{mx} \tag{185}$$

$$\Delta\phi_{my} = k_y \Delta_{my} \quad \frac{6\pi}{\lambda}(\tan E)\Delta_{my} \tag{186}$$

$$\Delta A_x = [(1 + \frac{L_x}{L_y} \sin A \tan E) \tan A] \frac{3\Delta_{mx}}{L_x} \quad (187)$$

$$\Delta E_y = (\tan \quad) \frac{3\Delta_{my}}{L_y}. \quad (188)$$

These three types of near field errors are the only ones which can produce a significant change in the boresight direction of the far-field pattern.

## 4.0 Application of Error Analysis Results to a Sample Antenna

In the previous sections, general relations have been developed to predict the errors in far-field parameters which are derived from PNF measurements. In this section we will apply the error equations to a phased array antenna, using typical values for the errors in near-field data. We will combine each source of error to arrive at an estimate of the total error which might occur in such a measurement.

The parameters of the sample antenna will be used in the derived expressions, along with typical and reasonable estimates of near-field errors to estimate the accuracy that can be expected. The pertinent antenna parameters are approximately;

| | |
|---|---|
| Width = $L_x$ = | 3.65 m |
| Height = $L_y$ = | 3.84 m |
| Highest operating frequency = f = | 4.0 GHz |
| Wavelength at f = | 7.5 cm |
| Antenna transmit gain = | 40.0 dB |
| Antenna receive gain = | 40.0 dB |
| Beam width = | 2.0° |
| Maximum steering angle, A = | ± 50° |
| Maximum steering angle, E = | +75°, -50° |
| Aperture efficiency = $\eta$ = | 50% |
| Difference pattern minimum = $\left\|\frac{\mathcal{D}(\underline{K}_b)}{D(K_b)}\right\|$ = | -30 dB |

The measurement parameters which are required to make PNF measurements on this antenna are assumed to be as follows:

Separation distance between probe and array = d = 25 cm
Scan length in x-direction = $L_x$ = 6.0 m
Scan length in y-direction = $L_y$ = 6.0 m
Data point spacings = $\delta_x = \delta_y = 0.40\lambda$ = 3 cm
Total number of data points = 201 x 201 = 40,401
Scan speed = 10 cm/sec
Time for one scan = 1 minute
Time for complete two dimensional scan ≅ 4 hours
Position accuracy, $\Delta_{mx} = \Delta_{my} = \delta_m = \lambda/100$ = .08 cm

Probe gain = $G_r(0)$ = 6.0 dB

Magnitude of normalization = $G_s(0) - G_r(0) = A_n$ = 34 dB

Instrumentation Errors

Phase error = $\Delta\phi_m$ = 5.0 deg

Amplitude linearity = $\mu$ = 0.02

Multipath reflection level

20 log $R_m(0) \cong$ -40.0 dB

w = 0.20 dB

Using these antenna and scan parameters and the appropriate equations, the following tables summarize the upper bound errors which could arise in the near-field measurements. Calculations and results are listed for the conditions where the beam is normal to the array and where it is steered to a representative direction far from the z-axis, A = 50°, E = 75°. These two conditions will be referred to in the tables as "normal" and "steered." The errors are combined by a direct summation and by a root sum square method to arrive at two estimates of total error. Since the errors are uncorrelated and each component is an upper bound, the RSS value is equivalent to at least a 3$\sigma$ confidence level.

Table 5. Summary of estimated errors in gain.

| Source of Error | Equation Used | Error in gain (dB) Normal | Steered |
|---|---|---|---|
| Receiver nonlinearity = $\mu$ | 142 | ±0.12 | ±0.12 |
| Probe gain = $G_r(0)$ | 167 | ±0.10 | ±0.10 |
| Multiple reflections | 152 | ±0.10 | ±0.10 |
| Normalization amplitude = $A_n'$ | 142 | ±0.12 | ±0.12 |
| Mismatch factors | 167 | ±0.02 | ±0.02 |
| x-y Position | 84 & 87 | ±0.003 | ±0.06 |
| z-Position | 132 | ±0.008 | ±0.0002 |
| Phase error | 144 | ±0.02 | ±0.02 |
| | RSS Sum | ±0.19 | ±0.20 |
| | Sum | ±0.42 | ±0.45 |

Table 6. Summary of estimated errors in monopulse difference minimum.

| Source of Error | Equation Used | Error in Difference Minimum Normal | Steered |
|---|---|---|---|
| Phase error | 144 | ±1.46 | ±1.46 |
| z-Position | 133 | ±1.30 | ±0.21 |
| x-y position | 85 & 88 | ±0.09 | ±1.20 |
| Receiver nonlinearity | 142 | ±0.12 | ±0.12 |
| Multiple reflections | 152 | ±0.10 | ±0.10 |
| | RSS Sum | ±1.96 | ±1.90 |
| | Sum | ±3.07 | ±3.09 |

Table 7. Summary of estimated errors in a -30 dB sidelobe.

| Source of Error | Equation Used | Error in -30 dB Sidelobe Normal | Steered |
|---|---|---|---|
| z-Position | 134 | ±4.18 | ±0.69 |
| x-y Position | 86 & 89 | ±0.04 | ±8.25 |
| Phase error | 146 | ±5.81 | ±5.81 |
| Receiver nonlinearity | 143 | ±1.86 | ±1.86 |
| Multiple reflections | 155 | ±3.00 | ±3.00 |
| | RSS Sum | ±8.0 | ±10.7 |
| | Sum | ±14.9 | ±19.71 |

In the above case of a sidelobe, combining of the four large sources of error leads to an estimate which is much larger than would ever be realized in an actual measurement. This is because each of these errors must be a periodic function of x and/or y with only one frequency component to produce an error of this magnitude in the sidelobe region, and all four errors must be of the same frequency to cause the combined error shown in Table 7. Since each of these errors is uncorrelated to any of the others, it is very unlikely that they all would be of the same frequency. The magnitude and periodic character of each of these errors can be easily determined before measurements are performed to determine where they will produce errors and how large the errors will be. The system can be adjusted, in the case of position errors, or corrections applied to the measured data, in the case of amplitude and phase errors, to guarantee that they will not achieve the worst-case values shown in Table 7 or combine at one given sidelobe to make the error even larger. With these factors in mind, it is not unreasonable to expect that each of the worst-case error components could be reduced by at least a factor of 3, and that in combining the errors, only one worst-case component should be added with the others reduced further by a factor of 10. This assumes that each error is a maximum in a different direction. With these modifications the sidelobe errors become as shown below in Table 8.

Table 8. Probable error estimates for -30 dB sidelobe.

| Source of Error | Equation Used | Error in -30 dB Sidelobe Normal | Steered |
|---|---|---|---|
| Phase error | 146 | ±1.94 | ±0.20 |
| z-Position | 134 | ±0.58 | ±0.10 |
| x-y Position | 86 & 89 | ±0.004 | ±2.75 |
| Receiver nonlinearity | 143 | ±0.19 | ±0.19 |
| Multiple reflections | 152 | ±0.30 | ±0.30 |
| | RSS Sum | ±2.06 | ±2.76 |
| | Sum | ±3.01 | ±3.54 |

Table 9. Estimates of error in beam width.

| Source of Error | Equation Used | Beam width error (deg) Normal | Steered |
|---|---|---|---|
| Amplitude nonlinearity | 142 | ±0.02 | ±0.02 |
| Phase error | 144 | ±0.001 | ±0.001 |
| x-y Position | 63a & 74 | ±0.0004 | ±0.009 |
| z-Position | 132 | ±0.0007 | ±0.00002 |
| | RSS Sum | ± .02 | ±0.02 |
| | Sum | ± .022 | ±0.03 |

Table 10. Estimates of error in boresight direction.

| Source of Error | Equation Used | Boresight Error Normal | Steered |
|---|---|---|---|
| Linear phase | 177 or 178 | ±0.02 | ±0.07 |
| Linear x-y position | 184 or 185 | 0.00 | ±0.001 |
| Linear z-position | 180 or 181 | ±0.0004 | 0.00 |
| | RSS Sum | ±0.02 | ±0.07 |
| | Sum | ±0.02 | ±0.071 |

## 5.0 Summary and Conclusions

The results of the error analysis developed in this report should have wide application to a broad class of planar near-field antenna measurements. They are valuable in estimating the errors which result from such measurements and have additional use in improving the design of future measurement systems.

The validity of these results has been demonstrated with the computer simulation, and has also been verified in some respects by two other studies on PNF errors. An earlier study [5] used computer simulation on a hypothetical near-field distribution to determine significant sources of error. Because of the specialized nature of the assumed distribution and error functions, the results were primarily of a qualitative nature and of limited generality, but where they are applicable, they do support the results obtained here.

Another analysis [6] has recently been done by Yaghjian which used a different analytical approach to study some of the same sources of error and antenna types. It is interesting to note that in all cases where Yaghjian considered the same antenna type and error source, as studied in this report, the functional form of the error equations was the same as obtained here. In most cases the cofficients differed, but this is not surprising for upper bound estimates.

It should be kept in mind that the error estimates presented here are upper bounds and that in actual measurements the probable values would be significantly less. Even with the upper bound estimates, we can conclude that the measurements performed using PNF techniques are as good, and in some cases better, than can be achieved on a typical far-field range. The near-field techniques have a number of other advantages which also are a strong consideration in their favor. The antenna can be measured in the production facility and does not have to be taken to a remote far-field range. This means that weather is not a factor in performing the tests and the antenna is not subject to possible damage during installation and measurement on a high rotator. If problems are discovered in the antenna, adjustments can be made much easier in the production facility than on a far-field range. It is also much easier to locate the specific cause of the problem from the near-field data than from far-field pattern measurements. The amount of information about the antenna is increased significantly with the near-field measurements and in addition to the parameters discussed in this report, such things as effective radiated power, ohmic loss in the antenna, and polarization parameters are easily obtained. In summary, especially in the case of a large steerable array which requires very special positioning equipment for far-field measurements, the Planar Near-Field Techniques are easier to implement and can produce higher accuracy and more complete results.

References

[1] D.M. Kerns and E.S. Dayhoff, "Theory of Diffraction in Microwave Interferometry," J. Res. Nat. Bur. Stand., Vol. 64B, pp. 1-13 (Jan.-Mar. 1960).

76-0-0948

[2] D.M. Kerns, "Correction of Near-Field Antenna Measurements Made with an Arbitrary but Known Measuring Antenna," Electron. Lett., Vol. 6, pp. 346-347 (May 1970).

[3] R.C. Baird, A.C. Newell, P.F. Wacker, and D.M. Kerns, "Recent Experimental Results in Near-Field Antenna Measurements," Electron. Lett., Vol. 6, pp. 349-351 (May 1970).

[4] D.M. Kerns, "Plane-Wave Scattering Matrix and Generalized Reciprocity Relations for Antennas and Scatterers," NBS Report (unpublished) (June 1972).

[5] G.P. Rodrique, E.B. Joy, and A.P. Burns, "An Investigation of the Accuracy of Far-Field Patterns Determined from Near-Field Measurements," Final Report, Contract No. DAAH01-72-C-0950, Georgia Inst. of Tech. (Aug. 1973).

[6] A.D. Yaghjian, "Upper Bound Errors in Far-Field Antenna Parameters Determined from Planar Near-Field Measurements," NBS Tech Note 667 (July 1975).

[7] E.B. Joy and D.T. Paris, "Spatial Sampling and Filtering In Near-Field Measurements," IEEE Trans. Antennas Propagat., Vol. AP-20, pp. 253-261 (May 1972).

[8] R.C. Johnson, H. Allen Ecker, and J. Searcy Hollis, "Determination of Far-Field Antenna Patterns from Near-Field Measurements," Proc. IEEE, Vol. 61, No. 12, pp. 1668-1678 (Dec. 1973).

[9] A.C. Newell, R.C. Baird, and Paul F. Wacker, "Accurate Measurement of Antenna Gain and Polarization at Reduced Distances by an Extrapolation Technique," IEEE Trans. Antennas Prop., Vol. AP-21, No. 4, pp. 418-431 (July 1973).

[10] A. Ludwig, J. Hardy, R. Norman, "Gain Calibration of a Horn Antenna Using Pattern Integration," J.P.L., Pasadena, Calif., Tech Report 32-1572 (Oct. 1972).

[11] A.C. Newell, M.L. Crawford, "Planar Near-Field Measurements on High Performance Array Antennas," National Bureau of Standards Internal Report, NBSIR 74-380 (July 1974).

[12] R. Bracewell, The Fourier Transform and its Applications, p. 108 (McGraw-Hill, New York, 1965).

[13] A. Papoulis, Systems and Transforms with Application to Optics, p. 177 (McGraw-Hill Book Company, New York, 1968).

[14] R. Bracewell, ibid., p. 112.